Structure and Kinematics of Late Cenozoic Deformation along the Western Margin of the Culverden Basin, North Canterbury, New Zealand.

A thesis
submitted in partial fulfillment
of the requirements for the Degree
of
Master of Science in Geology
in the
University of Canterbury.

By
Richard Mould.

University of Canterbury

1992

FRONTISPIECE.

An oblique aerial view (7000ft.) looking down the core of the Island Hills Syncline (North Canterbury) depicted by the prominent strike ridges of the Flaxdown Limestone Member. To the left (SE) of the syncline are the prominent ridges of the Mandamus Igneous Complex. The igneous complex is thrust over the syncline along the Island Hills Fault that strikes NE through the first valley between the syncline and the igneous rocks.

An oblique aerial photograph (3500ft.) looking NNE down the core of the Mt. Mason Syncline, North Canterbury. The prominent strike ridges in the cover rocks define the syncline and the Mt. Hilton Anticline (to the right) that unconformably overlie Torlesse Supergroup basement (right foreground). To the left the Torlesse basement can be seen to be overriding the syncline along the Tommys Stream Fault. In the right background is the straight range front of the western margin of the Culverden Basin.

ABSTRACT.

Along the western margin of the Culverden Basin, North Canterbury, on the SE edge of the New Zealand plate boundary zone, deformation in Late Cretaceous and younger cover rocks has produced synchronous faulting and folding about orthogonal NNE-NE and WNW-NW orientations that are younger than early Pleistocene. The folds in the cover sequence are asymmetric, steeply inclined, gently plunging structures that are parallel to the major faults. Non-classical irregular basin and dome interference patterns are defined by prominent marker horizons, and triangular, corrugated hose and irregular T-shaped fold surface geometries (defined by structure contours) are common. The main folds, which vary in shape along their hinge line, have secondary folds developed at various angles to their axial trace. The major NNE-NE trending folds are characterised by composite conical geometries and are defined by several distinct cone segments. Folding in the cover rocks has developed in response to both fault propagation and displacement in the basement, and to shortening within the fault bounded blocks. The axial surfaces of the folds that parallel the faults are truncated by the propagating faults. Fault-related folds have half wavelengths of 1.5-5km and amplitudes of 0.5-2.4km whilst folding within the fault bounded blocks have dimensions of 0.5-1.5km and 0.2-0.6km respectively.

Meso-scale faults, joints, calcite veins, fractures and pressure solution seams indicate two phases of post Late Cretaceous deformation: 1) a weak late Oligocene event related to the beginning of plate boundary inception, and 2) a post Pliocene phase related to widening of the plate boundary deformation during the last 2-3ma.

Analysis of fault and slickenside striation data suggests faulting is dominated by oblique-reverse faults and thrusts, which verge NW, SE and SW. Locally the stress and strain directions are variable but generally imply a predominant NW-SE compression comparable to local geodetic shortening and focal mechanism compression directions. Principal incremental shortening axes and stress tensors suggest the shortening and compression directions plunge gently to horizontally NW-SE but can switch with the intermediate stress to NE-SW. Movement planes tend to be less conclusive, often showing girdle distributions of M-plane intersections. Interspersed with the regional contractional faulting are local areas of oblique-normal NNE and normal faults indicating strain partitioning.

Late Holocene terraces incised into older Pleistocene aggradation gravels are dated by weathering rinds and document deformation. Two seismically triggered landslides and a ground rupture event of the Balmoral Fault appear to have occurred during the same seismic event, approximately 1700 years B.P. A magnitude 6.5+ event necessary to produce ground rupture and the landslides would cause both local, and possibly regional, destruction.

The main contractional deformation along the western margin of the Culverden Basin, commonly associated with thrusting to the southeast is atypical of North Canterbury structure, is distinct from the right-lateral tectonics of Marlborough and marks a transition between the inner and outer plate boundary zones and subduction related tectonics.

TABLE OF CONTENTS

LIST OF FIGURES

LIST OF TABLES

MAP POCKET CONTENTS

Geological map and cross sections of the western margin of the Culverden Basin.

A block diagram illustrating the structure of the top 12km of Pacific Plate crust along the western margin of the Culverden Basin.

CHAPTER ONE: INTRODUCTION.

1.1. REGIONAL SETTING.

Plate boundary deformation in the New Zealand continental block is taking place within a zone up to 200 kilometres wide (Walcott, 1978 & 1987), with associated strain in the South Island largely being accommodated by the Alpine Fault and the Southern Alps. This fault transects the New Zealand continent, joining opposite facing subduction systems (Figure 1.1).

On the east coast of North Island the Hikurangi Margin, and associated accretionary prism, have developed in response to west directed oblique subduction of the Pacific Plate. In the northern South Island subduction of the Hikurangi Margin merges with the strike-slip Marlborough Fault System. Relative plate motion in the northeastern South Island is estimated by de Mets et al. (1990) to be approximately 40mm/yr in a WSW direction. This closely parallels the NE-ENE strikes of the major dextral faults in Marlborough and North Canterbury. The faults of the Marlborough Fault System splay from the Alpine Fault, along which Mesozoic terranes display a 480km strike separation (Wellman, 1953). This has long been regarded as a measure of net displacement on the Alpine Fault, but this assumption is being reconsidered as the mechanisms of convergence are explored. To the south, near Fiordland, the Alpine Fault connects with east directed subduction of the Puysegur Trench system. The Alpine Fault, therefore, functions as a form of trench-trench transform (Le Pichon, 1968), but is atypical in that it links mirror image subduction systems.

The inception of the Alpine Fault as a major plate boundary structure is considered to have occurred during the Oligocene (Molnar et al., 1975; Carter & Norris, 1976; Cooper et al., 1987) or Miocene (Christoffel, 1971; Cutten, 1979; Kamp, 1986). Furthermore, the rate of oblique plate convergence along the Alpine Fault appears to have increased during the last 10Ma (Molnar et al., 1975; Walcott, 1978 & 1984; Cutten, 1979; Stock & Molnar, 1982).

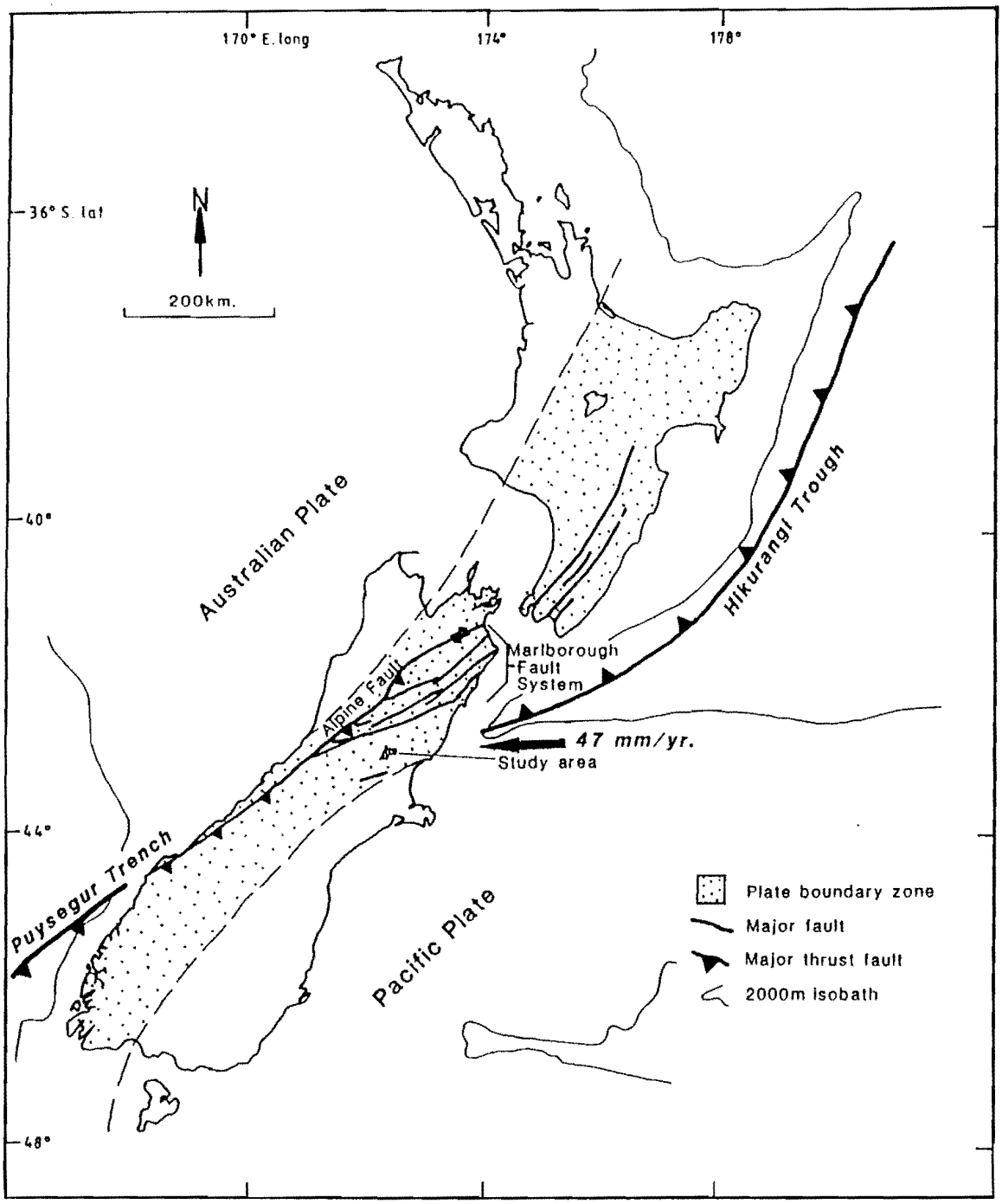

Figure 1.1. Map of the plate boundary through the continental crust (2000m isobath) of New Zealand. The arrow shows the motion of the Pacific Plate relative to the Australian Plate (Chase, 1978). The plate boundary zone limits are after Walcott (1987) where they are defined as "the outer limit of post-Miocene plate boundary zones". The large teeth denote areas of plate subduction.

Comparisons and analogies are often made between the Alpine Fault and the San Andreas Fault in California. Some comparisons are useful (Yeats & Berryman, 1987) but there are also fundamental differences between the two. One principal difference is in the large relative uplift which has occurred on the eastern side of the Alpine Fault. It is becoming increasingly evident that the Alpine Fault is not vertical (Norris et al., 1990) but dips eastward with the bulk of the shortening component being accommodated by extensive telescoping and crustal thickening accomplished by widespread folding and thrust faulting.

Strain is distributed across the entire Marlborough Fault System, although there is some evidence that deformation has migrated southward with time (Campbell, 1973). Presently the southernmost of the major faults, the Hope Fault, is the most active member of the system with horizontal slip rates estimated at between 10mm a^{-1} (Cowan, 1990) and 33mm a^{-1} (Bull, pers. comm.), for different fault segments. This fault currently may be accommodating up to 50% (Van Dissen & Yeats, 1991) or 60% (Kneupfer, 1984) of the relative plate motion.

Dextral displacements on the faults of the Marlborough system vary between 5-50km. (Lensen, 1962; Lamb & Bibby, 1989). Strain within the Marlborough Fault System is also taken up by deformation between faults. The main faults are complexly interconnected, with strain being accommodated by both faulting and associated folding within the fault bounded blocks. To the east, near to the Kaikoura coastline, Van Dissen (1987), Lamb (1988), Lamb & Bibby (1989) and Van Dissen & Yeats (1991) have suggested that the main faults of the Marlborough system progressively merge into a number of west dipping thrusts.

South of the Hope Fault, valley and range topography is associated with several basins which contain remnants of the Cretaceous-Tertiary cover sequence, together with extensive Quaternary fluvial and glacio-fluvial deposits. These basins are bounded by Mesozoic greywacke basement-cored elongate uplifts, developed in association with range-front thrusts, and have up to approximately 3km of structural relief. The largest

of these wide, but shallow depressions is the Culverden Basin, a structure that has been referred to as a composite pull-apart basin (Hicks, 1989). This interpretation is inconsistent with regional Canterbury geology, the Culverden Basin forming part of a chain of basins (e.g. Castle Hill, Lees Valley through to the Cheviot Basin; Figure 1.2) that appear to be predominantly contractional. These basins reflect the Pleistocene-Recent (0-2Ma; Nicol, 1991) development of plate boundary related deformation in North Canterbury.

The study area of this project incorporates a 25km long section of the western margin of the Culverden Basin, approximately an equal distance from the strike-slip Hope Fault in the north and thrust-related shortening to the south (Nicol, 1991). The area takes in both the basin floor and the bounding ranges including Mesozoic Torlesse Supergroup and Cretaceous-Cenozoic rocks exposed along the flanks of the basin. At the northern end of the study area the basement rocks include the Mandamus Igneous Complex and an outlier of Cretaceous-Cenozoic rocks at Island Hills. Typically the structures developed within this study area are asymmetrical, syncline-anticline fold pairs that are separated by moderately-steeply dipping oblique reverse (thrust) faults. These faults generally dip W-NW and strike N-NE. The west dipping faults are atypical of the North Canterbury deformation (Gregg, 1964) and appear to be a continuation of a zone extending from Charing Cross (M33/807292) in the north to at least Mt. Grey in the south.

1.2. STUDY AREA LOCATION AND CHARACTERISTICS.

The 230km^2 study area is located 80km north of Christchurch and 10km west of both the Hawarden and Culverden townships (Figure 1.3). Access is via unsealed roads which branch from State Highway 7. Elevations range from 230-940m.

1.3. THESIS OBJECTIVES AND METHODS OF INVESTIGATION.

The aims of this thesis are:

1). to map the western margin of the Culverden Basin, between Mt Mason and Island Hills;

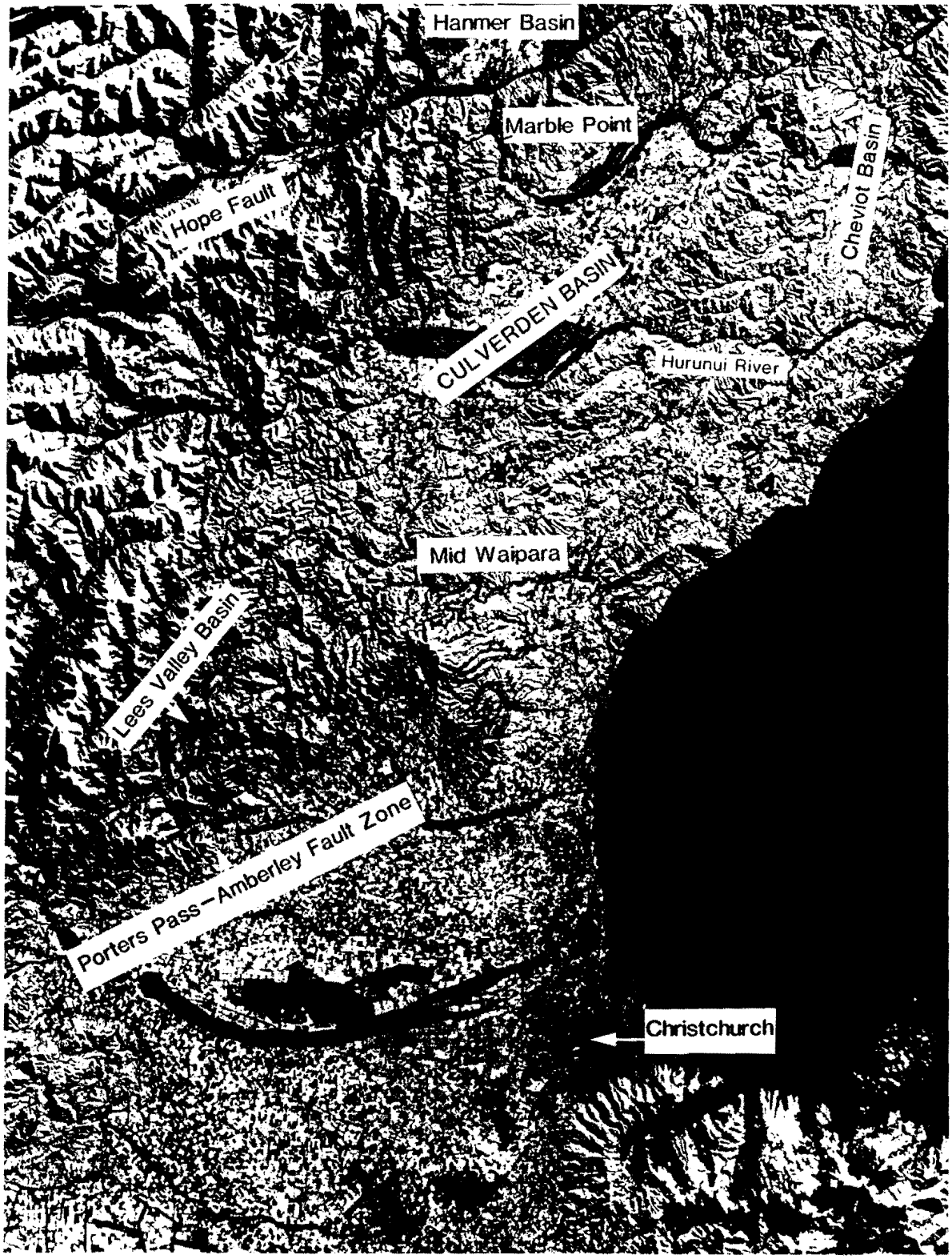

Figure 1.2. Landsat image of North Canterbury showing the rhomboidal shaped range front at the southwestern end of the Culverden Basin. Also highlighted are the Hope Fault, Hanmer Basin, Cheviot Basin and Lees Valley Basins.

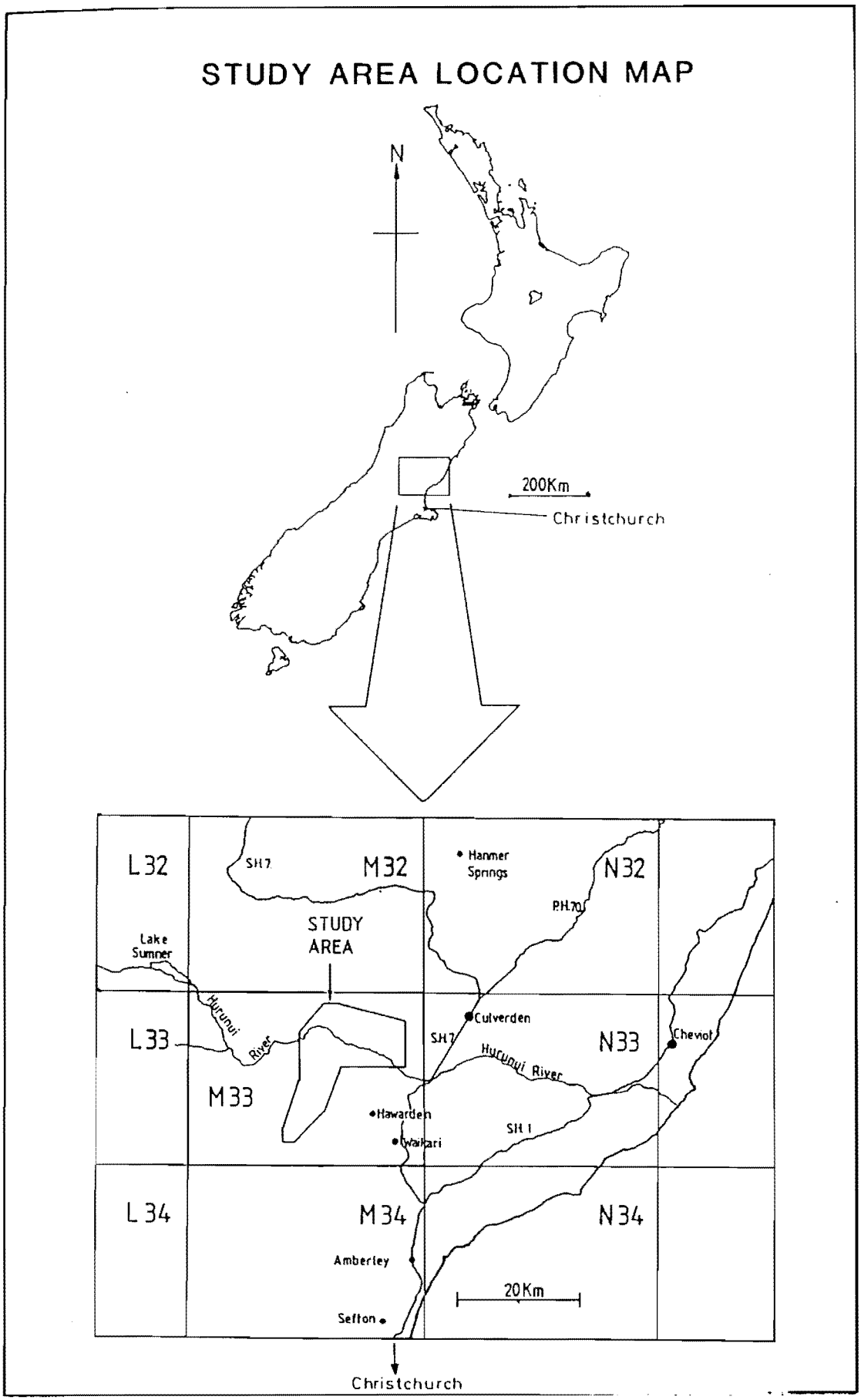

Figure 1.3. Study area location map. The study area is located 80km. north of Christchurch on sheet M33 (DOSLI Infomap 260 series).

2). to characterise the style(s), kinematics and history of deformation in this area;

3). to characterise the active faulting and recent deformation in this area;

4). to place some constraints on the origin of the Culverden Basin.

In order to achieve the principal objectives of this thesis it was necessary to apply a multi-disciplinary approach. This involved defining the stratigraphy and facies relationships so that the geometry and style of the macroscopic structures could be accurately determined. Within the framework defined by the macroscopic deformation small-scale structures provided a means of assessing the local kinematics and were examined in detail. A good understanding of Quaternary deposits was required to investigate active deformation.

Investigation of the stratigraphy and facies relationships involved detailed field mapping. This provided criteria for defining mappable units and data for locating formation boundaries. Aerial photos were used in the preliminary stages in order to locate changes in the topography, often associated with changes in rock type. Facies variations are complex locally and required detailed mapping and sample collection to adequately account for the stratigraphy. Field observations were augmented with petrography and microfaunal age determinations where necessary.

The geometry and style of the macroscopic structures were determined using a combination of detailed field mapping and aerial photo interpretation. Bedding and macroscopic fault orientation data was collected in the field. The data are presented in a number of forms (e.g. cross sections, block diagrams, structural contour maps and equal area stereonet plots). These help to define the three-dimensional geometric relationships of the main structural elements.

Small-scale orientation data were collected in two stages. The first involved preliminary data collection during the mapping stage of the investigation. This was followed by detailed examination and collection of information from localities where, either the small-scale structures were abundant or, they provide important data

constraining the kinematics of macroscopic faulting. Numerous meso-scale structures were examined including stylolites, faults, folds, veins, joints and fractures. Of these small-scale faults, and associated striations, proved the most useful. Two forms of movement indicators were found on small-scale faults: slickenside scratch striations and calcite fibre striations. The age relationships of small-scale structures determined in the field provided information for delineating the structural history of the area.

Active deformation analysis involved detailed mapping, aerial photo examination and structure contouring of the active Balmoral Fault. The age of movement on this fault was estimated using the modal thickness of weathering rinds on medium sand sized Torlesse cobbles from undeformed and deformed terrace surfaces adjacent to the fault. These rind dates made it possible to estimate rates of active deformation and, hence, seismic hazard in the region. Weathering rinds also proved useful in constraining the downcutting rates of local streams that drain across the fault scarp. The ages obtained from various terraces indicates that revision of the ages of many of the terrace surfaces assigned by Gregg (1964) is required.

Large landslides in the NW of the study area were investigated to determine their association with the active deformation of the basin. This involved detailed field mapping and examination of aerial photos. Lichenometry was used to try and date these landslides but the age of the landslide debris was older than the upper limit (1000ybp) to which lichenometry is useful. A minimum age for the landslide in the Mandamus River area was defined from the terrace surface on which the landslide debris rests.

1.4. THESIS BACKGROUND AND STRUCTURE.

This thesis forms part of the North Canterbury Active Tectonics Programme established in 1988 at the Geology Department, University of Canterbury. The programme aims to carry out reseach into the neotectonic processes operating in the region, to establish a database applicable to seismotectonic hazard assessment, to improve our understanding of plate boundary evolution, and to gather information on

the methodology of constructing neotectonic maps.

During the first five years of the programme research has concentrated on the area between the Porters Pass-Amberley Fault Zone and the Hope Fault (Figure 1.2). The Culverden Basin forms part of this priority region, with Nicol (1991) being the first to complete a thesis aimed at addressing the structure of the basin. This thesis represents a northwestern continuation of the area covered by Nicol (1991).

This thesis is presented in 6 chapters, including: local stratigraphy (Chapter 2), structure (Chpters 3 & 4), and aspects of Quaternary geology and active deformation (Chapter 5). The main body of this work concentrates on describing and accounting for the development of the local structures. Data and material not used in the text are presented in the appendices.

A total of approximately 64 days were spent in the field. Field mapping was carried out at scales of 1:25,000 and 1:12,500 from NZ. Aerial Mapping photos (runs 1807-1817) and NZMS 270 topographic maps (sheets M33 A,B,C, & D).

1.5. PREVIOUS WORK.

Although numerous references to parts of the Culverden Basin are scattered throughout the literature, no detailed geological structural investigation of the basin has been undertaken. The earliest reference to the geology of the area is in a report by Buchanan (1868), while Haast (1871) described the igneous and sedimentary rocks on the north and west sides of the basin in a survey of the Amuri district. Hutton (1878) visited the western and northern parts of the Culverden Basin in his report of the "Geology of the North-east Portion of the South Island". Haast (1879) further described the geology along the course of the Hurunui River.

McKay (1890) wrote an account of the geology of the Marlborough and Amuri counties, and followed this up with another report in 1892 on the origins of the

Speight (1915, 1926) discussed the Culverden Basin in a paper on the origin of some intermontane basins in Canterbury. In 1918 he described some of the geological features of the basin in a paper on the structural and glacial features of the Hurunui Valley. Mason (1949) followed Speight's 1918 work examining the Mandamus-Pahau area, noting the absence of late Cretaceous rocks and the Amuri Limestone. Mason (1951) investigated in detail the igneous rocks in the Mandamus-Pahau area.

Schofield (1949) presented a thesis on the Waikari and McDonald Downs areas, and Hamilton (1950) on the Waikari Valley. Falloon (1954) provides an overview of the geology of the Culverden Basin in his thesis, but gives little detail of the structure.

Andrews' (1960) thesis on the sedimentology of the lowermost Otaian horizon in North Canterbury addressed, in part, the sedimentary history of the Culverden Basin. Andrews presented further work on the sedimentology of North Canterbury, including the Culverden Basin, in papers during 1963 and 1967.

Powers (1962) gives a description of the warped and unwarped terraces of the Hurunui River. A thesis by Read (1964) deals mainly with the glacial geology of the Hurunui

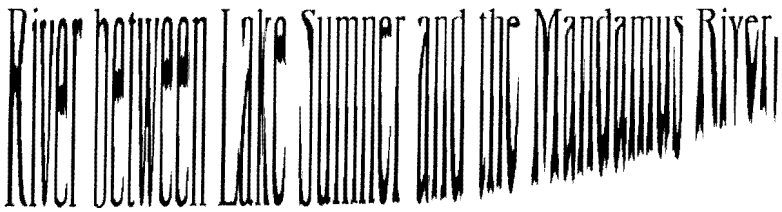

Sevon (1969) examined the geology of the Mandamus area, while Reid (1972) concentrated on the Mandamus Igneous Complex. In later years Shelley (1977), Tulloch (1991) and Weaver and Pankhurst (1991) have also dealt with the Mandamus Igneous Complex.

The Torlesse basement at Mt. Mason has received considerable attention from Bradshaw (1972, 1973), Jenkins and Jenkins (1971), and Middleton (1978). Bradshaw (1972, 1973) mapped the area to show facies variations and structure, and parts of this map have been used here. Jenkins and Jenkins describe the biostratigraphic

significance of the Mt. Mason Limestone. Middleton mapped and described the volcanics in the Torlesse basement. Andrews et.al. (1976) investigated, to a much broader degree, the Canterbury Suite (Torlesse Supergroup) of South Island, of which the Torlesse of this study area is part.

Gregg (1964) produced a Geological Survey 1:250,000 geological map of the Hurunui survey area which represents the most upto date interpretation of the structure of the basin. Field work has been carried out by Browne (1984a & 1984b) in the Culverden Basin, during the development of the Balmoral Irrigation Scheme, but the descriptions from this work are limited to file notes for the NZ Geological Survey.

Although the Middle Waipara and Weka Pass areas are not strictly included within the Culverden Basin, reference is made to the invaluable descriptions of the stratigraphy of these areas by Thomson (1920), Wilson (1963), McCulloch (1981), and Browne & Field (1985). The classification of the late Cretaceous and Cenozoic rocks has provided the framework for the discussion of the stratigraphy of the Culverden Basin.

Valuable descriptions of the structure, lithostratigraphy and volcanolgy at the northern margin of the basin, and to the south of the Hope Fault have been submitted as theses (Gregg, 1965; Lammerink, 1976; Coote, 1987; Endharto, 1987; Syme, 1991). Mason's (1947) paper on the Marble Point outlier is also of value for the correlation of the Omihi Formation from north to south. The stratigraphy and the structure at the southern end of the Culverden Basin has recently been addressed by Nicol (1991). It is this thesis, however, that forms the most recent and comprehensive work on the structure and neotectonics of the western margin of Culverden Basin.

CHAPTER TWO: STRATIGRAPHY.

2.1. INTRODUCTION.

The rocks in the Mt. Mason to Island Hills area comprise conglomerates, sandstones, mudstones, limestones and volcanogenic deposits of late Cretaceous to Pleistocene age unconformably overlying Triassic to early Cretaceous basement rocks (Figure 2.1). The late Cretaceous-Tertiary units form both unconformable and conformable sedimentary sequences and are generally well exposed. There are lithofacies changes across the study area; these are noted here, but not addressed in detail (Andrews, 1963 & 1968; Browne & Field, 1985; also see recommendations for further work).

The entire rock sequence is complexly deformed by folding and faulting, complicating both the estimation of sedimentary thickness of units and the construction of cross sections through the deformed areas.

2.2. THE PRE-TERTIARY SEQUENCE.

The pre-Tertiary rocks comprise basement rocks of the Torlesse Supergroup and Mandamus Igneous Complex, both are unconformably overlain by cover rocks comprising late Cretaceous coal measures, sandstones, mudstones and conglomerates of the Broken River and/or Conway Formations. The Torlesse basement beneath the unconformity surface is generally highly weathered, as at Flaxdown (M33/801256) and Coal Creek (M33/724252), and were the unconformity surface is exposed it ranges between 360m and 480m above sea level, values that are similar to those of the Mid Waipara, Lees Valley and Mt. Thomas areas.

2.2.1. Torlesse Supergroup.

The Torlesse Supergroup consists of grey, well indurated, bedded (mm to tens of metres), poorly-well sorted, intensely deformed, metamorphosed (to zeolite facies), quartzofeldspathic sandstones and mudstones with minor coal, red chert, marble, conglomerate and volcanics (Bradshaw, 1972, 1973; Andrews et al., 1976; Warren, 1978). The Torlesse rocks are well bedded and are characterised by the mudstones

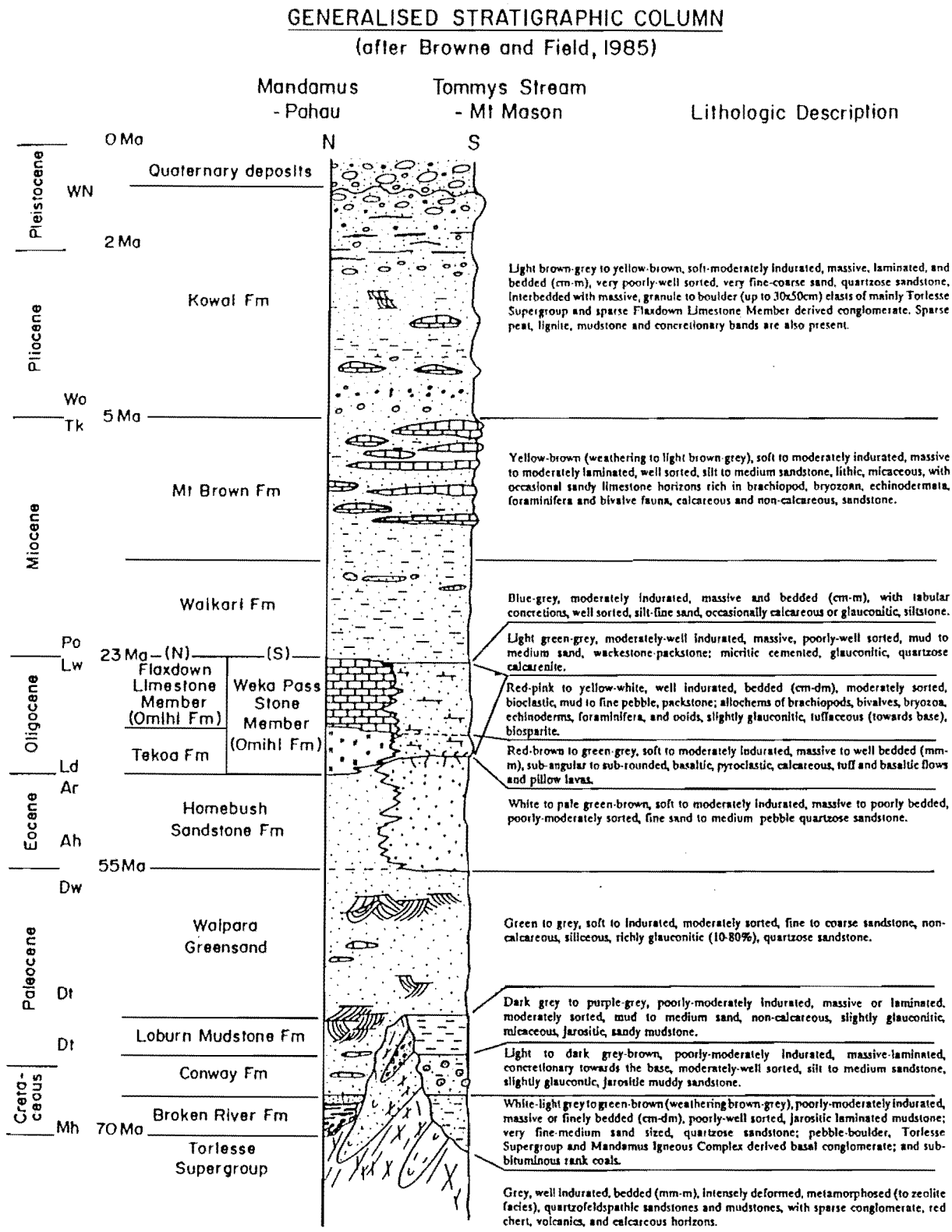

Figure 2.1. Generalised and schemmatic stratigraphic column (not drawn to scale) representing the lithological units between the Mandamus-Pahau to Tommys Stream-Mt. Mason areas. Ages and nomenclature after Browne & Field (1985), descriptions from this study.

forming thin beds (up to 2m) between thicker sandstones and conglomerates (up to 80m). The Torlesse Supergroup in North Canterbury ranges in age from Triassic to early Cretaceous (Gregg, 1964; Campbell & Warren, 1965; Wilson, 1976, 1978, 1984).

2.2.2. Mandamus Igneous Complex.

The rocks of the Mandamus Igneous Complex (after Reid, 1972), in the west of the Culverden Basin (Map 1), cut Torlesse rocks and were once overlain by late Cretaceous sediments. The $10km^2$ igneous complex comprises a monzodiorite-syenite core with associated trachytic and locally phonolitic lavas, tuffs and dykes. Whole-rock chemistry confirms an alkaline character, but both nepheline and quartz-normative rocks are present. The Mandamus Igneous Complex has a precise Rb-Sr isochron age of 97.0 +/- 0.5Ma (Weaver & Pankhurst, 1991). This age is in close agreement with the ages for the alkaline mafic rocks of the Tapuaenuku Igneous Complex and the basalt lavas of the Gridiron Formation, Marlborough (Weaver & Pankhurst, 1991; Tulloch, 1991).

2.2.3. Broken River Formation.

The Broken River Formation unconformably overlies weathered Torlesse basement at Coal Creek, (M33/728252) and Tommys Stream (M33/677056). The formation typically comprises a basal conglomerate passing up into sandstones, mudstones and lensoidal coals. Glauconite is not always present, and is usually less than 5%, but grains up to medium sand size do occur in the Mandamus area.

In the Mandamus area, Sevon (1969) reported conglomerate at the base of the formation containing well rounded clasts ranging from granule to 60cm, of quartz microsyenite, quartz trachyandesite, microsyenite, quartz trachyte, andesite and Torlesse sandstone and mudstone. The igneous clasts are derived from the Mandamus Igneous Complex. The matrix of the conglomerate is a light to dark brown-grey, moderately indurated, jarositic, carbonaceous, sandy mudstone and medium to fine sandstone. Lensoidal, low rank sub-bituminous coals (Appendix II) with minor pyrite nodules are interfingered with the conglomerates.

The environment of deposition is interpreted as non-marine to marginal marine at the base, becoming fully marine (inner shelf) towards the top. The formation is interpreted as being of Haumurian age (Browne & Field, 1985).

2.2.4. Conway Formation.

The Conway Formation, a concretionary, muddy sandstone, conformably overlies Broken River Formation and unconformably overlies Torlesse Supergroup at Tommys Stream (M33/675058). Conway Formation and the conformable overlying Loburn Mudstone Formation are absent in the Mandamus area.

A barred submarine depression, marked with gentle bottom currents and sedimentation from suspension, is the suggested depositional environment (Warren & Speden, 1978). The age of the Conway Formation ranges from Haumurian to Teurian (Strong, 1984).

2.3. TERTIARY ROCKS.

The Tertiary rocks comprise sandstones, mudstones, conglomerates, limestones and volcanogenic deposits that belong to the Eyre, Cookson Volcanics and Motunau groups.

2.3.1. Loburn Formation.

The Loburn Formation conformably overlies Conway Formation at Tommys Stream (M33/673059). Strong (1984) indicates a Teurian age for the Loburn Formation. Browne & Field (1985) suggest a similar depositional environment to the Conway Formation, but with less organic matter being preserved.

2.3.2. Waipara Greensand Formation.

The Waipara Greensand Formation unconformably overlies Torlesse basement, Broken River, and Loburn Mudstone formations. At Flaxdown (M33/801256) the underlying Torlesse basement is highly weathered for approximately 25m beneath the unconformity surface. The Waipara Greensand Formation is divided into two

members; the Mt Ellen and the Stormont members. The Stormont Member is the only member to crop out in the Island Hills and Waitohi Downs areas while both crop out in the Mt. Mason area.

The Stormont Member is generally bioturbated, massive, coarse sandstone, but scour-and-fill and metre-scale cross bedding are locally common. This member has been dated as ranging from Teurian to Waipawan (Hoskins, 1969; Field & Odin, 1981) in the south to Heretaungan in the Island Hills area (Sevon, 1969). In contrast the Mt. Ellen Member is unbioturbated, bedded and a fine sandstone that ranges in age from Teurian to Waipawan (Field & Odin, 1981).

The Waipara Greensand is a shallow marine deposit accumulated under conditions of slow sedimentation although periods of higher energy are represented by scour-and-fill and trough cross-bedding.

2.3.3. Homebush Sandstone Formation.

The Homebush Sandstone only crops out in the Mt. Mason area where it conformably overlies Waipara Greensand. Browne and Field (1985) place an Arnold age on the formation. The depositional environment for the formation is regarded as nearshore to beach (Van der Lingen, 1984).

2.3.4. Tekoa Formation.

The Tekoa Formation, which consists of marine volcanogenic sediments with minor flow units near the base, crops out along the northwestern margin of the Culverden Basin. The tuffs of the Tekoa Formation are an integral part of a volcanic phase which, in terms of age, is similar to the Cookson Volcanics. Browne and Field (1985) propose the Tekoa Formation to be a local formation of the Cookson Volcanics Group, and this nomenclature is adopted here.

The Tekoa Formation crops out in two localities, Waitohi Downs and Island Hills. Associated with the epiclastic deposits at Island Hills is a basalt flow at the base of the formation (M33/749268) which conformably overlies Waipara Greensand Formation. Further to the east, in the Pahau River, and to the north at Marble Point, the Tekoa Formation contains similar flows and pillow basalts.

A marine setting is proposed for the Tekoa Formation based on the presence of pillow lavas in the Pahau River area and the high degree of alteration and calcite infilling of the epiclastic deposits. Coote (1987) inferred a shallow marine setting for Cookson Volcanics in the Waiau area 45km to the NE and a similar environment is inferred for the Island Hills to Waitohi Downs area.

The thinning of the Tekoa Formation south of the Pahau River indicates an eruptive centre either in the Pahau River (Mason, 1949) or further to the north near Waiau. As defined, the Tekoa Formation does not occur south of Waitohi Downs in this study area, but Andrews (1963) notes a deposit to the south, (Dungeon Creek) in the Mid Waipara area, that he attributes to the Tekoa Formation.

Micro and macro-fossil assemblages support a Duntroonian age for the Tekoa Formation in this study area.

2.3.5. Omihi Formation.

The Omihi Formation has been divided up into six members (Andrews, 1963);

i). Flaxdown Limestone,

ii). Weka Pass Stone,

iii). Gorries Creek Greensand,

iv). Berrydale Greensand,

v). Isolated Hill Limestone,

vi). Marble Point Limestone.

The Flaxdown Limestone and the Weka Pass Stone members are the only two to crop out along the western margin of Culverden Basin.

2.3.5.1. Flaxdown Limestone Member.

The Flaxdown Limestone Member takes its name from the Flaxdown limestone quarry on the eastern edge of Hurunui Peak. The limestone also crops out as prominant 'dip and scarp' ridges at Island Hills and Waitohi Downs. The unit grades up from the underlying Tekoa Formation at these localities. The base of the limestone has a "handsome pink to red tint" (Mason, 1949), resulting from the inclusion of the underlying Tekoa Formation, and grades up into a white to cream colour at the top. The well indurated nature of the rock is a result of the precipitation of calcite around the bioclasts, which indicates diagenetic cementation.

In the Waitohi Downs-Kanuku Hills area the Flaxdown Limestone Member passes laterally into the upper portion of the Weka Pass Stone Member. In the north Mason (1949) correlated the Flaxdown member with the Isolated Hill Limestone and the Hamner Marble to the NE and NNE respectively.

On the basis of stratigraphic correlation Mason (1949) assigned a Duntroonian age to the member. This was later revised to Waitakian by Andrews (1963). Specimens of Rhizothyris kokoamuensis and Waiparaia elliptica have been collected from near the base of the pure limestone at Island Hills. These indicate a Duntroonian age (McKinnon, pers. comm. to Ward, 1989), and this age is adopted by the author for at least the base of the unit.

The Flaxdown Limestone Member is probably a shelf limestone which developed on the flanks of a submerged volcanic complex.

2.3.5.2. Weka Pass Stone Member.

The Weka Pass Stone Member crops out in the Waitohi Downs-Kanuku Hills area, where it is laterally equivalent to the Flaxdown Limestone Member, and in the Mt. Mason Syncline, where the base is bioturbated and highly calcareous.

In the Waitohi Downs-Kanuku Hills area the Weka Pass Stone Member disconformably overlies Waipara Greensand Formation. A sharp, unbioturbated contact between the two units and the absence of the Tekoa Formation indicates a period of erosion rather than non-deposition. The presence of re-worked tuff at the base of the Waikari Formation (M33/723203) suggests that the Tekoa Formation was present and is further support for an erosional episode. Andrews (1963) considered the Tekoa Formation to be a continuous body south to the Mid Waipara area, however, there is no conclusive field evidence to support this hypothesis.

2.3.6. Waikari Formation.

The Waikari Formation includes the blue-grey and grey sandstones and siltstones that disconformably overlie the Omihi and Homebush Sandstone Formations and underlie the Mt. Brown Formation. Andrews (1963) formally subdivided the Waikari Formation into five members;

i). Glenesk Sandstone,

ii). Tommys Creek Concretionary Sandstone,

iii). Gowan Hill Sandstone,

iv). Scargill Siltstone,

v). Pahau Siltstone.

Three of these members crop out in the Mt. Mason to Island Hills area, they being the Pahau Siltstone, Scargill Siltstone and Tommys Creek Concretionary Sandstone Members. Due to the thin nature of the Pahau Siltstone and Tommys Creek Concretionary Sandstone Members the three members have been mapped as a single entity, the Waikari Formation, for clarity.

The Pahau Siltstone Member forms the core of the Island Hills syncline where it disconformably overlies the Flaxdown Limestone Member. Pahau Siltstone, the basal member of the Waikari Formation, also crops out in the Mt. Mason area and is present along the eastern edge of the Green Hill downlands (Mason, 1949; Andrews, 1963). From foraminifera in the siltstone a Waitakian to Otaian age is proposed (Andrews, 1963).

The Scargill Siltstone Member contact with the underlying Pahau Siltstone Member is transitional at Mt. Mason but sharp at Green Hill (Mason, 1949; Andrews, 1963). Regularly spaced concretionary sandstone layers occur throughout the member. Mason (1949) reports that many of these concretionary sandstone layers contain a rich molluscan faunule towards their top.

Rich assemblages of foraminifera show the Scargill Siltstone to be Otaian at its base and Lillburnian at its top at Green Hill. An Otaian age is inferred for the Scargill Siltstone at Mt. Mason.

Conformably overlying the Scargill Siltstone, in the Mt. Mason to Waipara River South Branch area, is the Tommys Creek Concretionary Sandstone. In the Green Hill area the Scargill Siltstone is conformably and transitionally overlain by the Mt. Brown Formation.

The Scargill Siltstone Member to Tommys Creek Concretionary Sandstone Member contact is transitional at Mt. Mason and is marked by a change in colour from that of the Scargill Siltstone (Andrews, 1963). At Mt. Mason the rock is a medium blue-grey, sandy siltstone that alternates with cemented, concretionary, silty fine sandstone layers. From the rich foraminiferal content of the siltstone Andrews (1963) has inferred an upper Otaian age.

In the Mt. Mason area the Tommys Creek Concretionary Sandstone is conformably overlain by the Mt. Brown Formation. The contact between the two units is transitional and difficult to define.

2.3.7. Mount Brown Formation.

The Mt. Brown Formation conformably and gradationally overlies the Scargill Siltstone and Tommys Creek Concretionary Sandstone members of the Waikari Formation in this study area. Sandstone beds as thick as 10m occur and many contain tabular fine-sandy calcareous concretions (M33/840184) or are bioturbated (M33/725221). The

sandstone beds may or may not be fossiliferous; if fossils are present they commonly form lensoidal shell beds upto 3m thick or occur scattered throughout the bed. The constituent limestone members of the Mt. Brown Formation (Browne & Field, 1985), that are common in the Waipara region, can not be correlated into this study area.

The sandstones, shell beds and siltstones of the Mt. Brown Formation crop out in the Mt. Mason, Waitohi Downs and Green Hill synclines. It is absent at Island Hills, but presumably, at one time covered the Waikari Formation, now the highest preserved, in the core of the syncline. The Mt. Brown Formation also crops out at Hurunui Mound (M33/846188), which consists of interbedded sandstones, siltstones and shell beds,and forms an inlier in the Quaternary gravels of the Culverden Basin.

The Mt. Brown Formation has a maximum thickness of approximately 500m in the Waitohi Downs area. Browne and Field (1985) infer that the Mt. Brown Formation was deposited in a rapidly subsiding basin, and that the rate of subsidence increased when the overlying, conglomerate dominated Kowai Formation was deposited. The sand of the Mt. Brown Formation is thought to have been deposited as mass flows within a background of silt sedimentation. Depositional depths of neritic to sublittoral, not greatly different from the depositional depths of the earlier Omihi and Waikari formations, are interpreted for the Mt. Brown Formation.

From foraminiferal and macrofossil content, Browne and Field (1985) propose that the Mt. Brown Formation ranges from Otaian to Waiauan in age in most sections.

2.3.8. Kowai Formation.

The Kowai Formation consists of a diverse range of lithotypes including sandstones, conglomerates, mudstones and sparse peats and lignites. Kowai Formation rests disconformably on Mt. Brown Formation in the Waitohi Downs and Green Hill synclines.

Mason (1949) proposed that the first appearance of conglomerate should mark the contact between the gradational Mt. Brown and Kowai formations. Browne & Field (1985) define the contact as being the last appearance of limestone in the Mt. Brown Formation. This is difficult to apply in this study area as the limestone members of Wilson (1963) and McCulloch (1981) are very difficult to define and/or are absent. Therefore, Mason's (1949) method of recognising the contact between the two formations is adopted here. Furthermore, the appearance of conglomerates indicates a significant change in the tectonic setting. For the purposes of this study, it is therefore practical to use the first appearance of conglomerate to define the contact and thence when uplift exposed a basement source.

At Green Hill the base of the Kowai Formation is not now well exposed, but further to the north according to Mason (1949) it overlies weathered, yellow-brown, fine sandstone of the Mt. Brown Formation. The core of the Waitohi Downs Syncline consists of Kowai Formation.

Browne and Field (1985) propose that the Kowai Formation represents a shallow marine sequence, deposited at inner to mid-shelf depths, affected by periods of flucuating eustatic sea-level associated with non-marine deposition. Penecontemporaneous with sedimentation was the onset of deformation in a source area which provided the voluminous gravel deposits in the Kowai Formation. The formation marks a substantial pulse in tectonism in the late Cenozoic.

Browne and Field (1985) place a possible Kapitean-Opoitian, or more probably Opoitian, to Mangapanian or Nukumaruan age on the formation. It is here proposed that the base is probably Opoitian or Waipipian in this study area, a change in age being affected by placing the contact between the Kowai and Mt. Brown formations higher in the sedimentary sequence than Browne and Field (1985). The top of the formation is believed to be Mangapanian or Nukumaruan.

2.4. QUATERNARY STRATIGRAPHY.

Coarse, basement derived, gravels are deposited in the Culverden Basin, forming the Culverden Plains, and extend within discontinuous terrace remnants, along the rivers draining into the basin; the Pahau, Dove, Mandamus, Hurunui, Waitohi and North Branch Waipara River. Three fluvio-glacial deposits have previously been recognised in the Culverden Basin (Powers 1962; Suggate, 1965) and formally been assigned, in ascending chronological order, to the Windwhistle, Burnham and St Bernard Formations (Gregg 1964). These have been attributed by Gregg (1964) to the Otarama, Blackwater and Poulter glacial advances respectively.

A previously unrecognised and highest fluvio-glacial deposit is located on Torlesse basement on the Waitohi Peaks range (M33/714224) and is here termed Waitohi Formation. On the basis of the gravels being 260m above the current river level, the high degree of weathering of the matrix and Torlesse derived clasts, and the degree of oxidation, the unit may correlate to the Hororata Formation. It is outside the scope of this study to determine the stratigraphic relationship of this unit, but it may be that the Waitohi Formation results from the Avoca glacial advance.

Commonly all these fluvio-glacial deposits are coarse, unsorted, subrounded gravels in a silt to sand matrix. The formations differ in colour and composition. The oldest, Watohi Formation, is highly weathered with well developed weathering rinds on the Torlesse basement derived clasts and a larger proportion of clays and iron oxide than in the younger formations. The volume of clay and iron oxide in the matrix and the thickness of weathering rinds developed on the clasts decreases with the decreasing ages of the formations. The Holocene floodplain deposits consist predominantly of rounded, moderately well sorted, fresh Torlesse basement derived gravels and sands.

2.5. SYNOPSIS.

The Torlesse Supergroup rocks were deformed in two major orogenies; the Rangitata-I Orogeny during the late Triassic or early Jurassic, and the Rangitata-II Orogeny in the late Jurassic or early Cretaceous (Bradshaw et al., 1981; Botsford, 1983). During the

Rangitata Orogenies the Torlesse basement rocks were folded and faulted and regionally metamorphosed. The Mandamus Igneous Complex forms part of a belt of alkaline igneous rocks of Ngaterian age, the emplacement of which accompanied extension of the thin continental crust of the Pahau subterrane following collision and subduction of a spreading ridge (Weaver & Pankhurst, 1991). The basal conglomerate of the Broken River Formation indicates that erosion of the local basement ocurred in the late Cretaceous, a result of the basement being exposed during this period of N-S regional extension (Field et.al., 1989).

The Broken River Formation marks the onset of a widespread marine transgression which reached its maximum westerly extent in the late Eocene. The deposition of pillow lavas, shallow marine tuffs, and agglomerates in the Oligocene indicate mild extension ocurred from at least Culverden to Oamaru in the south. At the beginning of the Miocene a simple depositional basin occupied most of North Canterbury (Figure 2.2). The Miocene was characterised by an influx of sediment from the west, along the present day location of the Southern Alps, in response to uplift assoicated with the Alpine Fault. In the Pliocene-Pleistocene this uplift and associated regression continued. The late Pleistocene-Recent stratigraphy documents the development of basement cored, elongate, fault-propagated folding in North Canterbury. Active deformation structures developed in Quaternary and Holocene deposits of this study area are evidence of the continuation of late Cenozoic deformation.

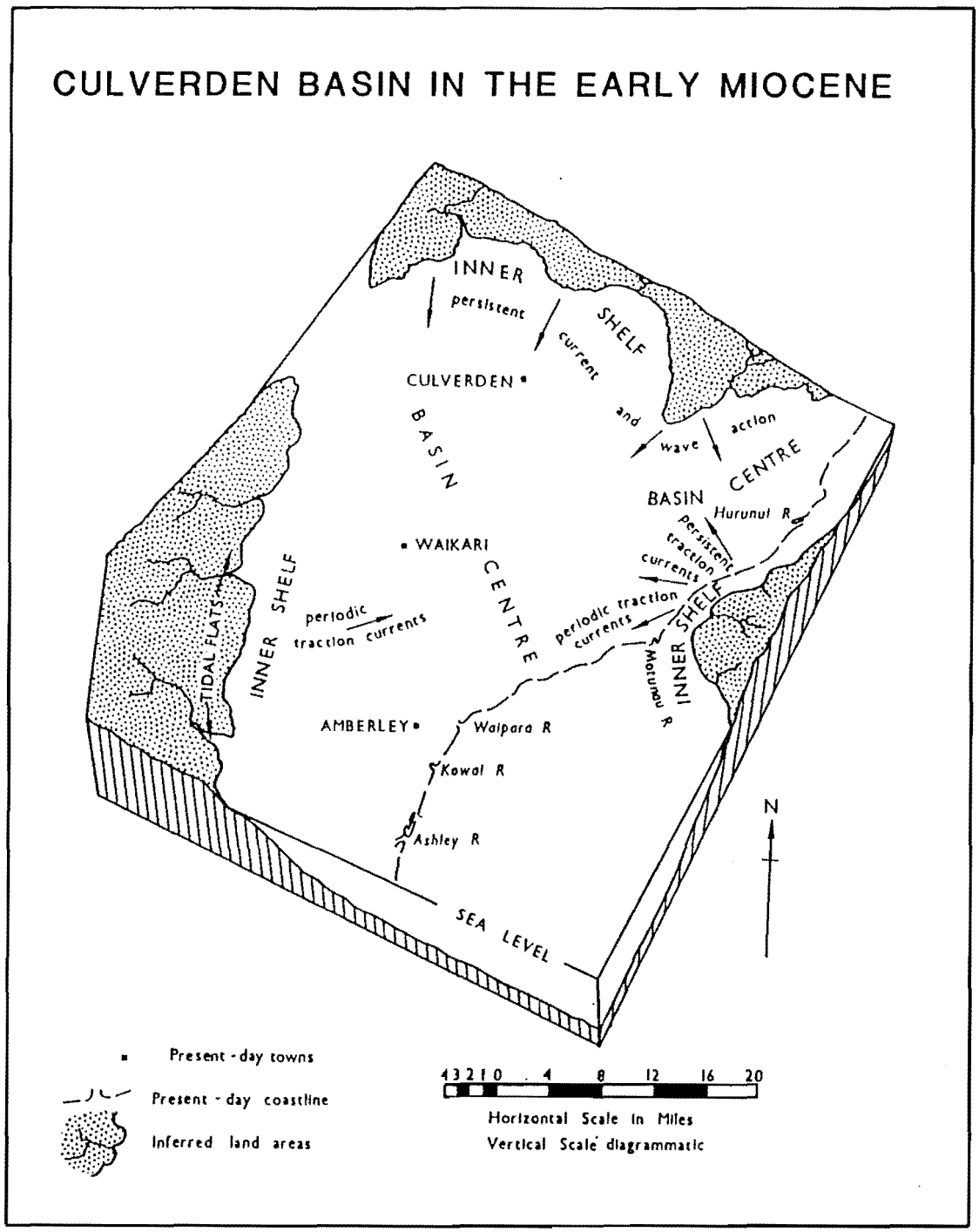

Figure 2.2. Diagrammatic sketch, showing the reconstructed geography/ bathymetry for Culverden Basin and North Canterbury during Miocene time (after Andrews, 1968).

CHAPTER THREE: STRUCTURE.

3.1. INTRODUCTION.

Analysis of the structures in this study area is limited to those developed in the Mesozoic basement and late Cretaceous-Quaternary sedimentary sequence along the western margin of the Culverden Basin. Typically the structural grain of the study area is dominated by approximately parallel striking macroscopic faults and folds. This chapter provides descriptions of the macroscopic structures and discusses their kinematics. The timing and kinematics of a variety of small-scale structures developed in the basement and cover rocks are also discussed.

3.2. MACROSCOPIC FAULTING.

Within this study area four major macroscopic faults have previously been identified and named, while the Taruna, Hurunui and Green Hill Faults are proposed from this study. A further possible macroscopic fault is inferred to strike WNW along the southern edge of Green Hill. No active trace or exposure of the fault exists but geomorphic features (Chapter 5) (Bull, 1984) developed along the range front of Green Hill are suggestive of a thrust fault that dips moderately-steeply NNE. Three macroscopic faults have developed at an oblique angle to the Waitohi Downs Fault at Kanuku Hills. A listing of the characteristic features of all these faults is tabulated in Table 3.1. and their location shown on Figure 3.1.

The orientation of the Waitohi Downs Fault in the north bank of the Hurunui River, the lineament of a large (9m) river terrace scarp and the alignment of the fault zone at Flaxdown Quarry warrant the inferrence that the Waitohi Downs Fault continues beneath the Quaternary gravels to crop out in the Flaxdown area. Similarly, the Tommys Stream Fault and the Green Hill Fault may be one continuous fault, although there is no evidence, other than the alignment of the fault traces, to prove this conjecture.

TABLE 3.1. Descriptions of the macroscopic faults in this study area.

FAULT NAME	ORIENTATION	DIP & DIRECTION	LATERAL EXTENT	FAULT ZONE WIDTH	BEST EXPOSURES (*1)	FAULT TYPE	UNITS JUXTAPOSED (*2)	AGE
TOMMYS STREAM FAULT	NNW-NE	24-53° WSW-NW	11km+	15-40m	Tommys St, North Branch Waipara R	Oblique thrust	Tor against Tor, BRF, CSF, LMF, WGF, HSF, WPSM, WF, Mt.BF.	Late Cenozoic
WAITOHI DOWNS FAULT	N-NE	36-65° W-NW	16km+	60-850m	Waitohi R, Kanuku St, Flaxdown St, Hurunui R	Oblique thrust	Tor against Tor, WGF, WPSM, FLM, WF, Mt.BF	Late Cenozoic
ISLAND HILLS FAULT	NE	55-64° SE	6km+	10-90m	Coal Ck, Mandamus R	Oblique thrust	Tor, BRF, WGF against Tor and Tr, Sy, LLT of the MIC	Late Cenozoic
HURUNUI FAULT	NW	60-67° NE	3.5km+	50m	Hurunui R	Oblique thrust	Tor against Tor	Late Cenozoic
GREEN HILL FAULT	NNE	70° WNW	3km+	50-120m	Cascade St, Awatui St,	Oblique reverse-oblique thrust	Tor, WGF against WGF, TTF, FLM?, WF, KF	Late Cenozoic
BALMORAL FAULT	NNW-N	27° steeply WSW-W	4.5km+	Not exposed	None	Thrust	Quat gravel against Quat gravel & WF	Late Cenozoic
KANUKU HILLS FAULTS	NE	80° NW-81° SE	0.2- 0.5km	Not exposed	None	Normal-oblique normal	Mt.BF against WF, WPSM, Mt.BF against Mt.BF, WF, WPSM, WGF against Mt.BF, WF, WPSM, WGF	Late Cenozoic
TARUNA FAULT	W-NW	15° NE-41° N	2.3km+	20m	Taruna	Oblique thrust	Tor against Tor	Late Cenozoic

*1. St= stream, R= river, Ck= creek.

*2. Tor= Torlesse Supergroup, BRF= Broken River Formation, CSF= Conway Sandstone Formation, LMF= Loburn Mudstone Formation, WGF= Waipara Greensand Formation, HSF= Homebush Sandstone Formation, TTF= Tekoa Tuff Formation, FLM= Flaxdown Limestone Member, WPSM= Weka Pass Stone Member, WF= Waikari Formation, Mt.BF= Mt. Brown Formation, KF= Kowai Formation, MIC= Mandamus Igneous Complex, Tr= Trachyte, Sy= Syenite, LLT= Lithic Lapilli Tuff, Quat= Quaternary

Figure 3.1. Location map of the major macroscopic faults along the western margin of the Culverden Basin, North Canterbury (see Table 3.1).

MACROSCOPIC FAULT LOCATION MAP

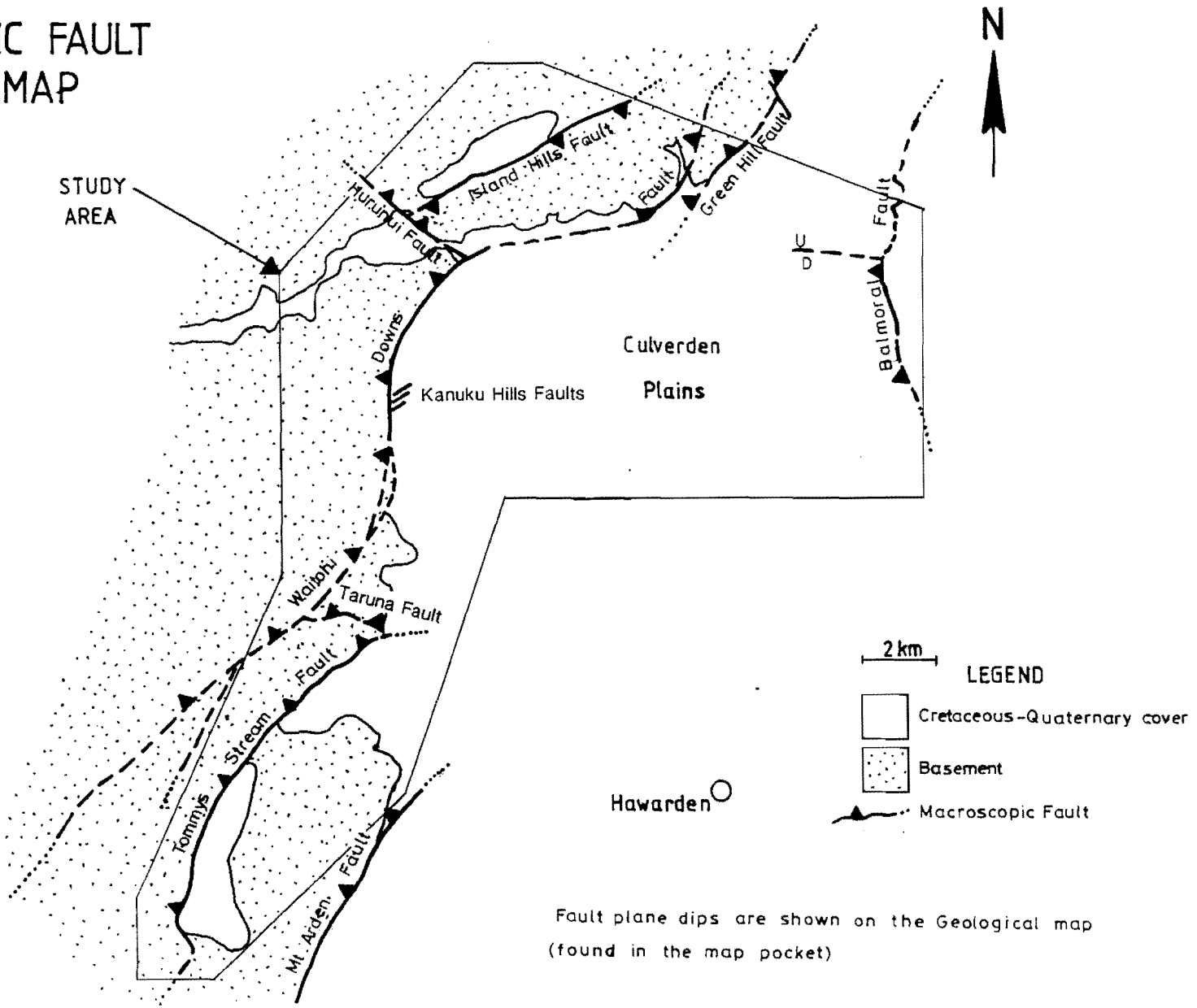

Fault plane dips are shown on the Geological map (found in the map pocket)

All the macroscopic faults, except those at Kanuku Hills, have gentle to steep dips and oblique-reverse to reverse displacements. The faults with dips of greater than 45°, could in Anderson (1951) terms, be classified as reverse, however, the author prefers the term thrust as it conveys a better perception of the tectonics. The oblique component to the vertical displacements of the macroscopic faults lowers the plunge of the slip vector of the fault resulting in thrusting rather than a pure reverse dip-slip motion.

Good exposure of all the macroscopic faults is limited to deeply eroded streams and farm tracks. Between exposures the fault trace is determined from hillslope morphology. Commonly saddles are developed in the ridges that strike across the less indurated and highly fractured rock of the fault zone. The width of the saddle provides a crude measure of the width of the fault zone. At Mt. Mason (M33/697115), for example, a strike ridge of Mt. Brown Formation is cut off by the Tommys Stream Fault. Between the rocks of the foot-wall and the Torlesse basement of the hanging-wall a 30m wide saddle has developed in the fault zone. Likewise, at Flaxdown Quarry a continuous line of saddles delineates the Waitohi Downs Fault.

Freshwater springs have developed ubiquitously along many of the fault zones. The highly fractured nature of the fault zone has resulted in increased porosity and permeability, the groundwater appearing to concentrate at the surface as small ponds and swamps. Occasionally the streams draining the ponds and swamps erode channels that strike parallel to the macroscopic faults. For example, a stream that joins the North Branch Waipara River (M33/682093) has eroded into the Tommys Stream Fault zone. Similarly, paleochannels of the Hurunui River have followed the crush zone associated with the Hurunui Fault.

The fault zones of the major faults, excluding the Balmoral Fault and the fault set at Kanuku Hills, exhibit a similar morphology. All the fault zones are highly fractured and sheared in the centre with the intensity of deformation decreasing laterally. Table 3.1 records field observations of the approximate widths of the fault zones.

A typical section across any of the faults is exposed where the North Branch Waipara River cuts across the Tommys Stream Fault (M33/682093). The fault contact between the cover rocks of the foot wall and the basement rocks of the hanging wall, is the zone of greatest deformation. In this zone phacoids of basement commonly occur in pugs derived from the shearing of the basement and occasionally from cover rock faulted into the basement. Slickenside striations developed on the phacoids exhibit strike-slip, oblique-slip and dip-slip movements suggesting many of the phacoids have undergone rotation. Away from the fault contact the intensity of the fracturing and shearing decreases, as does the width and occurrence of fault derived pugs. Although all the faults show similar characteristics, some warrant separate discussion.

3.2.1. Tommys Stream and Waitohi Downs Faults.

The Tommys Stream and Waitohi Downs Faults are laterally the most extensive of the major faults along the basin margin. The Waitohi Downs Fault can be traced to the SW of this study area and may continue SW into the upper reaches of the Okuku River and North Branch Waipara River. South of the Hurunui River both the Waitohi Downs and Tommys Stream Faults strike obliquely to the N-S striking western range front of the Culverden Basin. North of the Hurunui River the range front is parallel to the Waitohi Downs and Green Hill Faults, the latter being a possible continuation of the Tommys Stream Fault.

The large westard jog in the Waitohi Downs Fault where the Hurunui River runs into the Culverden Basin suggests the presence of some sort of structural high to the east of the fault. The thickness of the cover rocks, in particular the Kowai Formation (1.6km, from Green Hill), and gravity anomalies indicate that this area should in fact be a structural low. It may be that the jog is simply a wobble in the fault, however, the jog coincides with the N-S strike of the range front of the Culverden Basin. From the landsat image (Figure 1.2) the N-S lineament of the range front continues south of this study area to the Mid-Waipara region and north through the Mandamus River valley to the juction of the Kakapo and Hope Faults. This lineament may delineate a structurally weak zone in the Torlesse Supergroup basement rocks which has been

exploited, perhaps not only by the Waitohi Downs Fault, but also by the Mandamus Igneous Complex. The change in modal elevation across this lineament suggests that the western side may have been upthrown (Mason, 1949).

3.2.2. Island Hills Fault.

The Island Hills Fault is atypical of the faulting in this study area in that it dips southeast. The fault is, however, more in keeping with the west verging macroscopic faulting that occurs to the east from the Lower Waipara region to the Cheviot Basin in the north. The Island Hills Fault thrusts basement rocks of the Mandamus Igneous Complex and Torlesse Supergroup over the steepened limb of a syncline developed in the cover rocks. Secondary shearing associated with the fault extends back into the hangingwall, partially obscuring the primary relationship between the intrusive and extrusive rocks of the Mandamus Igneous Complex and the preservation of Cretaceous fracturing associated with intrusion.

There is debate (Tulloch 1991; Weaver and Pankhurst 1991) as to whether the contact between the syenite and trachyte of the Mandamus Igneous Complex is intrusive or fault controlled. Observations of numerous mesofaults, along the continuously well exposed banks of the Mandamus River, and small intrusive inclusions of syenite in the trachyte indicate the contact is not simply intrusive or fault controlled. Rather, it is a combination of small movements on numerous mesofaults associated with localized intrusion of the syenite into the trachyte. The relationship of the Island Hills Fault and the other the faults of this study to regional faulting is discussed in Chapter 6.

3.2.3. Hurunui Fault.

The WNW-NW striking Hurunui Fault is approximately orthogonal to, and has moved synchronously with, the NNE-NE striking, late Cenozoic Island Hills and Waitohi Downs Faults. The age of initial movement on the fault is difficult to determine from field evidence, the fault may have formed during late Cenozoic deformation or it may be a Late Cretaceous fault that has been reactivated in the late Cenozoic.

Much of the New Zealand continent was subjected to regional extension in the Late Cretaceous (Laird, 1981; Bradshaw, 1989). Fault bounded half grabens trending ENE to ESE on the Chatham Rise (Lewis et al., 1985; Browne & Field, 1988) and minor E-ESE trending faults and veins in the basement and E-ESE faults in the cover rocks of the mid-Waipara region (Nicol, 1991) have been attributed to this Late Cretaceous tectonism. The Hurunui Fault may have been normal in the Late Cretaceous with the NE block having been downthrown. This is suggested by the conglomeratic texture and wedge shape of the Late Cretaceous Broken River Formation, which is preserved on the relatively downthrown NE block but is absent on the relatively upthrown SW side. If this is so, the fault has provided a weak zone in the basement which has been exploited and reactivated in the present orogeny.

The narrow width of the fault zone (30m), which contains numerous oblique-slip and dip-slip striations, suggests that the Hurunui Fault may only have been initiated during the present orogeny. The lack of exposure of the areas where the Island Hills and Waitohi Downs fault may intersect the Hurunui Fault results in conjecture as to the relative age of the Hurunui Fault. If these sites were exposed the age relationships of the faults could be determined. Whatever the cross cutting relationships the Hurunui Fault has been and is active in the present orogeny.

3.2.4. Balmoral Fault.

The Balmoral Fault is a recently active, thrust-reverse fault that obliquely offsets Quaternary gravels. The fault strikes N to the SE corner of Green Hill where the trace is lost but may do one of two things:

i). the fault may abut against the inferred WNW striking fault at the southern edge of Green Hill or

ii). the fault continues, becoming bedding parallel and striking NNE, along the eastern edge of Green Hill.

The second scenario is preferred as exposure of the cover rocks that form Green Hill does not continue east of the strike of the Balmoral Fault suggesting the WNW striking fault may abut against the Balmoral Fault.

3.2.5. Kanuku Hills Faults.

A strike ridge in the cover sequence at Kanuku Hills is apparently dextrally offset by three macroscopic, vertically dipping, normal faults. The macroscopic faults are not exposed, but their presence and strike can be determined from field evidence and numerous small-scale faults in the cover rocks. The bedding of each of the offset blocks of the strike ridge is overturned and dips WSW. The southernmost offset block has a mean overturned dip of 68°, the middle block, 70°, and the northern block a mean dip of 80°. The overturned dips of the blocks is a manifestation of their proximity to the east verging thrusting of the nearby Waitohi Downs Fault (Figure 3.1). Small-scale faults on the blocks predominantly indicate normal slip motions with a minor population of oblique-normal faults. The progressive steepening of dip in the fault bounded blocks indicates that this is accompanied by block rotation. Stress tensor, movement plane and P and T-axes analysis (Chapter 4) of the small-scale faults supports the field evidence of normal faulting.

The apparent offset of the blocks is attributed to the variation in dip of the marker unit as the blocks undergo local NW extension and NE compression. The extension must post date the Oligocene to Miocene formations in which the normal faults have formed. Futhermore, the variation in dip and the resulting apparent dextral offset of the blocks suggest that the macroscopic normal faults at Kanuku Hills developed synchronously due to oblique reverse movement associated with the late Pliocene-Pleistocene compressional Waitohi Downs Fault.

3.2.6. Taruna Fault.

Taruna Fault is proposed for the unnamed WNW-ESE striking macroscopic fault to the NE of Mt. Mason that was first recognised by Bradshaw (1972). At the eastern most exposure of the fault the fault plane dips 15° NNE while closer to the Waitohi Downs Fault, which the Taruna Fault appears to abut, the fault dips moderately N. Kinematic analysis of the slickenside striated mesofaults developed in the volcanogenic facies of the Torlesse Supergroup at the ESE end of the Taruna Fault (Figure 3.2) indicates that the last movement on the low angle fault was oblique reverse.

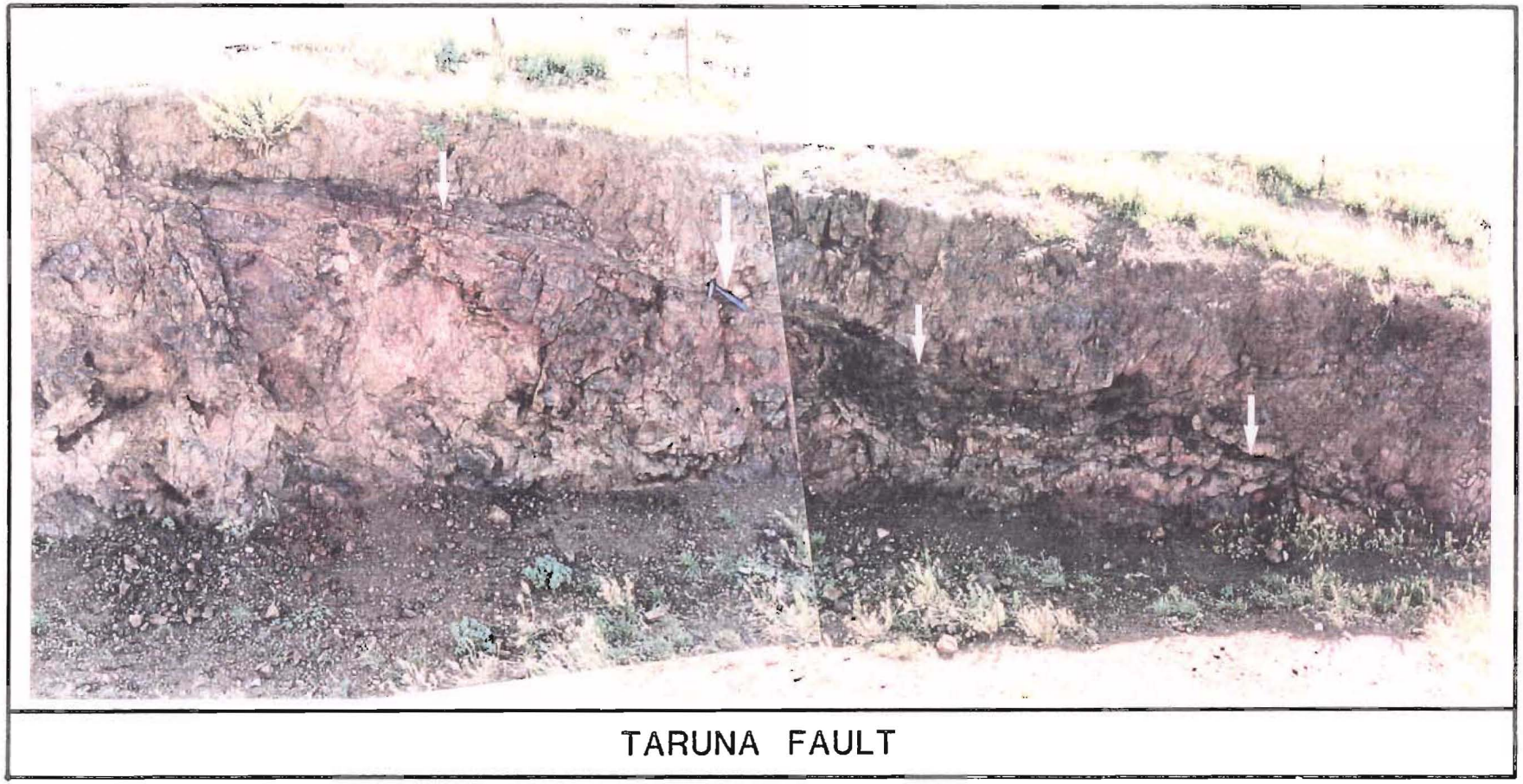

Figure 3.2. A view, northwest, of the Taruna Fault at its eastern most exposure. The fault is a low angle thrust that stikes WNW (note hammer for scale on the main fault plane).

3.3. SMALL-SCALE FAULTING.

The arbitrary separation of mesofaults from macrofaults is taken at a maximum displacement of about 5m and a maximum fault plane area of about $1000m^2$ (Hancock, 1985). Mesoscale faults are developed in both the cover and basement rocks in this study area.

In the field four types of slickenside striated mesoscale faults are found in the basement rocks: (1) a bedding parallel set that appears to be related to deformation in the Mesozoic; (2) a set at Island Hills that strikes in the NE-SW quadrants and is related to the Late Cretaceous emplacement of the Mandamus Igneous Complex; (3) an approximately NNW-SSE set that is oblique to the general NW strike of the Torlesse basement and which is commonly developed along calcite, laumontite, and quartz veins, possibly related to an inferred phase of Late Cretaceous, approximate N-S regional extension (Browne & Field, 1988); (4) the final set are developed in close proximity to, and in, the fault zones of the macroscopic faults.

Wherever possible type 1 and 2 mesofaults were excluded from the main population of faults prior to analysis but types 3 and 4 faults can rarely be distinguished and thus the data includes all four types of faults for kinematic analysis (Chapter 4).

Mesofaults within the cover sequence occur predominantly within the Tekoa Formation, Flaxdown Limestone Member, Mt. Brown Formation and occasionally continue into the overlying and underlying units. Displacements on the mesofaults, measured from either offset bedding or movement indicators, such as calcite fibre lineations or slickenside striations, range from 0.5-1cm to 3-4m. Narrow 1-20cm zones of brecciation, polishing, mineralization (calcite veins) or pressure solution are associated with these mesofaults. Two types have been recognised: (1) a widespread set of dip-slip faults parallel to sub-parallel with bedding and which have formed from movements associated with flexural folding, and (2) an orthogonal set of predominantly dip-slip to oblique dip-slip faults and minor lateral faults that are associated with the macroscopic faults.

The small-scale faults vary in geometry and several pronounced faulting styles are evident. Poles to fault planes for all small-scale faults within the basement and cover rocks have been divided into eight areas (Figure 3.3). The diagram exhibits a predominance of ENE-NE and NW-NNW faults. ENE-NE striking faults dominate the Kanuku Hills, Waitohi Downs, Flaxdown Quarry, and Waitohi River areas. Island Hills has a significant number of ENE-NE and NW-NNW faults of equal prominence. The Hurunui and Mt. Mason areas, as well as a significant number of faults at Flaxdown Quarry, show a NW-NNW orientation.

Four groups emerge from the total (basement and cover) fault population (Figures 3.3 & 3.4). These are: (1) approximately NE and NW striking, moderately to steeply dipping, oblique-reverse to reverse faults, (2) approximately NE striking, moderately-steeply dipping, oblique-normal to normal faults, (3) WNW-NNW striking, moderately-steeply dipping oblique normal-normal faults, and (4) WNW-NNW striking, gently to steeply dipping, lateral faults. In Figures 3.3 and 3.4 dip-slip faults are characterised by movement vectors oriented at 60° or more to the fault strike; oblique-slip faults have a motion vector striking between 30°-60° to the fault strike while lateral faults have motion vectors trending at less than 30° to the fault strike.

Oblique-reverse, reverse and oblique-normal faults were collected in approximately equal proportions while twice as many normal faults were recorded and left lateral were slightly more abundant than right. Avouca et al. (1992) have documented the growth of normal faults in the cover rocks that form fault-propagated folds associated with the El Asnam Thrust of North Africa. Oblique-reverse, reverse and normal movements are predominantly associated with the NE-ENE faults (Figure 3.4). Small-scale normal and oblique-normal faulting occurs at Flaxdown Quarry, Island Hills and Kanuku Hills (Figure 3.3). Oblique-reverse and reverse faults that strike NE-ENE occur in the Island Hills and Waitohi Downs areas. The change in the predominant movement sense on the NE-ENE faults from area to area is indicative of local strain partitioning, the style of strain being a manifestation of the movement sense on the nearby macroscopic faults.

Figure 3.3. Fault map showing the orientation and distribution of the major faults (labelled). Fault dip directions are indicated by the thrust teeth (for dips see main map in the Map Pocket). Lower hemisphere equal area nets display orientation and distribution of poles to fault planes for reverse, oblique-reverse, normal, oblique- normal and right and left lateral faults within basement and cover rocks.

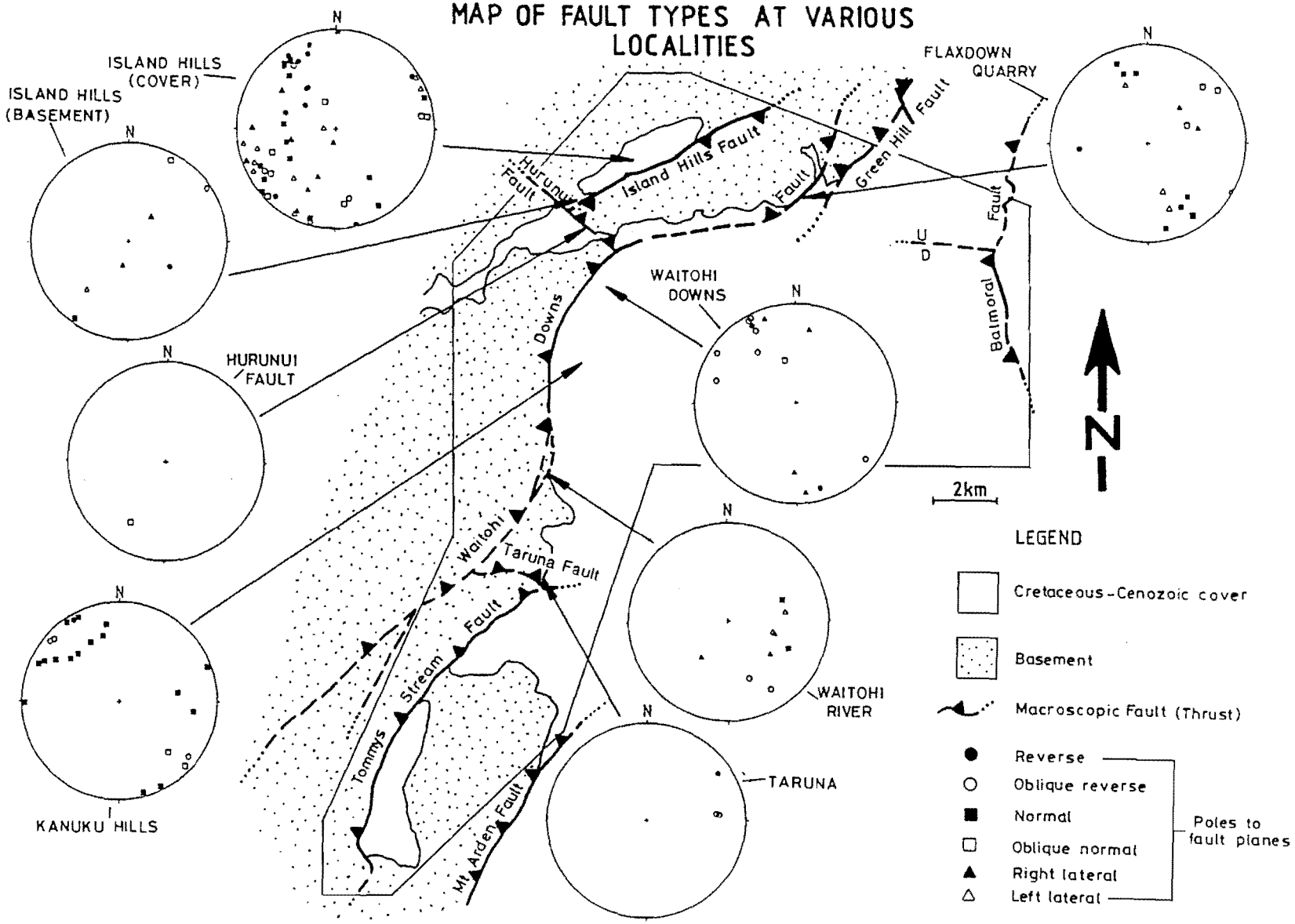
MAP OF FAULT TYPES AT VARIOUS LOCALITIES
ISLAND HILLS (COVER)
ISLAND HILLS (BASEMENT)
HURUNUI FAULT
KANUKU HILLS
FLAXDOWN QUARRY
WAITOHI DOWNS
WAITOHI RIVER
TARUNA
Hurunui Fault
Island Hills Fault
Green Hill Fault
Fault
Downs
Balmoral
U
D
Waitohi
Taruna Fault
Fault
Stream
Tommys
Mt Arden Fault
2km
N
LEGEND
Cretaceous-Cenozoic cover
Basement
Macroscopic Fault (Thrust)
Reverse
Oblique reverse
Normal
Oblique normal
Right lateral
Left lateral
Poles to fault planes

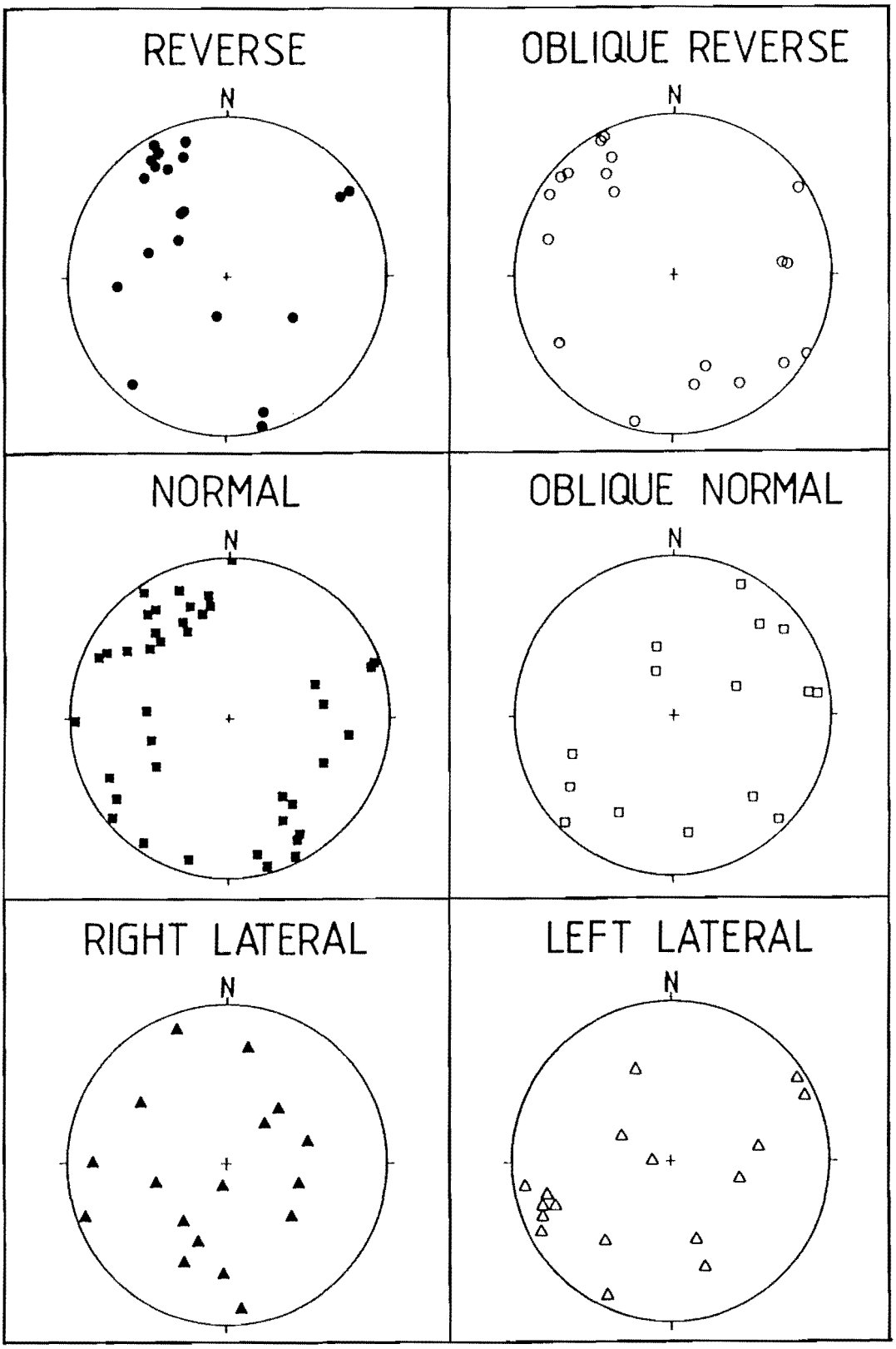

FAULT TYPE ORIENTATIONS - ALL FAULTS

Figure 3.4. Lower hemisphere equal area nets of poles to reverse, oblique-reverse (top), normal, oblique-normal (middle) and lateral faults (bottom) on which a motion sense could be determined from the entire study area.

The timing of generation of the mesofaults in the cover sequence will be discussed in Section 3.8.4.

3.4. MACROSCOPIC FOLDING.

Folding is the most common macroscopic manifestation of deformation in the basement and cover rocks in North Canterbury. At least two sets of folds are present in the basement and pre-date the development of the Cretaceous unconformity. Although the existence of folding in the cover sequence in this study area was recognised over 120 years ago (Hutton, 1871), fold interference was not. The fold patterns, apparent in only the late Cretaceous-Cenozoic cover rocks are complex and associated with two fold sets orientated perpendicular to each other. These folds commonly strike NNE-SSW and ESE-WNW producing non-classical and irregular (Ramsay, 1962) basin and dome fold interference.

3.4.1. Basement Folding.

Bedding within in the Torlesse basement commonly dips steeply, with strikes predominatly in the NW quadrant (Map 1). At least two sets of folds are present, one a late Mesozoic, NE, trending set of macroscopic rounded flexures and an earlier set of NW-SE trending macroscopic folds (Bradshaw, 1972). The evidence for the earlier folds is of four types: mesoscopic folds, megascopic fold hinges, the relationship of fossil localities and younging directions, and stratiform belts of cataclastic rock (Bradshaw, 1972). The mesoscopic folds associated with the earlier fold set commonly plunge moderately-steeply towards the NW and SE quadrants. These folds are generally close with rounded to acute fold hinges and are either conical with steeply plunging axes or cylindrical. The younger rounded macroscopic folds appear to have warped the earlier folds that are responsible for the general NW strike of the Torlesse basement.

3.4.2. Cover Sequence Folding.

Macroscopic folding is the most common manifestation of late Cenozoic deformation in this study area and is preserved in the late Cretaceous-Cenozoic cover sequence.

Three macroscopic synclines (Table 3.2) are developed along the western margin of the Culverden Basin with a fourth syncline to the west of the basin at Island Hills (Figure 3.5). These folds are non-cylindrical, asymmetric and reflect fold interference patterns. A fifth syncline, the Green Hill Syncline, lies on the northern edge of the study area, only the southern poorly exposed third of this syncline was mapped. A sixth, and only partially exposed, syncline is preserved at Flaxdown Quarry. Only two macroscopic anticlines are preserved, one at Mt. Hilton and the other at Flaxdown Quarry. Early Miocene strata form an inlier, Hurunui Mound, in the Quaternary gravels of the Culverden Plain. Exposure of bedding in the Mt. Brown Formation is limited to a section along the north bank of the Hurunui River and along the railway and road cutting. The limited bedding data collected, however, indicates a syncline-anticline-syncline train of folds from east to west (Figure 3.6).

All the macroscopic folds trend parallel to sub-parallel with nearby macroscopic faults (Figure 3.5), and generally plunge gently N to ENE or SSW-SW. The axial planes are always steeply dipping in the same direction as the dip of the nearby macroscopic faults (see cross sections in map pocket). Generally the hinge shape is angular and the fold tightness close near the macroscopic faults broadening to sub-rounded and open, respectively, with greater distances from the faults. The folds are always asymmetric with the limb closest to the fault being the steepest and occasionally being overturned. Fold geometry typically comprises composite partial conical sections although the steepest limbs may appear straight when the limb is near vertical.

The cross sections, whenever possible, have been constructed perpendicular to the axial traces of the macroscopic folds and the strike of macroscopic faults so as to illustrate the folds in profile views. In the unexposed hinge zones of the folds the author has generally retained constant bed thicknesses for the cover rocks, thus the shapes of the folds are interpretive. Competent units, such as the Flaxdown Limestones Member of the Omihi Formation, are likely to deform in this manner. However, less competent units like the Tekoa Tuff Formation may well be deformed such that the

TABLE 3.2. Description of macroscopic folds.

NAME OF FOLD	AXIAL TRACE ORIENTATION (STRIKE & DIP)	AXIAL PLANE ORIENTATION	AXIAL TRACE LENGTH	HINGE SHAPE	FOLD TIGHTNESS	LIMB SHAPE	LIMB DIPS
TOMMYS STREAM SYNCLINE	NNE & SSW 06° SSW & gently NNE	SSW/steep	4.8km	Angular?	Open?	Conical	15-35°
MT. HILTON ANTICLINE	015° & SSW 026° NNE & gently SSW	205°/75-80°	7.5km +	Sub-angular-sub-rounded	Open	Conical?	?
MT. MASON SYNCLINE	035-048° 12-20° NNE-NE	215-228°/ 70-75°	3.7km +	Angular-sub-angular	Close-open	Straight (NW limb) Conical (SE limb)	81-22°
WAITOHI DOWNS SYNCLINE	005-067° 10-25° N-ENE	185-247°/ 60-80°	5.0km +	Angular-sub-rounded	Close-open	Conical	39-83°
ISLAND HILLS SYNCLINE	040 & 246° 07-15° SW & 05° NE	040°/75-80°	3.0km	Sub-angular	Close-open	Conical	42-87°
GREEN HILL SYNCLINE	209° steeply-gently	209°/70-85°	5.0km +	Sub-angular-angular	Close?	Conical?	27°-?
HURUNUI MOUND INLIER FOLDS	230-244° gently SW	SW/steep	0.7km +	Sub-angular-sub-rounded	Close-open	Conical?	09-72°
FLAXDOWN QUARRY SYNCLINE	SSW gently SSW	SSW/steep	1.0km +	?	?	?	64-85°
FLAXDOWN QUARRY ANTICLINE	SSW moderately-gently SSW	198°/75-80°	2.0km +	Sub-angular	Close	Conical?	?

Figure 3.5. Location map of the major macroscopic folds (labelled) in relation to the major faults (unlabelled, see Figure 3.1) developed from late Cenozoic deformation along the western margin of the Culverden Basin.

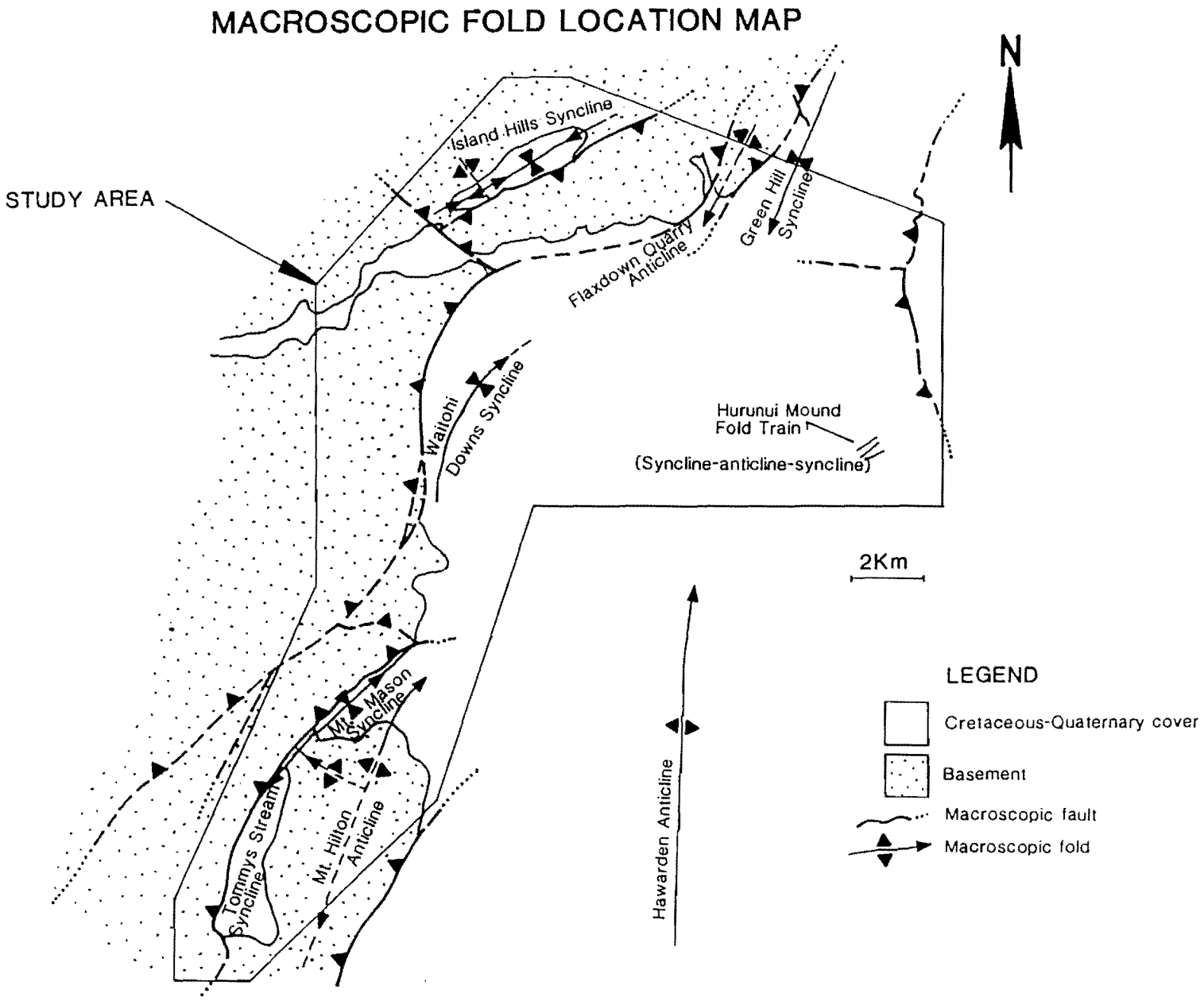
MACROSCOPIC FOLD LOCATION MAP
STUDY AREA
N
Island Hills Syncline
Green Hill Syncline
Flaxdown Quarry Anticline
Waitohi Downs Syncline
Hurunui Mound Fold Train
(Syncline-anticline-syncline)
2Km
Mt. Mason Syncline
Tommys Stream Syncline
Mt. Hilton Anticline
Hawarden Anticline
LEGEND
Cretaceous-Quaternary cover
Basement
Macroscopic fault
Macroscopic fold

Figure 3.6. A schematic cross section through the Hurunui Mound Inlier, using exposure in the norhteast bank of the Hurunui River. Form lines are derived from marker horizons in the Mt. Brown Formation.

CROSS SECTION OF HURUNUI MOUND INLIER

Scale 1:3,125

Vertical = Horizontal

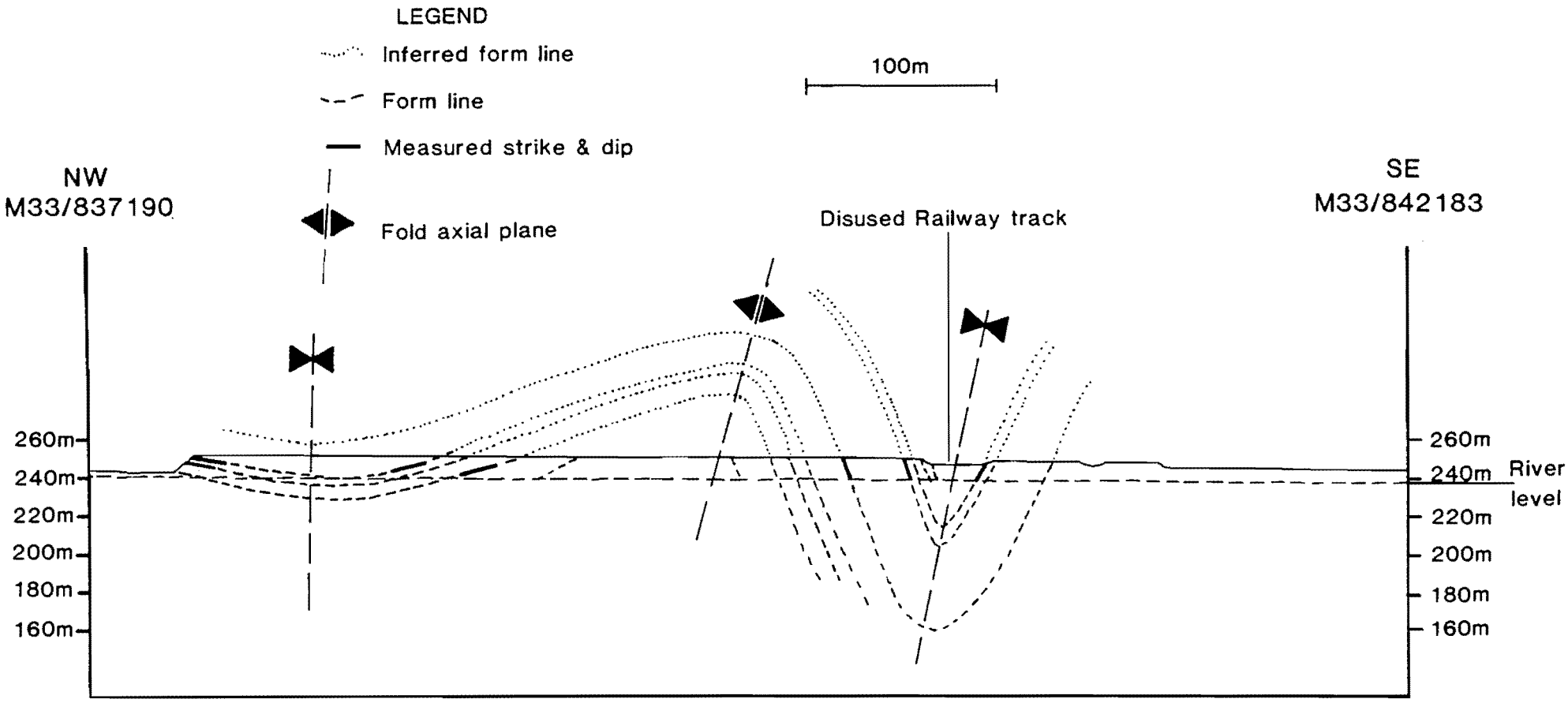

folded unit increases unit thickness in the hinge zones and this may modify the profiles from those shown. A further assumption with regard to the cross sections is that the conglomerates and volcanic beds of the Torlesse Supergroup wedge out with depth. This was done because the author found the conglomerates and volcanics to be lensoidal in lateral extent and because no field evidence was found to control their geometry at depth.

3.5 CONICAL FOLDS RESULTING FROM BASIN AND DOME FOLD INTERFERENCE

Conical folds are one member of a larger group of non-cylindrical folds which are distinctive in that they are easy to define geometrically with the aid of equal area stereographic projections. A conical fold is defined by a mathematical cone and must have a geometric axis which is oblique to the conical surface (Figure 3.7), (Stauffer, 1964; Systra & Skornyakova, 1980). The inclination of the cone axis and the angle between the axis and the cone surface, half the apical angle of the cone, are used to define the orientation and curvature of a conical fold.

Conical folds commonly form in two environments: 1) at the termination of a cylindrical fold (Webb & Lawrence, 1986), and 2) as a result of fold interference (Systra & Skornyakova, 1980). It is commonly acknowledged that conical folds develop in association with fold interference (Ramsay, 1962; Systra & Skornyakova, 1980), however, not all fold interference patterns are defined by conical folds (Stauffer, 1988; Nicol, 1991 & 1992). Many of the techniques developed and used by Nicol (1991 & 1992) have been applicable to analysing the development and kinematics of the structures, in particular the folding, in this study area. In this section it will be documented that macroscopic folds in the western Culverden Basin are defined by more than one cone; a consequence of the variations in development of the interfering fold sets.

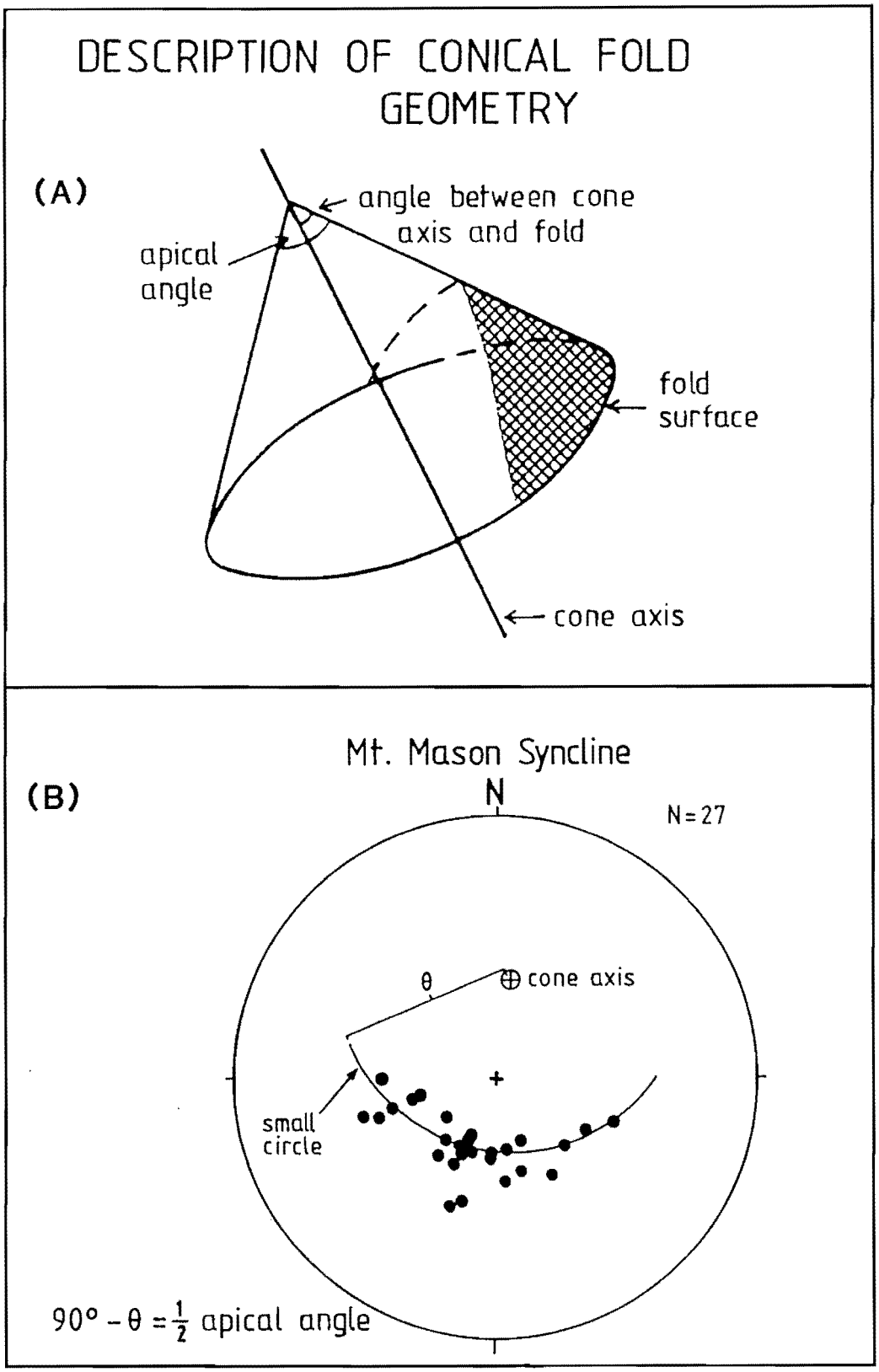

Figure 3.7. Geometric description of conical fold surfaces. A) Diagramatic sketch of cone shape and geometric elements, including cone axis and apical angle. (After Nicol, in press). B) The same elements represented in lower hemisphere equal area plot of poles to bedding for the Mt. Mason Syncline.

3.5.1. Cone Geometries

The Tommys Stream, Mt. Mason, Waitohi Downs and Island Hills Synclines have been divided into sub-areas each of which was analysed, by plotting poles to the fold surface (bedding) on an equal area net, for the presence of conical fold surfaces. Table 3.3 is a summary of the conical fold geometries found in the four macroscopic synclines.

The Island Hills Syncline has moderately inclined cone axes and small (30-60°) apical angles. The other areas are all characterised by steeply inclined cone axes with moderate (60-100°) and large (100-130°) apical angles. The variations in conical fold geometry occur both across and along the interfering fold sets as a consequence of changes in fold tightness, hinge zone angularity, and limb dips. Fold tightness and hinge zone angularity affect the cone shapes in this study area and are discussed below. The effect of changes in limb dips on the folds in this study area have been indeterminable due to lack of exposure. In general, however, if an upright fold with variable limb dips is subjected to interference folding each limb will be defined by cones with different geometries. Provided the cone axis remains steep and as the limb dips increase, the apical angle of a conical fold surface will decrease.

3.5.2. Fold Tightness

The ratio of fold wavelength to amplitude of the two interfering fold sets, and the subsequent tightness of the fold sets, which affect the geometry of the conical folds have been estimated from cross sections constructed perpendicular to the fold axes. With different combinations of fold set interlimb angles changes in cone geometry occur. Nicol (1991) has found in the mid-Waipara region, that only if both fold sets are upright and have similar interlimb angles do the resulting cones have an apical angle approximately equal to the interlimb angles, with a steep cone axis and circular cross section (Figure 3.8. cones 1,5,8 and 10). Increases in the wavelength to amplitude ratio (i.e. increases in interlimb angles) results in increases of the apical angle.

Where the fold dimensions are different, such as the Island Hills and Mt. Mason Synclines, the subsequent cones are flattened with an elliptical cross section

TABLE 3.3. Summary of all conical fold data and fold set interlimb angles for the Tommys Stream to Island Hills areas. All numbers represent the mean, in degrees, for the subareas of Figures 3.10., 3.11., and 3.13.

FOLD NAME	Cone axis plunge	Cone and fold axis angular separation	Apical angle	Interlimb angle (Fold set 1)	Interlimb angle (Fold set 2)
Tommys Stream Syncline	80°	45°	148°	?	132°
Mount Mason Syncline	59°	43°	72°	74°	144°
Waitohi Downs Syncline	69°	50°	67°	49-91°	?
Island Hills Syncline	42°	31°	41°	58°	135°

Figure 3.8. Predicted changes in the geometry of conical folds produced by changes in the tightness of the interfering fold sets. These changes in the fold set interlimb angles are inferred for areas of basin and dome fold interference where fold limb dips are equal. Hinge zone curvature effects are neglected. (After Nicol, in press).

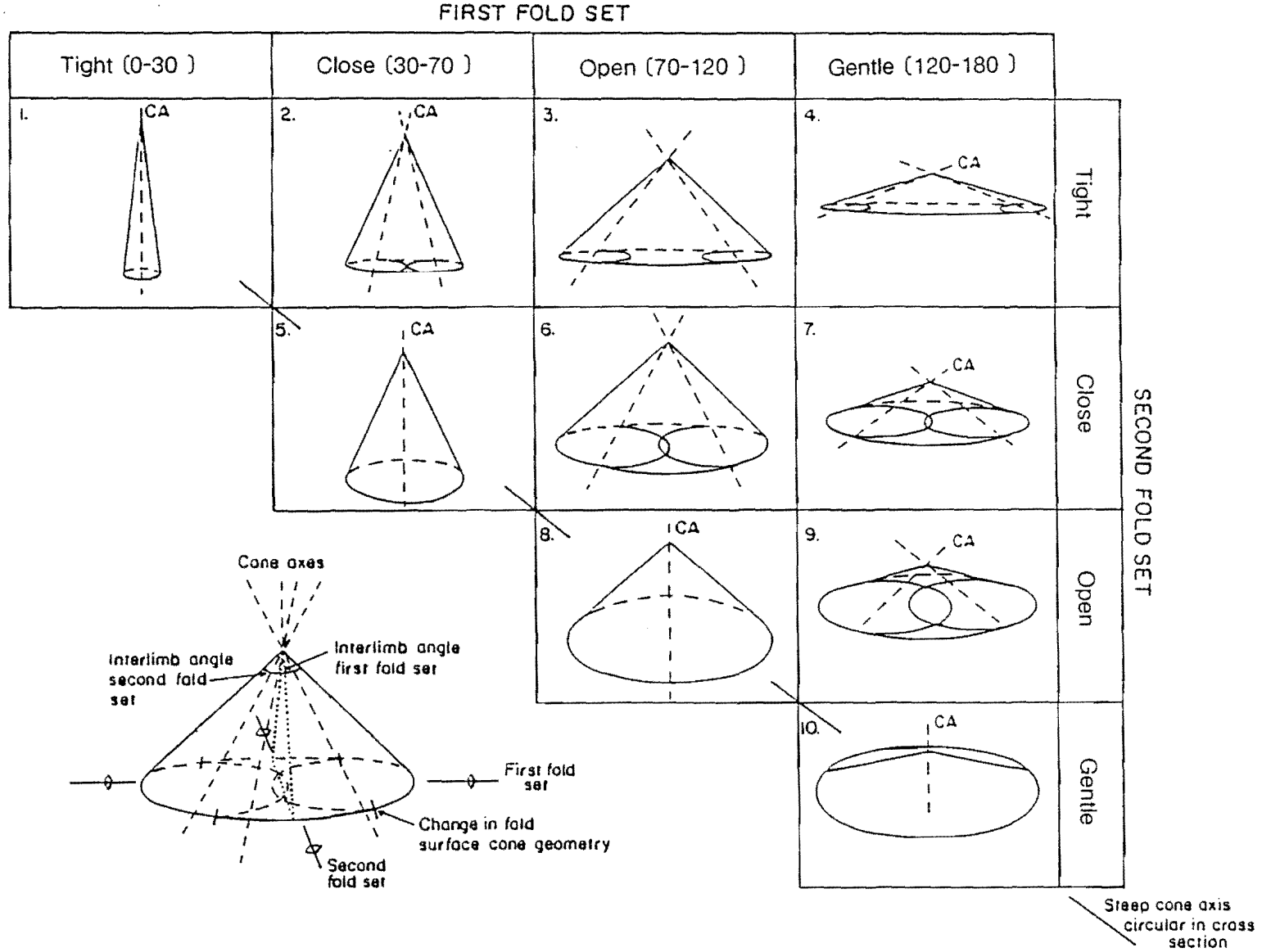

INTERFERING FOLD SET TIGHTNESS AND CHANGES IN CONE GEOMETRY

perpendicular to the trend of the tightest fold set. The amount of flattening increases with greater differences in fold set interlimb angles (Nicol 1991) (Figure 3.8). Once the cone becomes flattened the fold surface cannot be defined by a single cone. Several partial cone surfaces with increasingly inclined axes, particularly the two axes parallel to the axial surface of the tightest fold set, will best describe the flattened cone. Furthermore, as the interlimb angle of one fold tends towards zero or 180°, the second fold set becomes approximately cylindrical. The Mt. Mason Syncline is best defined by a flattened cone similiar to that of type 9 in Figure 3.8. The Island Hills Syncline is best defined by a slightly more flattened cone, type 7, due to the larger differences in the interlimb angles than at Mt. Mason.

3.5.3. Hinge Zone Curvature.

The effects of hinge zone curvature on cone geometry are often difficult to determine because the hinge zones are commonly not exposed to the same extent as the fold limbs. This commonly results in more data being collected from the limbs than the hinge zones. The hinges zone of the macroscopic folds in this study area, other than in the Mt. Mason and Waitohi Downs Synclines, are poorly exposed. The best exposure of the hinge zone from the Mt. Mason Syncline, were found on the limb of the interfering fold set.

Frequently the interference of two folds at a high angle to each other results in a flattening of the fold surface into basin and onto dome structures. Figure 3.9 illustrates the predicted change in distribution of poles to the fold surface (normally bedding) and cone geometry, into a rounded, fold interference basin. A decrease in limb dip towards a basin or dome produces an increase in the apical angle which describes the fold surface (heavy line in Figure 3.9A). Similarly, as the limb dips decrease so does the diameter of the small circle that represents the cone. The apical angle for rounded folds must continually change to house the curvature of the fold surface. The angular folds in the mid-Waipara (Nicol, 1992) region and the Mt. Mason Syncline of this study, are easier to describe as only one or two cones (Figure 3.10) are required to define the fold surfaces.

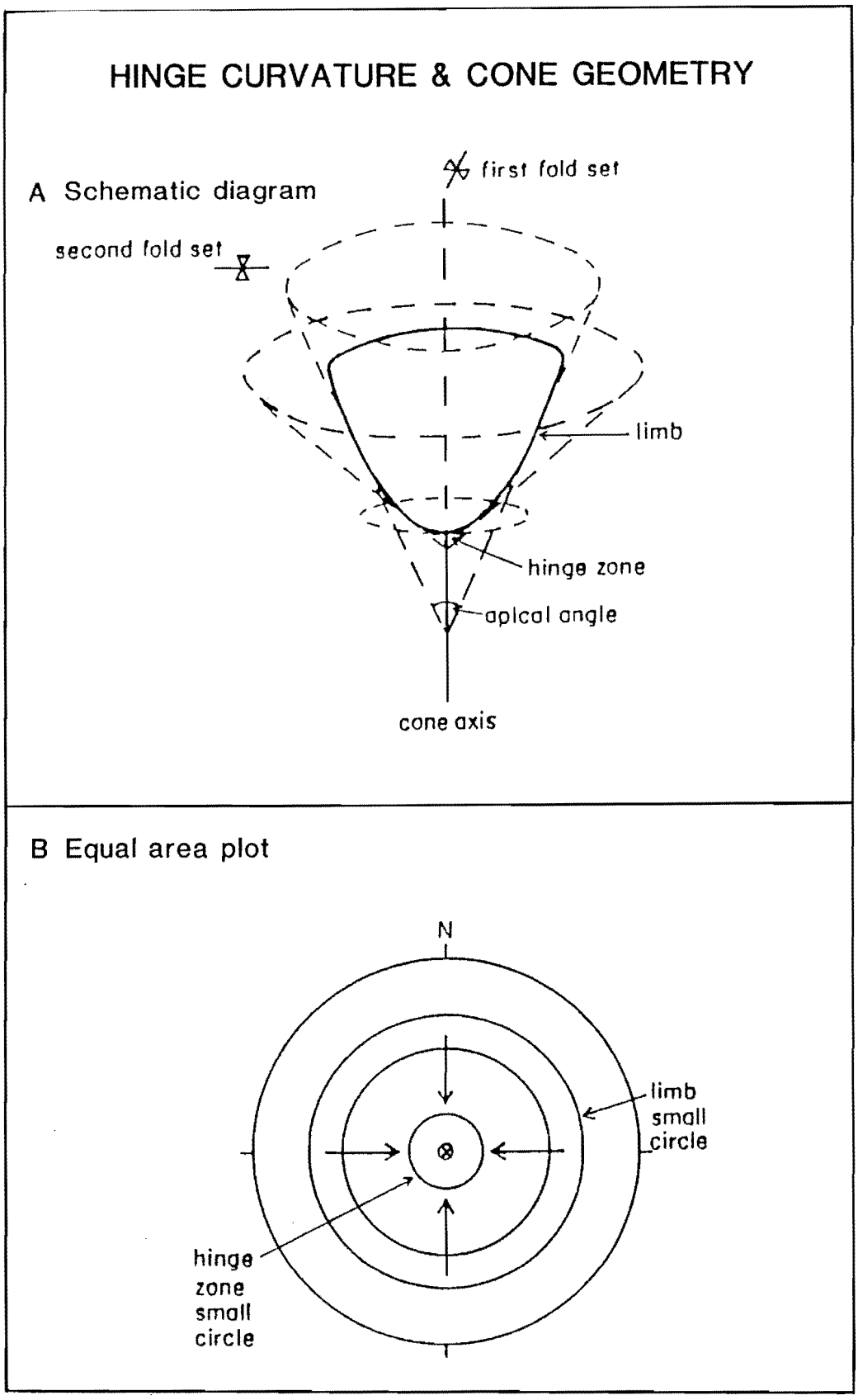

Figure 3.9. Schematic diagram and lower hemishere equal area plot demonstrating the expected changes in cone geometry into fold interference basin structures. The arrows on the equal area net indicate the reduction in small circle size into the basin. (After Nicol, in press).

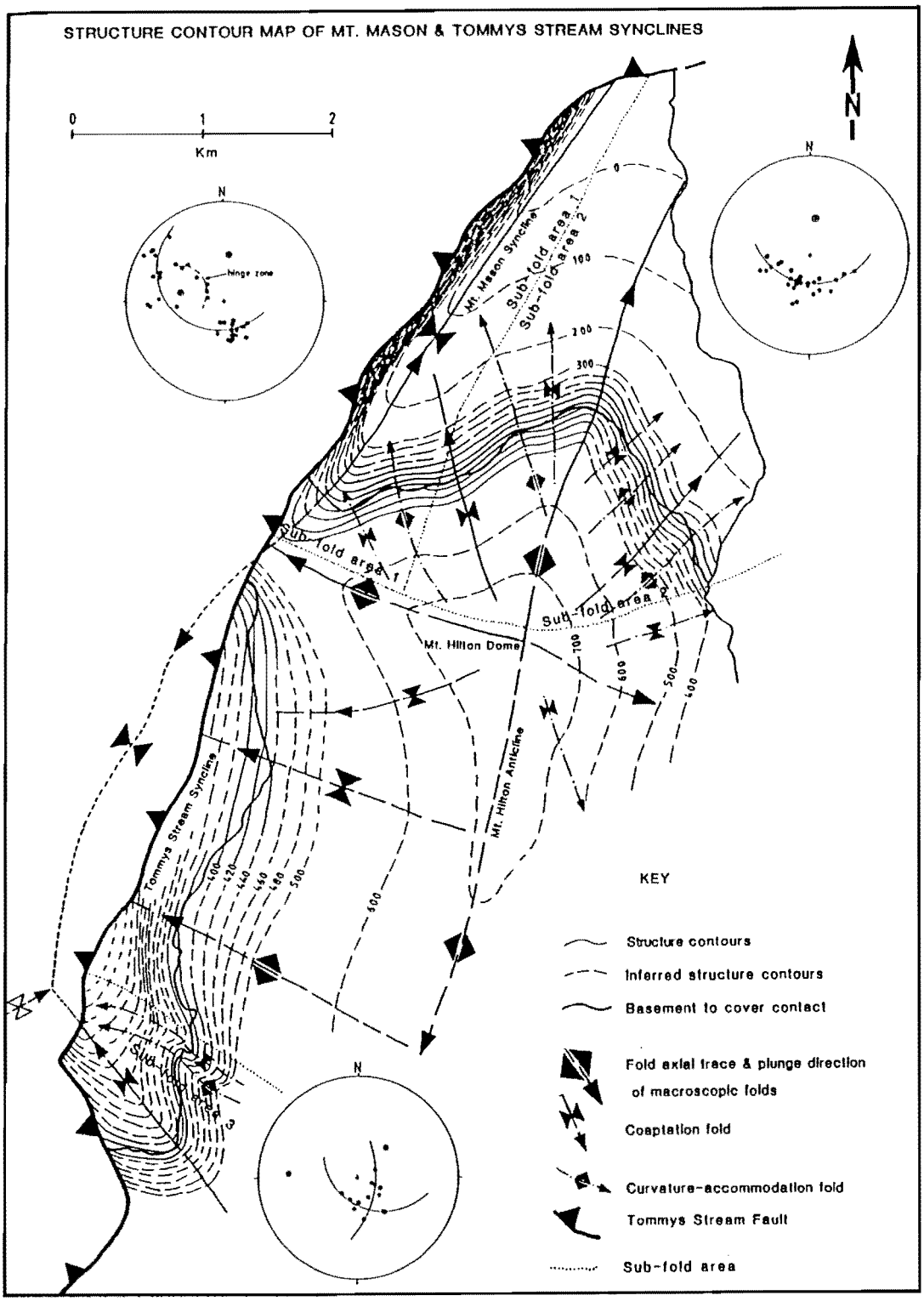

Figure 3.10. Structure contour map and lower hemisphere equal area nets displaying changes in fold interference cone geometries along the Tommys Stream and Mt. Mason Synclines and the Mt. Hilton Anticline, North Canterbury. Structure contours are drawn on the basement to cover unconformity surface. Poles to bedding of cover rocks are presented on the equal area nets. Also represented are the coaptation and curvature-accommodation folds that strike obliquely to the main orthogonal fold axes.

The combined effects of fold interference may produce conical folds with geometries that are irregular and apparently non-conical. Conical fold shapes change both along and across the fold due to variations in the geometries of the interfering fold sets. The Island Hills Syncline, for example, exhibits changes in its fold surface geometry due to slight variations in the morphologies of the interfering fold sets (Figure 3.11). The fold geometry is defined by three cones with moderately inclined axes and small apical angles. Simple conical folds define the fold surfaces of the three sub-fold areas with the variations in cone geometry of the three sub-fold areas reflecting variations in fold tightness. The reduced apical angle of sub-fold area 2 (Figure 3.11) reflects the termination of the Flaxdown Limestone fold surface from which all the fold surface data was collected.

An equal area plot of the total bedding-pole data exhibits a distribution that is more scattered than the distributions for the individual sub fold areas. A similar trend is observed with fold surface data from the Waitohi Downs and Mt. Mason Synclines. The plots of total fold surface data are diffuse, and it is difficult to define a conical fold surface. It is therefore, advisable to divide the fold into sub fold areas which have a similar geometry. In this study the sub-fold areas have been defined by placing lines through the inflexion points of structure contours drawn on the fold surfaces of the interfering folds.

3.6. NON-CLASSICAL BASIN AND DOME FOLD INTERFERENCE.

The fold patterns, apparent only in the Late Cretaceous-Cenozoic cover rocks, are complex and associated with two fold sets orientated perpendicular to each other. These folds commonly strike NNE-SSW and ESE-WNW, interfering to produce basin and dome fold interference. The interference pattern is dissimilar to the classical interference patterns documented by Ramsay (1962, 1967), Thiessen and Means (1980) and Thiessen (1986). In this study fold interference is subtle and varies in geometry from area to area as a consequence of the effects of changing fold morphologies and topography.

Figure 3.11. Structure contour map and lower hemisphere equal area nets displaying changes in fold interference cone geometries along the Island Hills Syncline, North Canterbury. Structure contours are drawn on the basement to cover unconformity surface. Poles to bedding of cover rocks are presented on the equal area nets. Also represented are the coaptation folds that strike obliquely to the main orthogonal fold axes.

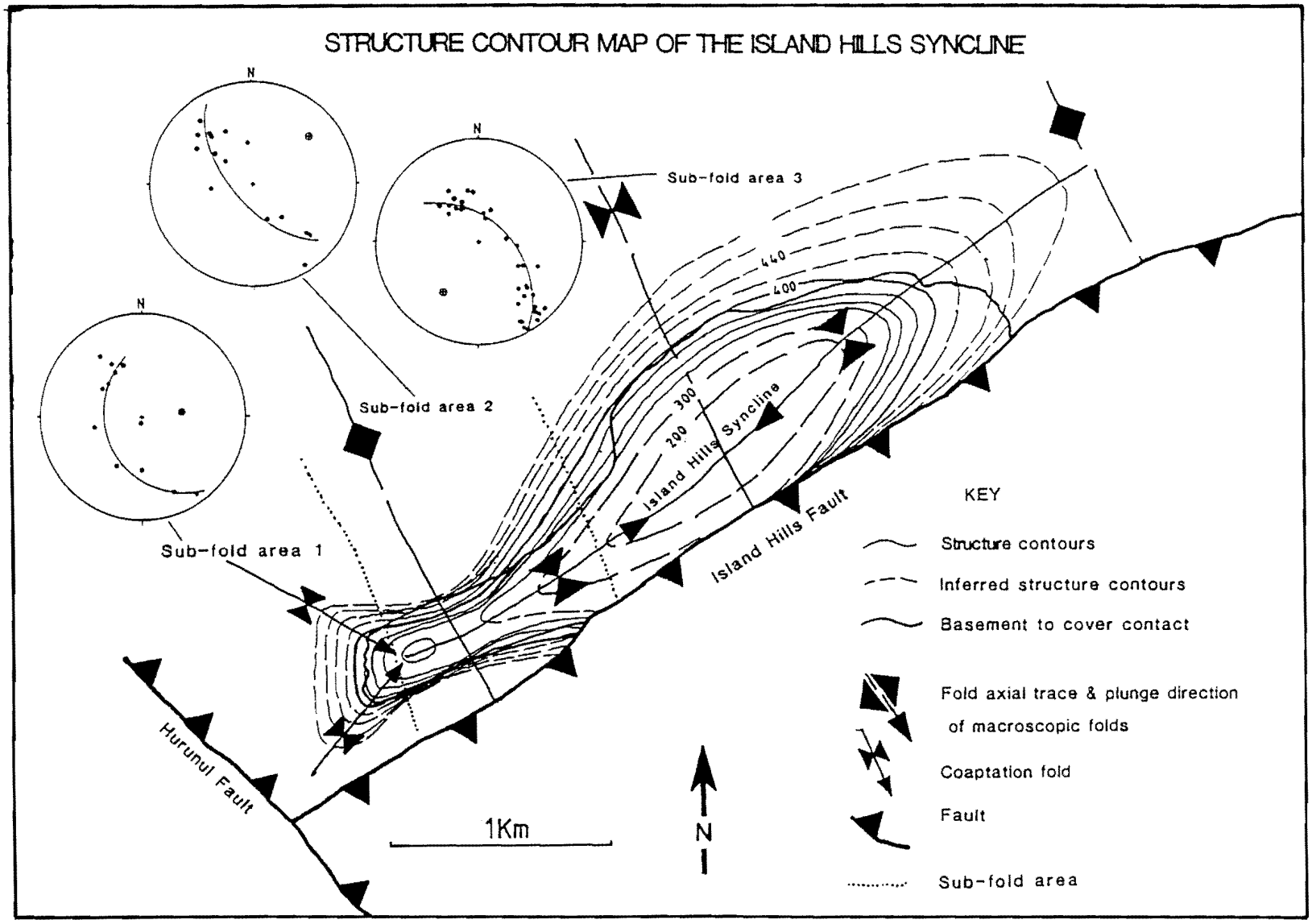
STRUCTURE CONTOUR MAP OF THE ISLAND HILLS SYNCLINE
N
N
N
Sub-fold area 1
Sub-fold area 2
Sub-fold area 3
440
400
300
200
Island Hills Syncline
Island Hills Fault
Hurunui Fault
1Km
N
KEY
Structure contours
Inferred structure contours
Basement to cover contact
Fold axial trace & plunge direction of macroscopic folds
Coaptation fold
Fault
Sub-fold area

3.6.1. Fold Morphologies.

As documented in Section 3.4.2, the N-NE macroscopic folds are the most prominently preserved of the two interfering fold sets. Both fold sets are mainly steeply inclined to upright, sub-horizontal to occasionally moderately plunging structures, with angular to sub-rounded hinges and rarely straight to mainly conical limbs. Fold amplitudes, estimated from cross sections constructed perpendicular to the fold axes, range between 0.5-2.4km. Commonly half fold wavelengths range between 1-3km, but reach up to 5km.

3.6.2. Interference Patterns.

Basin and dome structures are the classical product of two fold sets interfering. In this study area the interfering folds produce only partial basins and domes which are commonly poorly preserved and are only recognisable from detailed studies of bedding orientations. The irregular T-shaped Mt. Hilton dome is the most protuberant interference feature in this study area (Figure 3.10). Structure contours constructed on the Late Cretaceous unconformity surface (Figure 3.10) show the dome to be asymmetric to the NNE and to the ESE. Furthermore, Figure 3.10 shows that the dome is flanked by numerous secondary folds trending at various oblique angles to the two main NNE and WNW striking fold sets.

Dome and basin interference patterns are not limited solely to the Mt. Hilton area. At Island Hills fold interference patterns are defined by the basement-cover unconformity surface and the Flaxdown Limestone Member of the Omihi Formation. The interference pattern is characterised by changes in the fold axes orientations across interfering fold sets and by secondary folds developed oblique to the two main fold sets. Similar structures are developed in the cover sequence of the Waitohi Downs, Mt. Mason, Tommys Stream Synclines. Nicol (1991) has documented similar interference patterns to the SE in the mid Waipara region, while Bradshaw (1975) has found similar interference folding in the Castle Hill Basin.

Seven recurring interference features were noted from field work and construction of structure contours on the fold sufaces:

1). two sets of folds trending approximately NNE-SSW and WNW-ESE in the south of the study area changing to ENE-WSW and NNW-SSW in the north.

2). fold axes that mutually change orientations where the fold axes intersect.

3). conical fold surfaces.

4). corrugated hose shaped fold surfaces and outcrop patterns.

5). T-shaped, and triangular shaped fold surfaces.

6). secondary folds that commonly trend oblique to, and often bifurcate from, the troughs and crests of the basins and domes respectively.

7). folds that change their geometry along the hinge line in accordance with the position of the interfering fold sets.

The first two features are typical results of fold interference (Ramsay 1962, Wilson 1967). Conical fold surfaces are also commonly associated with fold interference (Ramsay, 1962; Wilson 1967, Systra & Skornyakova, 1980), and have been discussed earlier in this chapter. Field examples of the last four features are not well documented in the literature on fold interference, and so are given attention here.

3.6.2.1. Corrugated Hose Patterns.

Where interfering fold sets have different wavelengths and amplitudes and the folds trend at high angles to each other, corrugated hose fold interference patterns develop (Figure 3.12). The outcrop patterns of the interfering folds is dominated by the larger set of folds, with interference preserved as small warps on the steep limbs of the dominant fold set. The Waitohi Downs Syncline represents the best example of this type of interference pattern. The dominant N-ENE trending syncline has a half wavelength of approximate 3.5-4km and an inferred amplitude of 1-1.5km. From fold mapping and structure contouring (Figure 3.13) of the steep western limb of the syncline it was found to have gentle warps in strike exhibiting wavelengths of 0.5km to 1km and small amplitudes. The outcrop pattern of the Waitohi Downs Syncline, and in particular the western limb is similar to the analogy that Nicol (1991) proposes of

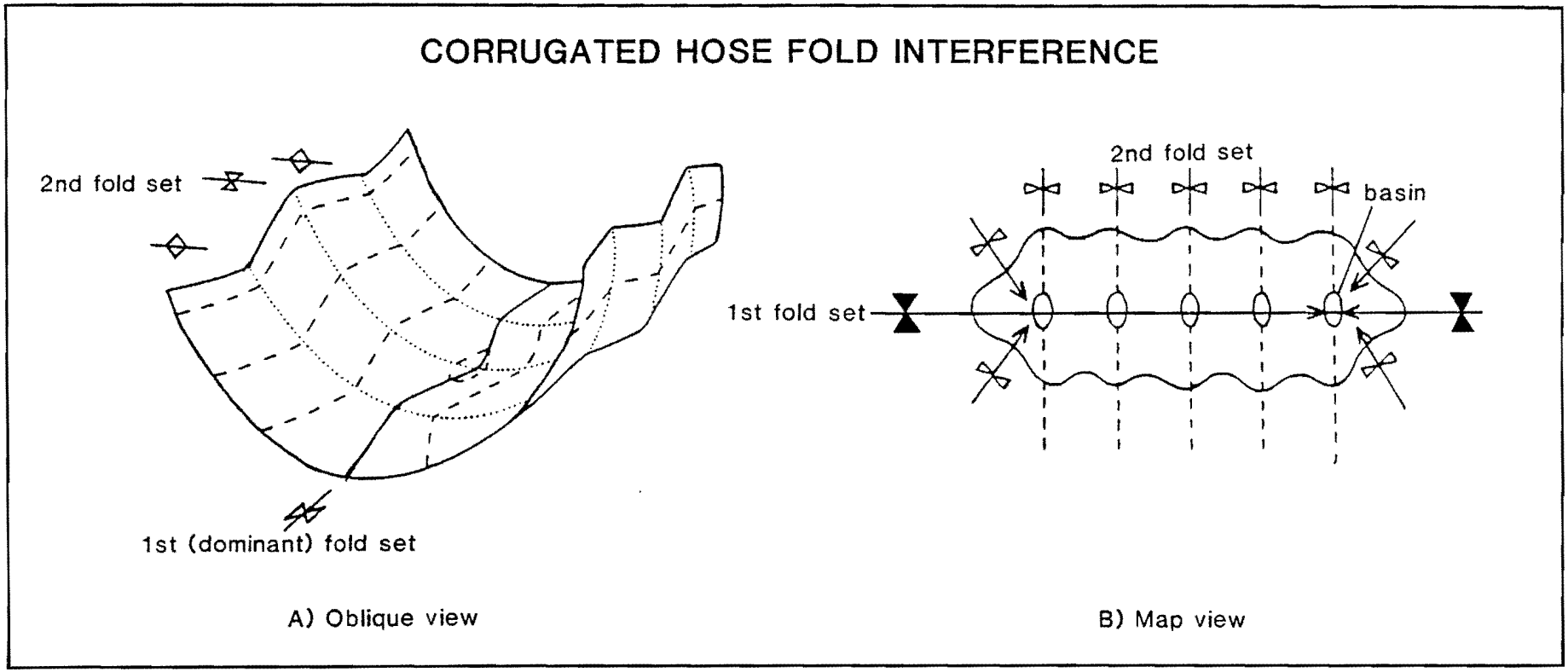

Figure 3.12. Schematic three dimensional oblique (A) and map view (B) representation of corrugated hose fold interference patterns. This pattern is developed where the interfering fold sets have different wavelengths. (After Nicol, 1991).

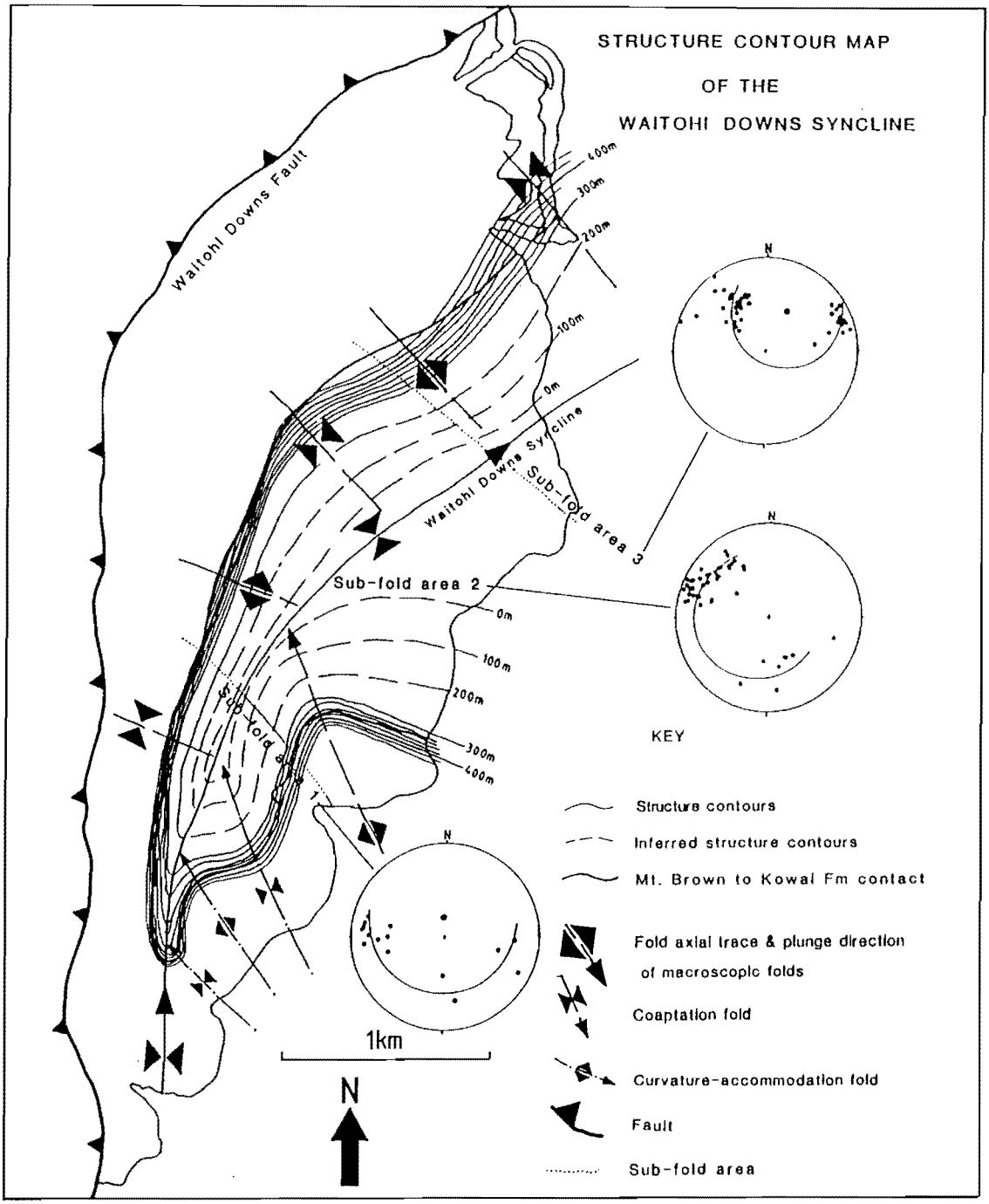

Figure 3.13. Structure contour map and lower hemisphere equal area nets displaying changes in fold interference cone geometries along the Waitohi Downs Syncline, North Canterbury. Structure contours are drawn on the contact between Mt. Brown and Kowai Formations. Poles to bedding of cover rocks are presented on the equal area nets. Also represented are the coaptation folds that strike obliquely to the main orthogonal fold axes.

the interference pattern being like a corrugated hose cut in half perpendicular to the corrugations.

3.6.2.2. T-shaped and Triangular Patterns.

In this study area fold interference has produced T-shaped (partial stars) and triangular (or half diamond) outcrop patterns and fold surface geometries, where anticlines (Figure 3.14) and an anticline and syncline (Figure 3.14) interfere respectively. The outcrop patterns of the Mt. Hilton Dome and the southern end of the Island Hills Syncline (Figures 3.10 & 3.11) represent only partial developments of fold interference structures that form as a consequence of like folds (syncline-syncline or anticline-anticline) and different folds (syncline-anticline) interfering.

Where secondary folds develop at oblique angles to the two main sets of folds, the resulting outcrop patterns are typically either star-shaped, heart to boomerang-shaped, or in the form of the outline of bicycle seats (T-shaped) (Stauffer 1988), although the more classical (Ramsay 1962) ovoid to box-like interference patterns may also be produced. Occasionally only the points of the star may be preserved. The Mt. Hilton Dome represents a partial star preserved as an irregular T-shaped interference pattern (Figure 3.10). Triangular shaped patterns are best exemplified by the outcrop patterns of the basement-cover unconformity surface at the southern ends of the Tommys Stream, Mt. Mason and Island Hills Synclines. The western halves of the triangular interference patterns in the Tommys Stream and Mt. Mason have been obscured by thrusting of basement over the cover rocks on the Tommys Stream Fault. The southern terminations of all three synclines is a consequence of the interferences of the synclines with adjacent WNW-NE trending anticlines to the south of the synclines (Figures 3.10 & 3.11).

3.6.2.3. Secondary Folds.

Two types of secondary folds are developed oblique to the two macroscopic fold sets. 1). coaptation folds (Stauffer, 1988) which form along the intersection line of the two macroscopic interfering fold set limbs.

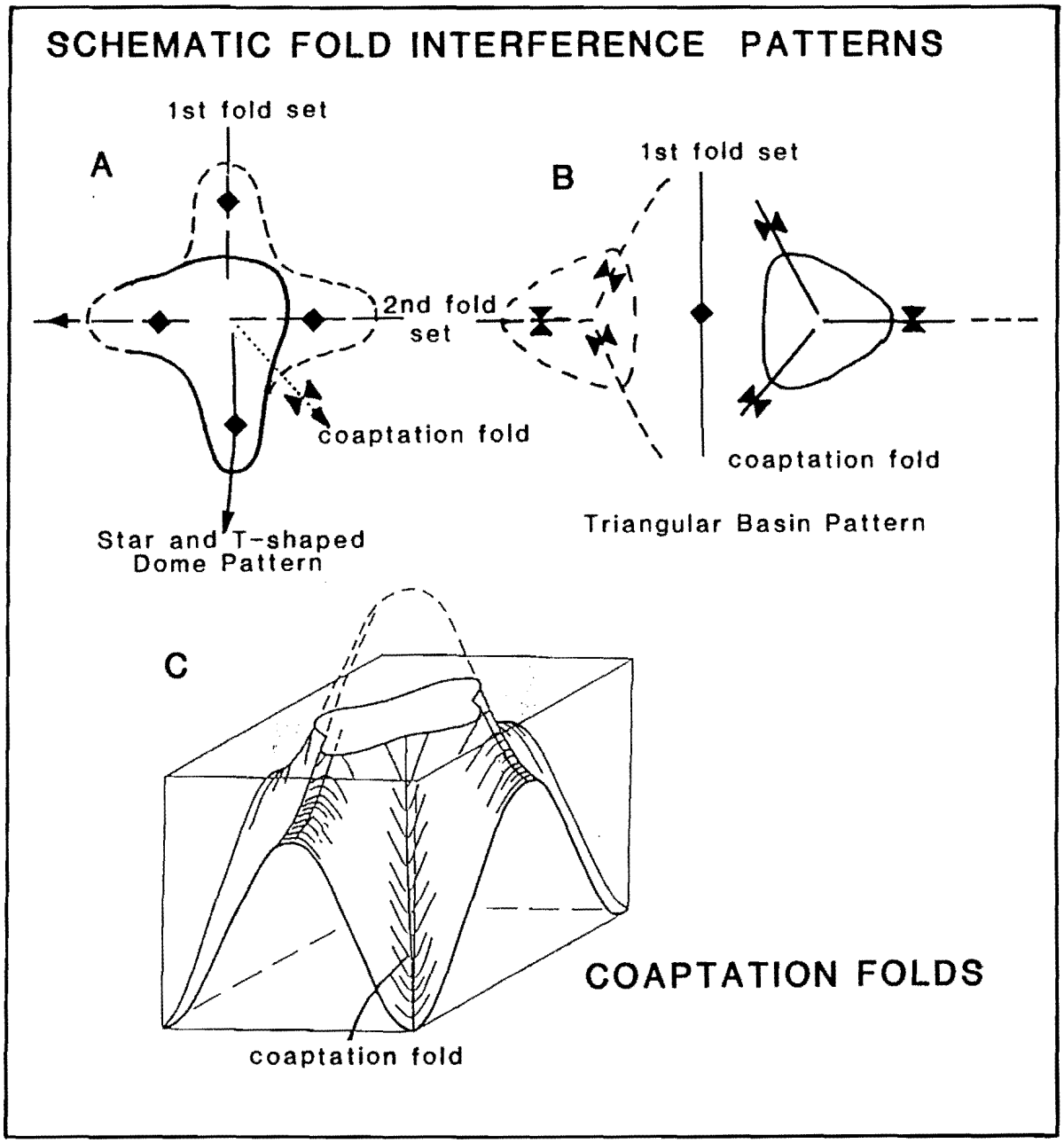

Figure 3.14. Schematic diagrams showing the fold outcrop patterns developed in North Canterbury in association with basin and dome interference of angular folds. The solid lines in (A) and (B) represent simplified versions of the interference patterns in the Mt. Hilton Dome and Island Hills Syncline areas respectively. (C) is a three dimensional sketch of synclinal coaptation folds on a dome. (After St auffer, 1988).

2). curvature-accommodation folds (Lisle et.al., 1990) which develop on the flanks of basin and dome structures.

Coaptation folds form only where the intersecting folds have axial surfaces at a moderate to high angle to each other (Figure 3.14). Commonly the coaptation folds in this study area trend NNW-ENE and WSW, approximately 45° to the main fold sets. The presence of coaptation folds trending in three directions precludes the possibility that the folds may represent further refolding of structures.

Coaptation folds form as both discrete and bifurcating structures depending on whether like folds (anticline-anticline or syncline-syncline) or different folds, (anticline-syncline) (Figure 3.14) respectively, interfere with each other. Discrete coaptation folds appear never to reach the centre point of the basins or domes. The NNW and NE trending synclinal coaptation folds on the Mt. Hilton Dome are probably the best example of the secondary folds dying out before they reach the intersection of the axial planes of the two main fold sets. Bifurcating coaptation folds, on the other hand, form a triple junction of fold axial traces. Synclinal coaptation folds formed due to the interfering of an anticline with a syncline bifurcate from the termination of the main syncline fold axis. The synclinal coaptation fold developed at the SE end of the Tommys Stream Syncline is inferred to be the only remnant exposed of the triple junction, the Tommys Stream Syncline having been terminated against an adjacent and dominant anticline to the south of the study area. Similarly, the coaptation folds at the SW termination of the Broken River Formation on the Island Hills Syncline is a result of an interfering NW trending anticline. Likewise, synclinal coaptation folds are present on the upper contact of the Flaxdown Limestone Member of the Omihi Formation at the south western most exposure of the limestone at Island Hills (Figure 3.15) explaining the box-shaped end to the limestone.

Curvature-accommodation folds on the flanks of basins and domes are analogous to pleats or flutes. These folds are generally discontinuous and converge towards the centre point of the basins and domes. Curvature-accommodation folds developed on

Figure 3.15. Vertical aerial photograph of the coaptation folds developed in the Flaxdown Limestone Member, Omihi Formation, at the southwestern end of the Island Hills Syncline, North Canterbury.

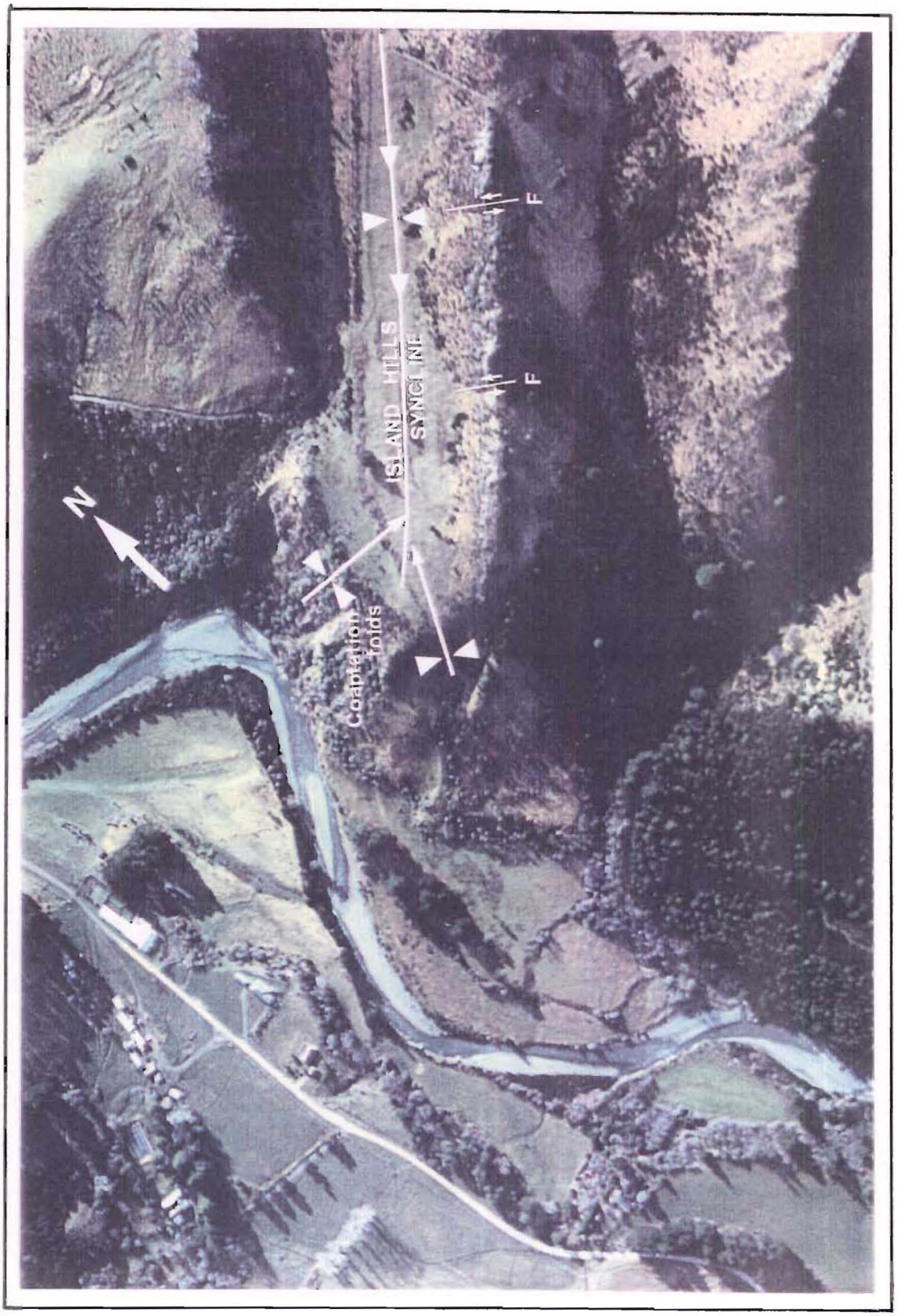
N
ISLAND HILLS
SYNCLINE
F
F
Coalalgion folds

the Mt. Hilton Dome (Figure 3.10), and which trend at varying angles to the main fold sets, are best developed in the more competent units (Lisle etal 1990).

Debate exists as to whether coaptation folds (Stauffer, 1988) are a distinct fold type or simply another curvature-accommodation fold (Lisle et al., 1991). It has been found in this study that coaptation folds do accommodate curvature of the fold surfaces on the basins and domes. However, it has also been found that coaptation folds have a regular geometric relationship with the main interfering folds. Coaptation folds are a distinctive type of curvature accommodation fold and should therefore be acknowledged as such. The author has heeded the advise of Stauffer (1988) and not placed the axial traces of the secondary folds on the geological map as they have no tectonic significance other than confirming the presence of interference folding.

3.6.3. Changes in Fold Geometry.

The approximately NNE-NE trending fold set exhibit variations in fold geometry along their hinge lines. These changes are best exemplified in cross sectional profile. Typically where a macroscopic syncline is cross folded by an anticline the syncline interlimb angle tightens and the hinge zone increases in angularity. Futhermore, where like folds interfere the interlimb angle increases and the hinge zone becomes more rounded. The interference of like folds has the local effect of increasing the wavelengths of the folds while interference of dissimilar folds reduces fold wavelength.

3.7. FAULT-RELATED FOLDING.

Orthogonal macroscopic folding in the cover rocks is consistent with the orientation of both macro- and meso-scale fault trends in the basement. The macroscopic folding of the cover rocks is either in direct response to fault displacement or, within blocks bounded by the macroscopic faults. The NNE-NE trending fault-related macroscopic folds are the most readily identifiable fold set.

Suppe (1985) has recognised four main types of folds associated with vertical fault displacement; drape folds, drag folds, fault-bend folds and fault-propagation folds.

Fault-related folds have been the basis of numerous field (Berg, 1962; Prucha et al., 1965; Stearns, 1971 & 1978, Bradshaw, 1975; Reches, 1978; Cook, 1983; Brown, 1988) and theoretical (Stearns & Weinberg, 1975; Friedman et al., 1976; Gangi et.al, 1977; Reches & Johnson, 1978; Weinberg, 1978; Chester et al., 1988) modelling studies.

3.7.1. Fault control of Fold Morphologies.

In North Canterbury the macroscopic faults and folds commonly exhibit similar orientations (Gregg, 1964; Bradshaw, 1975; Nicol, 1991) and, in this study area, a similar relationship is found. In Figure 3.5 it can be seen that the macroscopic faults and fold axial traces share similar orthogonal NNE-NE and WNW orientations. To the south in the mid Waipara region many of the macroscopic faults were observed to disappear in the cores of folds, termed fault-propagation folds. These folds develop due to the deformation that takes place just in front of the propagating fault surface (Suppe, 1985). In this study area fault-propagated folding predominates with all the faults being exposed rather than concealed in the core of folds. Locally, close to the macroscopic faults, minor drag folding of both basement and cover rocks occurs. Principally the folding is by buckling and flexure slip with associated brittle fracture and mesoscopic faulting. The fault-related folds are usually asymmetric and have axial surfaces that dip steeply sub-parallel with the fault plane. Generally, the folds exhibit one vertical to steeply inclined limb while the other is gently to moderately inclined.

Folds with this asymmetric shape have developed in association with the Tommys Stream, Mt. Mason, Waitohi Downs, Island Hills and Green Hill faults. Anticline-syncline fold pairs occur along range fronts (Reches, 1978; Cook, 1988) such as the western margin of the Culverden Basin. Each fold in the fold pair lie on opposite sides of the fault, the syncline always resting on the relative downthrown side of the fault. Occasionally the fold axial trace is truncated by the fault plane as happens with the Tommys Stream and Mt. Mason synclines.

It has been documented that angular folds may develop in association with faulting (Stearns, 1978; Cook, 1988; Nicol, 1991). Similarly, the folds in the thin (1km) cover

rocks along the western margin of the Culverden Basin are predominantly angular in shape.

Determining the dimensions, wavelength and amplitude, of the folds is complicated by the lack of exposure and the low structural level at which the cover sequence crops out along the western margin of the Culverden Basin. Fold wavelengths is the most readily determinable property. Fault-related folds have half wavelengths of 1.5-5km while the folds developed in fault bounded blocks have half wavelengths of 0.5-1.5km.

Measurements of fold amplitudes of both fault-related folds and folds formed in fault bound blocks are indeterminable in the field because of the lack of preservation of any marker bed on the relative upthrown block. However, the fold amplitudes have been estimated, from the construction of cross sections, on the assumption that the ridge crests of the basement on the upthrown blocks have not been significantly lowered by erosion below the Cretaceous unconformity, to range from 0.5 to 2.2km for the fault-related folds and from 0.2 to 0.6km for the folds developed in the fault bounded blocks. It is inferred that the amplitudes of the fault-related folds are controlled by the amount of vertical fault displacement, and the fold wavelength by the perpendicular distance between the macroscopic faults. Furthermore, as the fault displacement increases likewise so will the fold amplitude.

3.7.2. Kinematics of Fault-related Folding.

Fault slickenside and fold axial surface data have been used to determine the orientation of strain accommodated by macroscopic faulting and folding in this study area. Figure 3.16 indicates the fold shortening directions are orientated WNW-ESE and NE-SW. Furthermore, shortening on the macroscopic faults crudely parallels the WNW-ESE and NE-SW fold shortening. Slickenside striations developed within the cover rocks of the study area due to bed over bed slip also crudely parallel the macroscopic fault slickensides. It is noted that the macroscopic fault slickensides are formed predominantly on steep faults and plunge more steeply than the fold shortening directions. The strain has been accommodated by movement on steeply

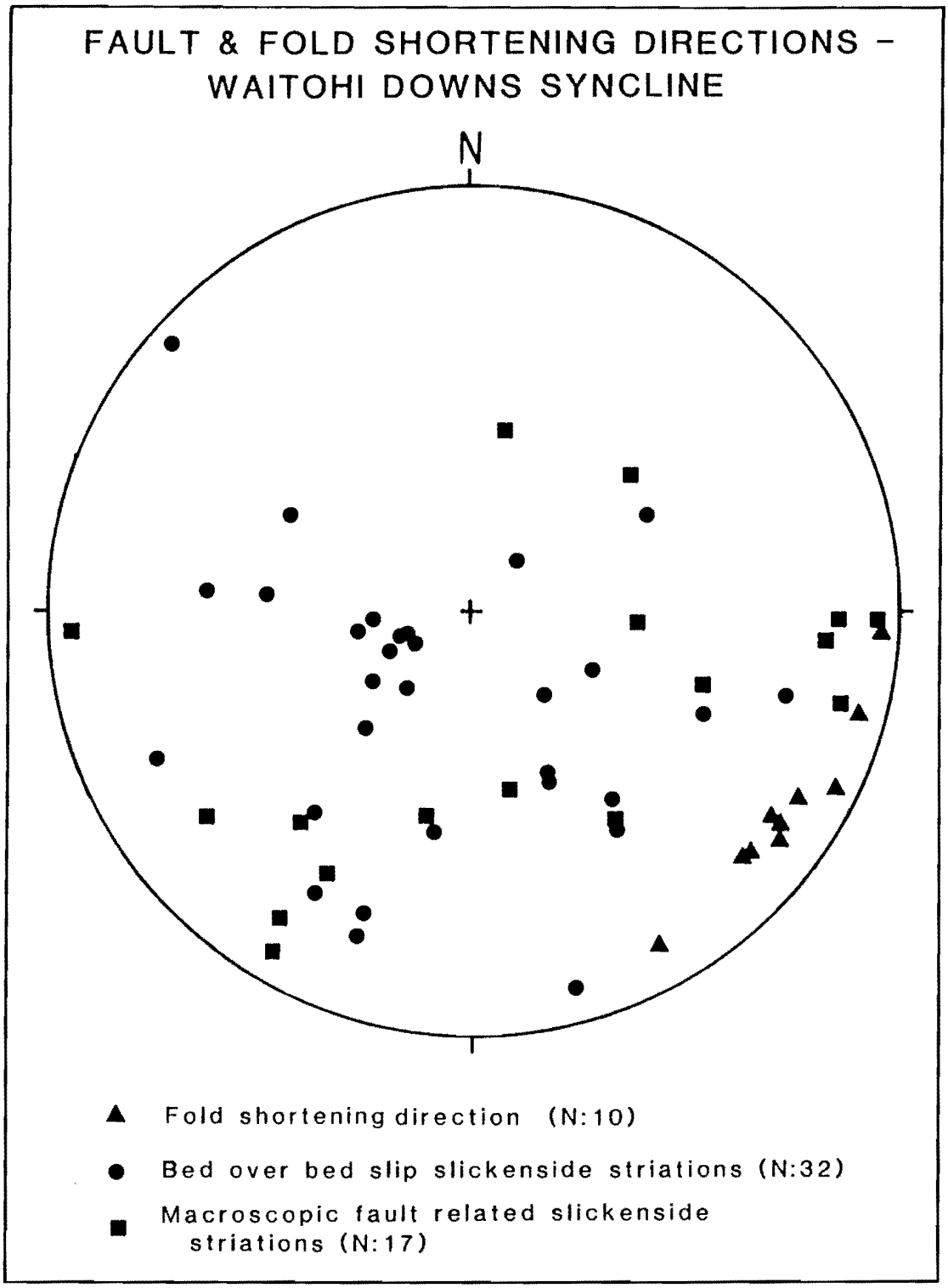

Figure 3.16. Fault and fold shortening directions for the Waitohi Downs area, North Canterbury, inferred by slickenside striations and the orientation of the axial surface of the Waitohi Downs Syncline. All data points are plotted on a lower hemisphere equal area net.

dipping faults and folding of anisotropic, horizontally bedded rocks.

3.7.3. Faulting at Depth.

Commonly folds are formed from movements on deep seated faults (Suppe, 1985; Yeats, 1987a & 1987b). In North Canterbury it can not be assumed that all folds are directly related to faulting. In general and in North Canterbury many macroscopic faults are poorly exposed or are not expressed at the surface. Analysing the morphologies of folds cropping out at the surface can be useful for determining the presence of faulting at depth and, if faulting is present, constraining the nature of faulting. Firstly, however, it must be determined that the folds are related to faulting.

All the steeper limbs of the folds are truncated by the macroscopic faults which dip moderately-steeply in the same direction as the fold axial surfaces. This means the vertical displacement of the anticline hinge and the syncline hinge is likely to be much larger than the displacement at the fault tip (Figure 3.17).

It has been found by Nicol (1991) that when fold amplitudes are plotted against vertical fault displacement for 15 fault-related folds in North Canterbury (Figure 3.18) the slope of the the estimated mean line of the data decreases with increased fault displacement. Furthermore, the graph (Figure 3.18) may be indicative of a decrease in the rate of fold growth with increasing vertical fault displacement. Figure 3.18 indicates that in the early stages of formation fold growth is likely to be greater than fault displacement and that above the developing fault vertical displacement is zero while fold amplitude is greater than zero. The graph (Figure 3.18) suggests that fold amplitudes of fault-related folds in North Canterbury may reach values of one to three hundred metres before the stratigraphy is displaced by faulting. The author believes that if a marker bed existed across the macroscopic faults in this study area, a similar relationship would exist between fold amplitude and vertical fault displacement as that observed by Nicol (1991).

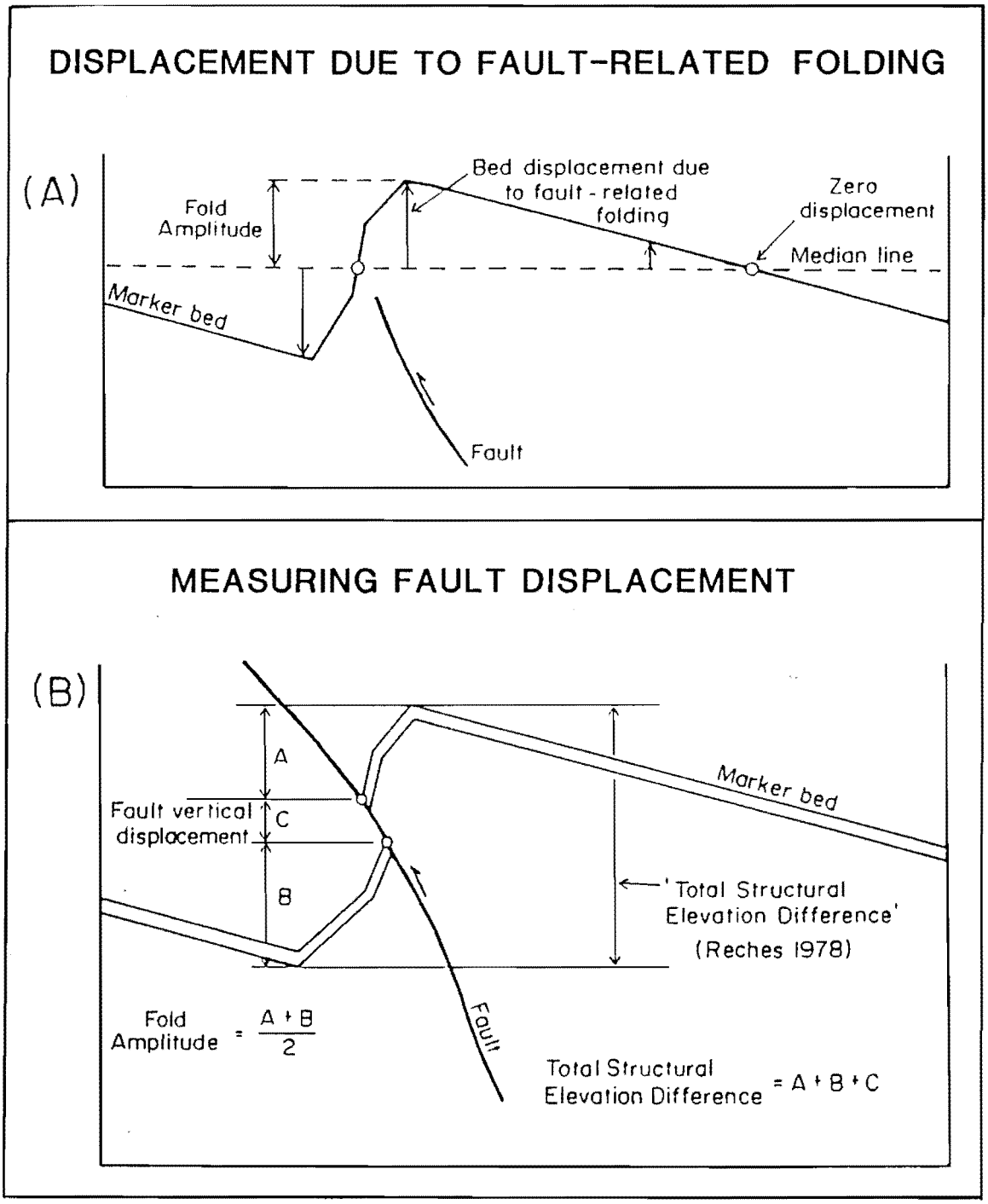

Figure 3.17. The measurement of fault related displacement by faulting and folding. (A) Fault-related fold displacement due to buckling and bed over bed slip can be measured from the fold median line. Prior to the displacement of the marker bed the `total structural elevation difference' across the fault is equal to twice the fold amplitude. (B) After the fault has displaced the marker bed the `total structural elevation difference' is equivalent to twice the fold amplitude plus the fault displacement. (After Nicol, 1991).

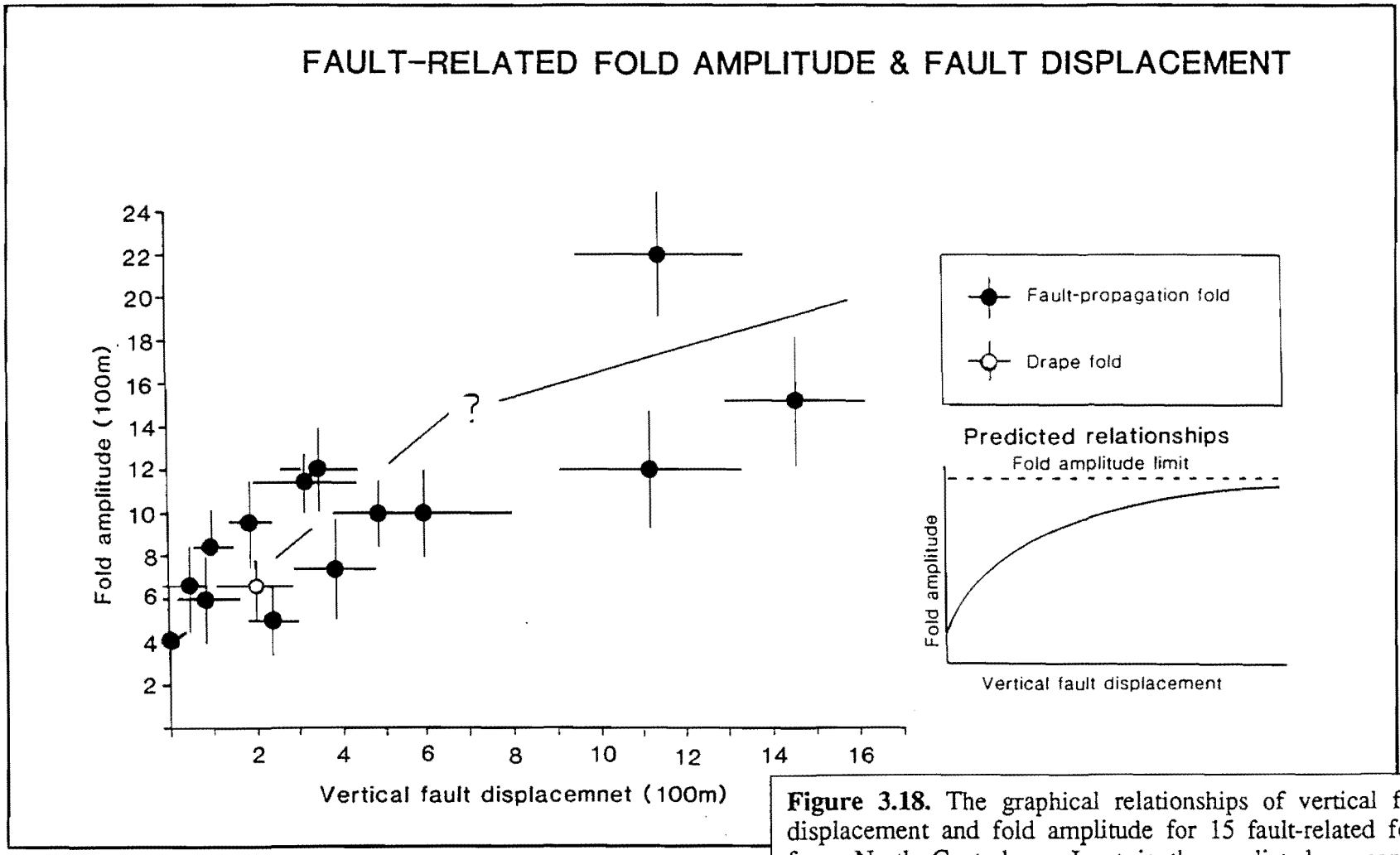

Figure 3.18. The graphical relationships of vertical fault displacement and fold amplitude for 15 fault-related folds from North Canterbury. Inset is the predicted conceptual relationships for these variables. The amplitude limit represents the limit of folding by buckling and bed over bed slip.

It is important to realise that vertical fault displacement is only a portion of the total difference in elevation across a fault that extends to the surface in a fault-related fold. Reches (1978) used the term "total structural elevation difference" to define the change in elevation across a fault that has formed in a macroscopic fold. Therefore, to measure, or estimate, the total structural elevation difference of the asymmetric fault-related folds of North Canterbury, two times the fold amplitude needs to added to the vertical fault displacement. Previous estimates of fault displacements in this study area and other parts of North Canterbury are probably more indicative of the total structural elevation difference. Field et al. (1989), using data of Gregg (1964), for example, have probably overestimated the "maximum vertical throw" of the Waitohi Downs and Tommys Stream Faults. Field et al. (1989) do not recognise the anticline-syncline fold pairs associated with the faults and hence, in the authors view, overestimate the vertical fault displacement. The values of Field et al. (1989) are probably more indicative of the total structural elevation difference across the Tommys Stream and Waitohi Downs faults. Total structural elevation differences across the Tommys Stream, Waitohi Downs, Island Hills and Green Hill Faults have been estimated from the cross sections to be 1.2km, 3.2km, 2.0km and 2.2km respectively. The basement is faulted against cover rocks in both these areas indicating that folding has accommodated some fault-related strain. Therefore, it may even be invalid to compare the difference in elevation between the relatively downthrown cover rocks and the upthrown basement range height with the minimum fault displacement.

3.7.4. Pseudo-Folding of the Basement.

The unconformity between the cover and basement rocks truncates bedding planes and folds within the Mesozoic basement rocks but follows the form of folds in the cover harmonically. This suggests that the cover rocks are not detached from the basement rocks and the latter appears to be 'folded' in conjunction with the cover rocks. However, the folds and bedding in the basement rocks do not show systematic changes in orientation as if they had been refolded by the late Cenozoic deformation that has formed the macroscopic folds in the cover sequence. Rather, basement has been deformed in a brittle fashion by movement on the main faults and numerous small

scale faults, accommodating the overlying folds. Late Cenozoic small scale deformation of the basement has been facilitated by the widespread preexisting Mesozoic faults and joints in the Torlesse. A similar form of deformation has taken place in the Torlesse basement in the mid Waipara region, the basement having deformed like a beanbag when a load is placed on it (Nicol, 1991).

Predominantly the small scale beanbag or triboplastic deformation of the basement is confined to zones flanking all the macroscopic faults and underlying the hinge zones of the late Cenozoic folds. Beneath the gently dipping limbs of the synclines in the cover rocks the small scale faults are far less abundant and do not offset the unconformity surface. For example, the eastern limb of the Tommys Stream Syncline rests on relatively intact Torlesse basement in comparison to the basement rocks adjacent to the fault and near the fold hinge. Similarly, the SE limb of the Mt. Mason Syncline rests on relatively intact Torlesse bedding when compared to the basement near the Tommys Stream Fault and the fold hinge zone. It appears that the brittle basement deformation is largely confined to a wedge shaped envelope which is defined by the main faults and their adjacent anticline and syncline fold hinges. Chester et al. (1988) and Friedman et al. (1976) have found similar wedge shaped envelopes of small scale deformation in experiments on basement cored folds. Similarly, Cook (1983 & 1988) has found wedge shaped zones of small scale deformation in basement beneath fault-related folds in the Rocky Mountains Foreland. Along the western margin of Culverden Basin, the width of the small scale brittle deformation zone decreases with increasing depth (lower structural level) and increasing confining pressure.

3.7.5. Interference Folding.

In this study area it has been found that the main influence on the macroscopic fold orientations is the strike of the macroscopic faults. Fold interference patterns along the western margin of Culverden Basin have formed in response to WNW-ESE and NNE-SSW oblique-slip faulting. These macroscopic orthogonal faults are termed thrusts (at depth (5km) the author believes that the faults flatten to thrusts) although sensu stricto the faults are often steep enough to be called reverse at the surface. The

oblique-slip motion explains the azimuth of fold shortening directions (Figure 3.16). It is also indicative of the regional NW-SE compression while the vertical component of movement is responsible for the folds being parallel to the macroscopic faults. In this study area both orthogonal fault sets are contractional resulting in two contractional fault propagated fold sets that interfere to produce irregular and non-classical basin and dome interference patterns. The interfering fold sets have formed synchronously and it is inferred that the faults have also developed synchronously during the late Cenozoic. Synchronous development of the orthogonal faults appears to be confirmed by the truncation of the NNE striking Island Hills Fault against the WNW striking Hurunui Fault which is itself apparently truncated by the Waitohi Downs Fault. This implies that the two fault sets, rather than having discrete sequential phases of movement have moved spasmodically, but during the same or an overlapping time interval. The inference from this is that the folds have also developed synchronously. Synchronous fold development is further implied from interpretating the structure contouring and from apparent warping of Holocene terrace surfaces at the southern end of the Culverden Basin (Nicol, 1991).

If one fault set is dominant then one fold set will dominate and a corrugated hose interference pattern will develop. This appears loosely to be the case with the Tommys Stream and Mt. Mason synclines which are located between two NNE striking thrusts, the Tommys Stream and Mt. Arden faults. The major folds parallel the major faults while the WNW cross folds, developed in the area between the NNE faults, are also accommodating shortening. The smaller fold amplitude and wavelength of these folds is not directly related to known macroscopic fault displacement, but NW striking mesoscopic faults in the basement are widely distributed. Where both orthogonal fault sets are well developed, such as at Taruna and Island Hills, both interfering fold sets are well developed producing more equant interference patterns.

3.8. SMALL-SCALE STRUCTURES.

Deformation in this study area has resulted in the formation of mesoscale faults, veins, joints, fractures, and, within the competent limestone lithologies of this study, stylolitic pressure solution seams. Mesoscale structures such as these have been found useful in determining the deformational histories in stable cratonic regions (Arthaud, 1969; Letouzey & Tremolieres, 1980). They are indicative of small strains, and can be used as kinematic indicators of shortening and extension (e.g. Fletcher & Pollard, 1981) and to determine the orientation of the principal stress axes (e.g. Engelder & Geiser, 1980; Buchner, 1981; Angelier, 1979 & 1984; Marrett & Allmendinger, 1990). Recent studies by Nicol (in press) and Syme (1991) in the North Canterbury area demonstrate that mesoscale structures also provide valuable information in New Zealand's active plate boundary setting. A detailed examination of the mesoscale structures developed in this study area was undertaken to determine the relationship of the mesoscale structures to the macroscopic structures, and to provide a means of assessing the timing and kinematics of the local deformation.

3.8.1. Pressure Solution Seams.

Fractures subjected to pressure solution are termed solution seams (Hancock, 1985). These are often associated with stylolite columns (here up to 4mm long) orientated perpendicular to the seam surface. Solution seams are best developed as irregular and discontinuous fractures within the tuffaceous basal portion of the Flaxdown Limestone Member at Island Hills and Waitohi Downs, where the seams are highligthed by the truncation of body fossils and concentrations of insoluable tuffaceous and iron oxide materials on the fracture surface (Figure 3.19). These solution seams are folded in the Island Hills Syncline, commonly striking NNE-NE, and dipping steeply WNW-NW or ESE-SE. The solution seams are parallel to bedding (within measurement errors) and probably formed as a consequence of lithostatic loading imposed on the Flaxdown Limestone Member by the overlying mid-late Cenozoic sediments. At Green Hill late Oligocene and younger sediments reach a thickness of approximately 1.6km, considerably more than the post-limestone strata preserved at Island Hills. The solution seams at Island Hills suggest that a considerable thickness of sediments

Figure 3.19. Bedding parallel pressure solution seams in Flaxdown Limestone Member, Omihi Formation, from the Island Hills Syncline. Arrow (4cm long) points to a fossil fragment truncated by a pressure solution seam.

Figure 3.20. Photograph of orthogonal joints in the Flaxdown Limestone Member, Omihi Formation on the northwest limb of the Island Hills Syncline, North Canterbury.

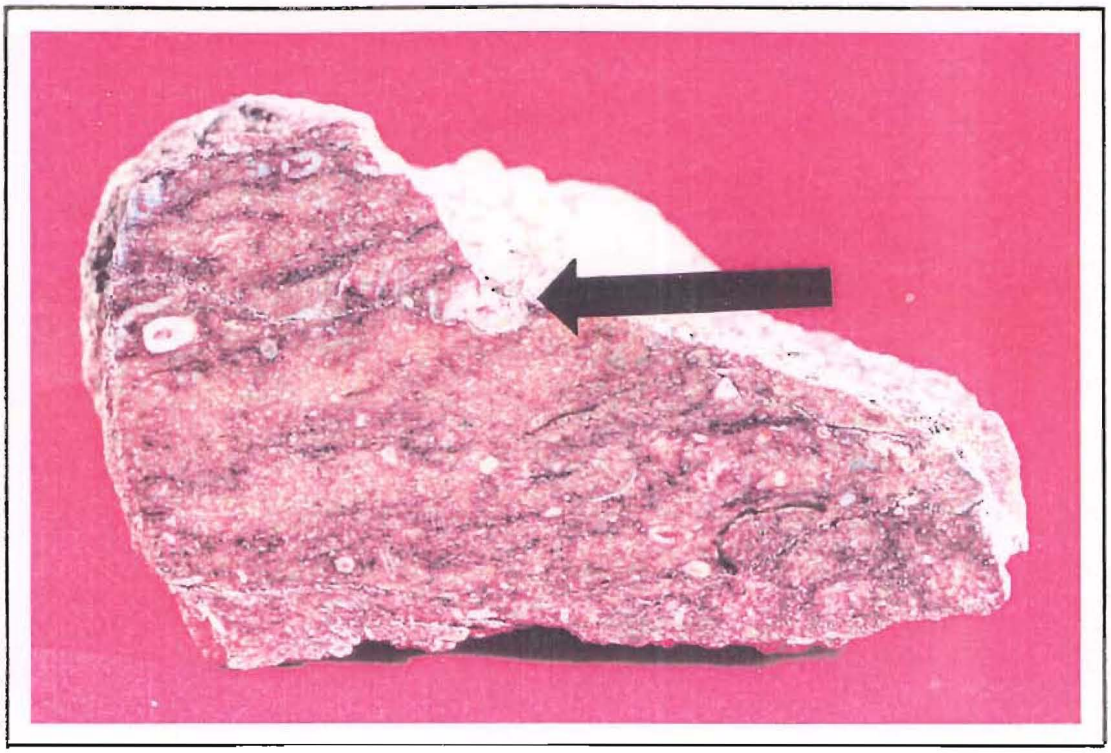

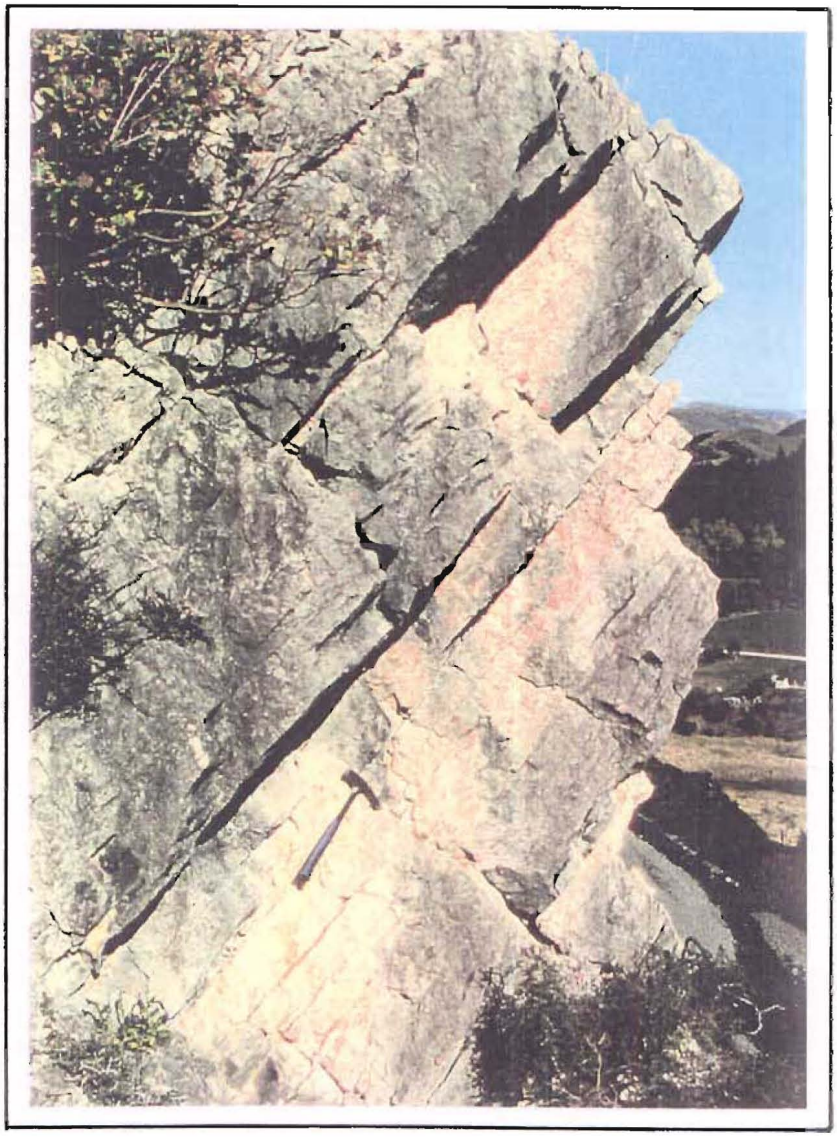

(possibly up to 1.6km -inferred from Green Hill) once overlay the limestone and have subsequently been eroded.

3.8.2. Orthogonal Joints.

The name 'joint' is a field term used to describe a barren, closed fracture on which there is no measureable slip or dilation (Hancock, 1985). Joints are widespread, but not ubiquitous, and appear to be preferentially developed in the more competent units of the cover sequence in this study area. They are most commonly observed in the Flaxdown Limestone Member (Figure 3.20) and the calcareous beds within the Mt. Brown Formation. However, in the Waitohi Downs area where Mt. Brown Formation overlies Flaxdown Limestone the joints are predominantly developed in the Flaxdown Limestone. The joints are generally planar and are spaced from 5-10cm in the Flaxdown Limestone Member and up to 2m apart in the Mt. Brown Formation. Commonly the joints are less than 5m in length and always appear to post date the solution seams.

The joints form two sets, often steeply dipping (>60°) (where bedding dips less than 35°), which are locally orthogonal to each other and always approximately perpendicular to bedding. In the field one joint set strikes from N-ENE and the other W-NNW. The N-ENE joint set generally bisects the fold axes of the two sets of macroscopic folds and may strike at up to 30° on either side of the fold trend, although the joints may become parallel to the macroscopic fold axes.

In Figure 3.21 the effects of folding on the orientations of the joints have been removed. The equal area plot shows that all the joints were vertical to sub-vertical to bedding prior to the late Cenozoic folding. The joints appear to have been extensional, suggesting approximately NE-SW and NW-SE extension, with both joint sets being orthogonal to the vertical compression inferred from the pressure solution seams.

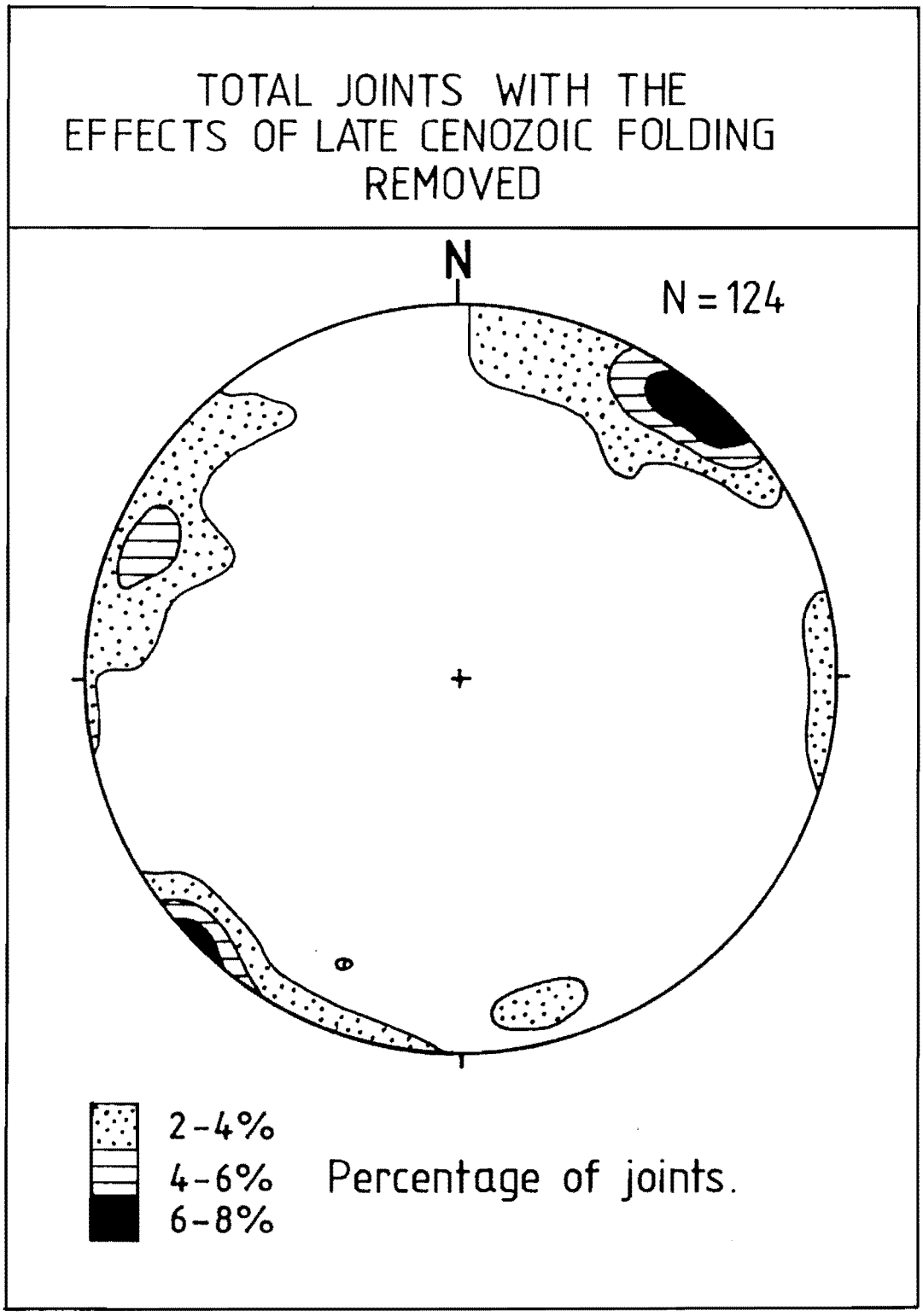

Figure 3.21. Spherical gaussian contoured poles to orthogonal joints collected from within the Flaxdown Limestone Member, Omihi Formation in the Island Hills and Waitohi Downs Synclines, North Canterbury. Bedding dips have been removed for all nets.

3.8.3. Macrofractures.

Macrofractures are fractures that cannot be differentiated as either joints or faults (Hancock, 1985). Although not strictly small-scale structures they place constraints on the deformation of the cover rocks. The best example of macrofractures crop out in the Mt. Brown Formation at Waitohi Downs. Aerial photos of the area suggest that the macrofractures are continuous across the numerous strike ridges for up to 300m. The macrofractures are commonly orthogonal, one set steeply dipping to the NNE and SSW and the second set dips steeply to the WNW and ESE, respectively. The NNE-SSW striking and steeply WNW and ESE dipping set of macrofractures are locally parallel to the fold axes of the macroscopic N-ENE trending Waitohi Downs Syncline. It appears that the macrofractures have developed contemporaneously with buckling of the limestones and, therefore, reflect local fold strain.

3.8.4. Mesofaults and Veins.

Within the cover rocks, two groups of mesofaults have been described (Section 3.3): (1) a steeply dipping set of orthogonal faults that strike approximately NW-SE and NE-SW, and (2) a widespread set of faults parallel to sub-parallel with bedding. The first set appear to have exploited the zones of weakness associated with the steep NW-SE and NE-SW striking orthogonal joints and macrofractures. The second set appear to have exploited bedding planes and possibly the bedding parallel pressure solution seams, and accommodate layer over layer slip associated with flexural folding.

Both mesofault sets contain faults that have scattered orientations when the effects of folding are not removed. On the other hand when the effects of folding are removed some mesofaults become increasingly scattered. This indicates that the mesofaults are late-stage structures having started to develop just prior to the onset of folding and have continued to develop with the late Cenozoic folding. Both sets of mesofaults appear to have exploited previously formed structures during the early Pleistocene to Recent period.

Calcite veins, up to 2cm wide, are present in the Flaxdown Limestone Member. The veins measured are commonly parallel to the orthogonal joints. It is inferred that they formed from calcite mineralization in the joints. The thickest precipitation of calcite occurs in the NW-SE striking joint set. Typically the calcite grows perpendicular to the vein wall suggesting continued NE-SW dilation after joint development. Many of the veins have been faulted and contain numerous calcite fibre lineations. On many of the faults two sets of calcite fibres are observed, commonly separated by a period of calcite mineralization. Multiple periods of vein mineralization and fault movement indicate a complex fracture history, and vein mineralization probably obscure many fault movements. In the field the NW-SE striking veins, more commonly than the NE-SW mesofaults, exhibited two, or occasionally more, phases of faulting and mineralization.

3.8.5. Timing of Mesoscale Structure Development.

The time of formation of the mesoscale structures is shown in Table 3.4 while the arguments for the ages are discussed here:

(1). The solution seams are developed in Oligocene limestone and are inferred to have formed due to lithostatic loading by the overlying sedimentary cover strata. The cover sequence reached a maximum thickness after the deposition of the Pliocene Kowai Formation. Late Oligocene and younger sediments are approximately 1.6km thick at Green Hill and it is likely that these pressure solution seams formed at, or close, to the time of maximum cover rock thickness (i.e. late Pliocene-early Pleistocene).

(2). The orthogonal joints are formed in Miocene limestone units and are therefore post Miocene. In addition the joints cut across the pressure solution seams, therefore post dating them (i.e. post late Pliocene-early Pleistocene). The joints also pre-date folding which in the mid-Waipara region began about 0.6ma (Nicol, pers. comm.). Using these data the joints formed between 0.6 and 2.0ma. ago.

(3). The macrofractures have formed contemporaneouly with folding as they cut across the orthogonal joints and are therefore of mid Pleistocene-Recent age.

TABLE 3.4. A summary of the brittle small-scale structures developed in the cover rocks, as well as their relative sequence of development and estimated ages.

TECTONIC STRUCTURES	ESTIMATED AGE	DEFORMATION EVENT
Bedding parallel pressure solution seams	Pliocene	Uniaxial gravitational loading by overlying sedimentary cover.
Steep orthogonal joints	late Pliocene	Onset of regional uplift associated NW-SE shortening and NE-SW dilation, on the outer edge of the New Zealand plate boundary zone.
Macrofractures	early Pleistocene to Recent	Associated with onset of folding related to NW-SE shortening and NE-SW dilation.
Mesofaults and veins	early Pleistocene to Recent	Related to continued folding, NW-SE and NE-SW shortening. Veins developed in joints. Mesofaults activated along bedding planes and pre-existing fractures and joints.

(4). The mesofaults and veins both pre-date, and have formed contemporaneously with, mid Pleistocene-Recent folding, suggesting these are both older and of similar age to the mid Pleistocene-Recent folding.

3.9. CONCLUSIONS.

Macroscopic folds developed in the late Cretaceous-Cenozoic cover rocks along the western margin of the Culverden Basin display axial traces that are sub-parallel to parallel with the macroscopic oblique reverse and thrust faults. The folds are typically steeply inclined, gently plunging, asymmetric syncline-anticline fold pairs. Two, locally orthogonal (approximately NNE-SSW and WNW-ESE), fold sets are developed producing irregular basin and dome fold interference patterns. The fold dimensions reflect their proximity to the macroscopic faults, the larger fold wavelengths and amplitudes form near the faults while smaller fold dimensions occur away from the faults. Commonly, more than one cone is required to define the fold surface. This is a consequence of changes in fold geometries along the folds resulting from the differences in the dimensions of the two fold sets. Where like folds (syncline-syncline) interfere the folds broaden while the interference of different folds (anticline-syncline) results in the folds tightening.

The non-classical fold interference produces corrugated hose, T-shaped and triangular outcrop patterns. Corrugated hose patterns have formed where folds of different dimensions interfere while T-shaped patterns result from the interference of like folds with similar dimensions. Triangular interference patterns are developed commonly at the southern ends of the N-NE trending folds where they are truncated by an interfering anticline. Two types of secondary folds are developed on the limbs of the basins and domes. Both synclinal and anticlinal coaptation folds are formed in the cover rocks and trend approximately 45° to the two main sets of folds. Curvature-accommodation folds are analogous to pleats or flutes in the cover sequence and are developed at various angles to the two main fold sets and the coaptation folds.

Synchronous orthogonal macroscopic faulting has propagated up from the basement into the cover rocks producing synchronous orthogonal folding of the cover. Beneath the cover rocks the basement has been deformed not by folding but in a way that is analogous to the movement of beans in a beanbag, that is, movement has occurred on numerous small-scale faults and a few macroscopic faults. The wedge-shaped deformation of the basement is greatest near the major faults and beneath the hinge zones of the folds developed in the cover rocks.

Various small-scale structures in the basement and cover rocks have proven useful for constraining the ages of the deformational phases. Pressure solution seams and orthogonal joints developed in the cover rocks prior to the onset of late Cenozoic deformation. Macrofaults and calcite veins both pre-date and, along with the macrofractures, have developed synchronously with mid Pleistocene-Recent folding of the cover rocks along the western margin of Culverden Basin.

CHAPTER FOUR: MESO-SCALE FAULT KINEMATICS

4.1. INTRODUCTION.

Numerous studies have found that movements on small-scale structures are useful indicators of the kinematics of macroscopic structures (e.g. Sporli & Anderson, 1980; Reches, 1987; Frizzell & Zoback, 1987; Hardcastle, 1989; Nicol & Campbell, 1990; Nicol, 1991; Syme, 1991). Faults, folds, tectonic joints, tension gashes, stylolites and veins are small scale structures that can prove useful for kinematic analysis (Angelier 1989). It is particularly useful to use small-scale structures for kinematic analysis in areas, (e.g. along the western margin of the Culverden Basin) where the exposure of the macroscopic structures is limited. Late Cretaceous-Tertiary cover rocks in this study area were largely undeformed prior to the onset of the late Cenozoic deformation. During late Cenozoic deformation of the cover rocks numerous outcrop scale faults were formed and provide reliable movement indicators. It is these faults that provide the best means of analysing the local kinematics.

4.2. MOVEMENT INDICATORS.

There are various small-scale structures developed in the cover rocks in the western Culverden Basin (Chapter 3), but it is only the mesofaults that record the movements of the late Cenozoic deformation. Two forms of movement indicators are developed on the mesofaults; 1) calcite fibre striations and 2) slickenside striations.

4.2.1. Calcite Fibre Lineations.

Calcite fibres (Figure 4.1a & b) often grow on fault planes in response to fault motion, and the subsequent development of voids between the walls. The long axes of the calcite fibres are orientated parallel to fault slip direction (Durney & Ramsay, 1973).

The calcite fibres lineations are developed on calcite veins in the Tekoa Formation and on fractures and calcite veins in the Flaxdown Limestone Member of the Omihi Formation. The Mt. Brown and Kowai Formations also contain small populations of calcite fibres within lenticular limestones horizons.

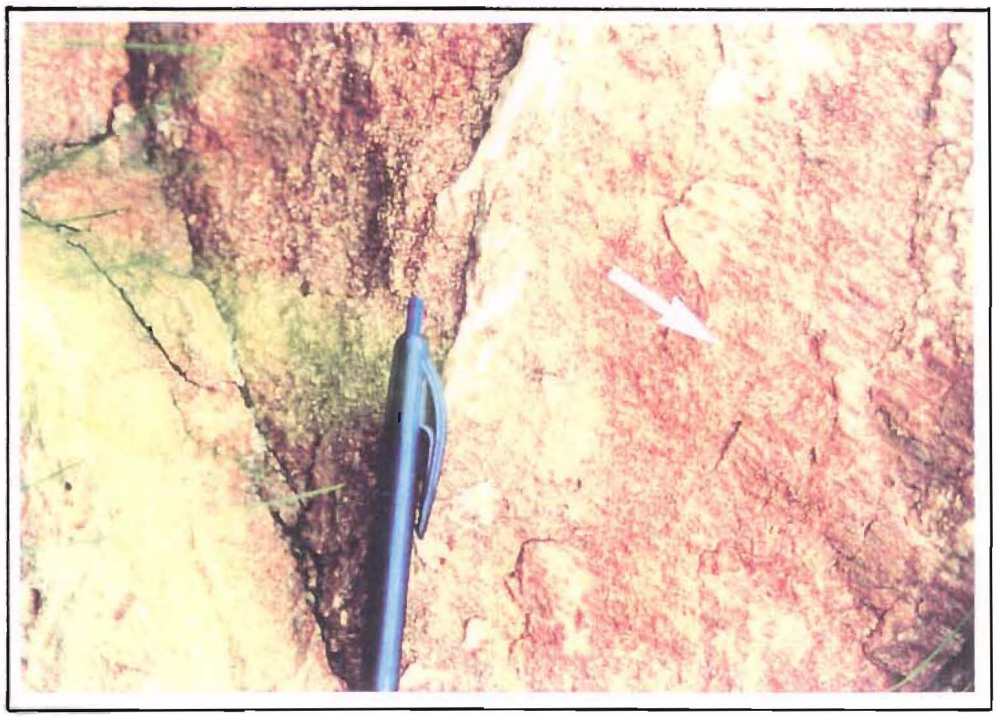

Figure 4.1 a). Stepped calcite fibre striations on a meso-scale fault plane within the Flaxdown Limestone Member, (Omihi Formation) Waitohi Downs. The arrow indicates the movement direction on the fault.

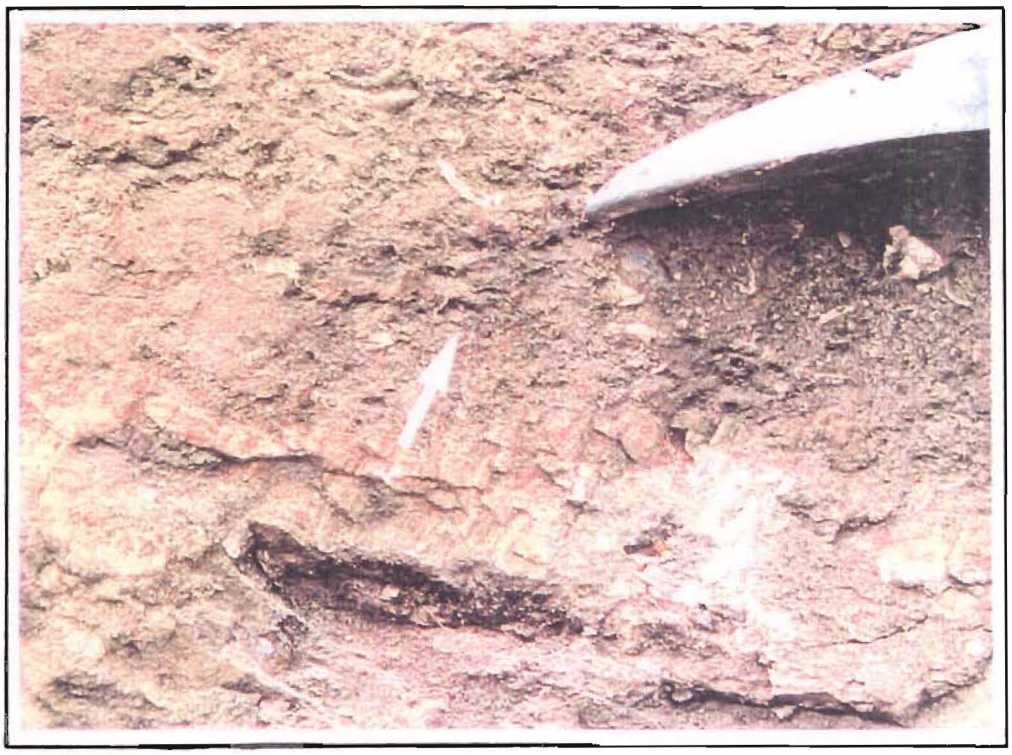

Figure 4.1 b). Calcite fibre striations on a meso-scale fault plane within the Mt. Brown Formation, Kanuku Hills. The arrow indicates the movement direction on the fault.

The sense of movement of faults containing calcite fibres determined in the field by the presence of stepped calcite risers. The risers, which are predominantly perpendicular to the lineations, are termed congruous (the risers facing towards the movement of the missing block) (Durney & Ramsay, 1973). Occasionally both walls of the fault were preserved and commonly calcite fibres were growing on both walls indicating a syntaxial model (Durney & Ramsay, 1973) for fibre growth. In this situation the fibres are an overgrowth of the original wall-rock grains.

Calcite fibres appear most likely to represent strain induced by multiple fault movement events, and therefore provide a longer term record of the strain history than slickenside striations.

4.2.2. Slickenside Striations.

A slickenside fault surface (Figure 4.2a & b) exhibits the effects of abrasion during fault movement, often forming smooth or shiny fault surfaces (Means, 1987). It is common to find that the slickensided fault surfaces are finely grooved. These striations are a consequence of abrasion on the fault surfaces as the fault moves. The striations are always parallel to the direction of fault movement (Petit, 1987). It follows that one set of commonly directed striations records a discrete fault movement. Furthermore, intermittent fault movements mean that the striations observed on the fault are probably only the youngest set of striations, any previous striations being largely overprinted by subsequence fault slip.

Along the western margin of Culverden Basin slickenside striations are most readily developed in the Flaxdown Limestone Member of the Omihi Formation, Waipara Greensand, Tekoa, Broken River, Conway Sandstone, and Loburn Mudstone Formations. The Flaxdown Limestone Member, Tekoa Formation and the Waipara Greensand Formation provided the most mesofaults on which fault movement could be readily determined in the cover sequence. Slickenside striations are also abundant in the Torlesse Supergroup basement rocks, particularly within the highly fractured zones of the macroscopic faults.

Figure 4.2 a). Slickenside striations developed on a meso-scale fault plane within the Flaxdown Limestone Member (Omihi Formation), Flaxdown Quarry. The arrow indicates the direction of movement on the fault.

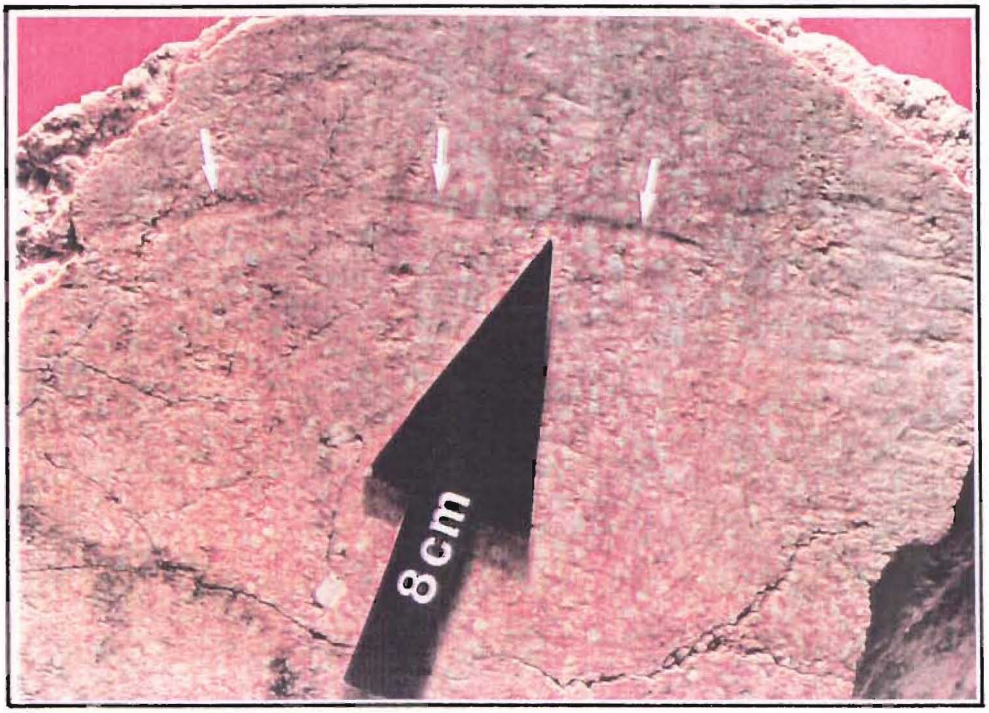

Figure 4.2 b). A curved slickenside striation developed on a meso-scale fault plane within the Flaxdown Limestone Member (Omihi Formation), Flaxdown Quarry. The arrows indicate the striation.

In the Flaxdown Limestone the fault surfaces often exhibite accretion steps (Petit, 1987) where the surface of the step is striated but the lee side is locally crystalised with calcite. Similarly, the Tekoa Formation occasionally exhibited accretion steps with up to 3mm long calcite crystals developed on the lee side of the step. These accretion steps are congruous (i.e. the riser faces towards the movement of the missing block), where euhedral calcite crystal faces are observed on the risers (Petit, 1987). The Waipara Greensand Formation on the other hand does not exhibit accretion steps, rather the glauconite is smeared out and striated along the leading side of the risers. The risers are congruous with the risers facing towards the movement of the missing blocks. On faults that exhibited stepped risers and slickenside striations the sense of movement and orientation of slip was determined.

4.3. METHODS OF DATA ANALYSIS.

Many methods for determining the kinematics of faults have been descibed since the early work of Wallace (1951), Anderson (1951) and Bott (1959).If the stress state is known, then the shear stress and the slip orientation expected on any fault plane can be determined. The first attempt at formulating and solving the inverse problem was published by Carey & Brunier (1974): knowing the slips and hence the shear stress orientations on various planes, one determines the average stress state. Subsequent methodological developments include those of Angelier (1975, 1979, 1984 & 1989), Armijo & Cisternas (1978), Ethchecopar et al. (1981), Angelier et al. (1982), Gephart & Forsyth (1984) & Michael (1984). Recent years have seen rapid progress in the use of computers to process lengthy numerical methods (Ethchecopar et al., 1981; Angelier, 1984; Hardcastle & Hills, 1991).

In this study the author has used three methods to analyse the relationship of faulting to stress and strain. Three methods were used so that a comparison of the techniques and results could be made. Two of the three methods, the P and T-axes method and M-plane method, are graphical, both requiring relatively little data manipulation. The other technique, the reduced stress tensor method, is a numerical iterative method designed for processing by computer. All the techniques require the fault plane

orientation and direction of fault slip. For the reduced stress tensor and P and T-axes methods the sense of movement of each individual fault is required. In addition, the reduced stress tensor method requires that the observer give a confidence value for the sense of movement. From here on the term slip vector is used to describe the measured movement vector on the fault plane, regardless of whether the vector was measured from a slickenside striation or calcite fibre lineation.

4.3.1. Graphical Methods.

For both the graphical methods it is assumed that for any individual fault the intermediate stress axis (σ_2) lies within the fault plane, and has not been involved in the development of the slip vector. This implies that the shear stress on the fault plane is related purely to axial tension and axial compression. Movement planes (M-planes) for the fault containing the maximum compressive stress (σ_1) and minimum compressive stress (σ_3) can then be defined (Figure 4.3). The M-plane is defined on a stereonet by a great circle that passes through the pole to the fault on which movement has occurred and the corresponding slip vector (Aleksandrowski, 1985). Once the M-planes are defined the poles to the M-planes, M-poles, can be plotted.

4.3.1.1. Intersection of M-Planes Method.

Arthaud (1969) proposed a graphical method for determining the principal stress directions based on the concept of movement planes. In Arthaud's (1969) method the sense of movement on each fault need not be known, in this method it is sufficient to know movement sense merely for a part of the slip vectors. Aleksandrowski (1985) modified the Arthaud (1969) technique so that both axial and triaxial stress fields could be taken into consideration. In the Aleksandrowski (1985) method the magnitude of intermediate stress on the motion is considered which distinguishes the method from other graphical methods. For triaxial stress methods secondary grouping of M-plane intersections (3 or more) are searched for and tested to see if they lie on great circle zones. Spurious intersections and inherent errors of a few degrees in plotting M-planes can produce sufficient noise to make the method impractical.

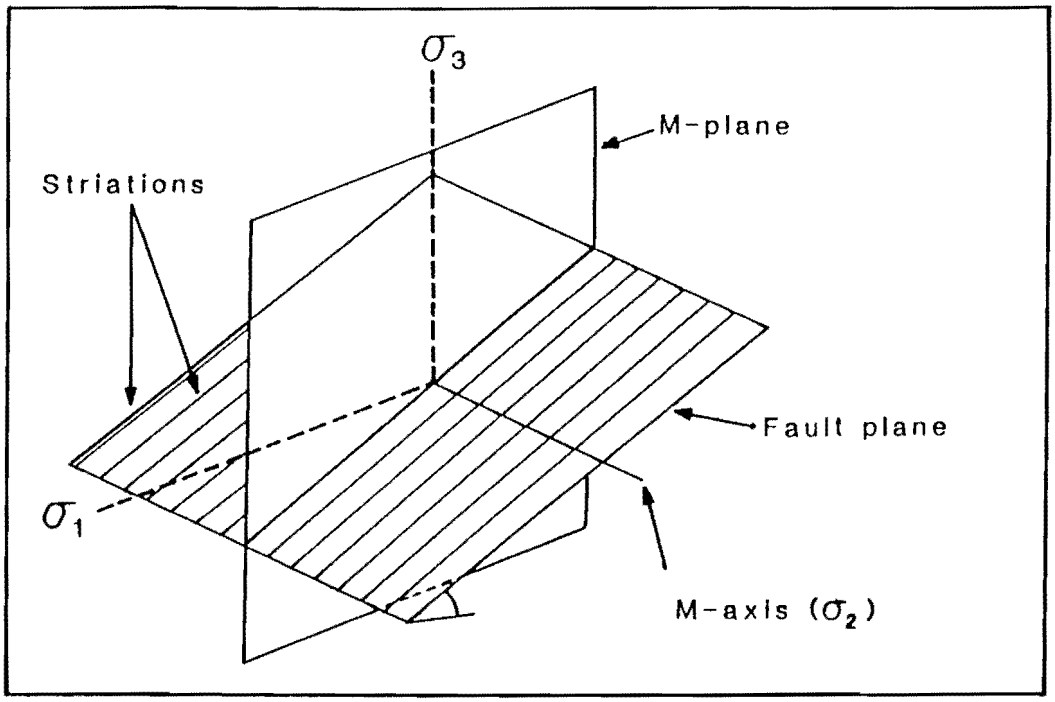

Figure 4.3. A schematic sketch of a reverse fault plane with striations developed on it and the corresponding movement plane (M-plane) of one of the striae (After Nicol and Campell, 1990).

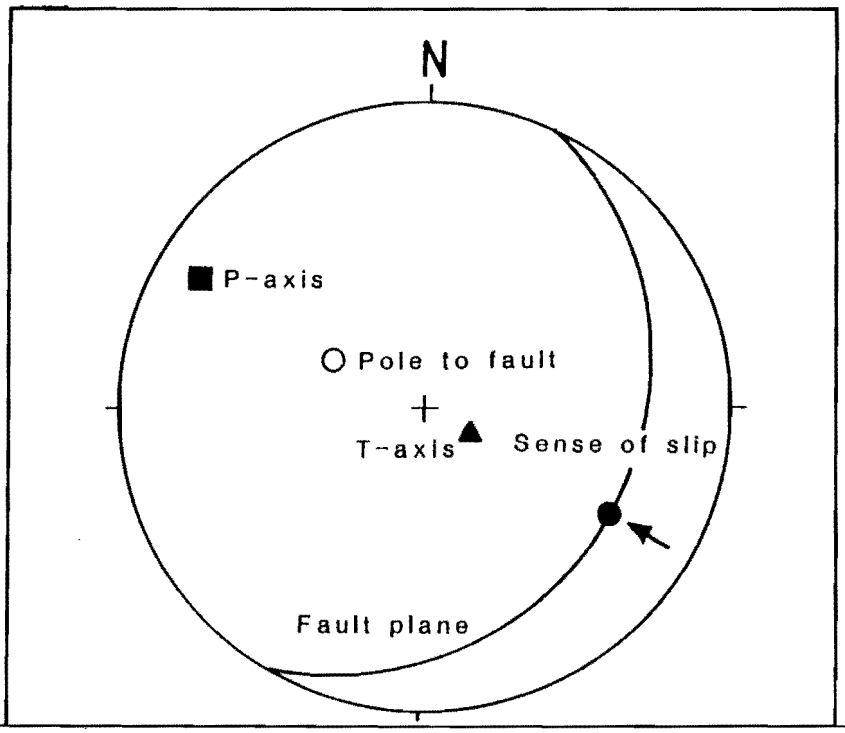

Figure 4.4. Geometry of fault-slip kinematics using the P and T-axes method in lower hemisphere, equal area stereographic progection. The principal incremental shortening axis (P-axis), principal incremental extension axis (T), the slip direction and pole to the fault lie in a common great plane. Each of the principal axes form angles of 45° with both the slip direction and pole to the fault.

For an axial stress field, where $\sigma_2=\sigma_3$ or $\sigma_1=\sigma_2$, the M-planes will intersect at a common point which defines the position of σ_1. The corresponding M-poles define a great circle in which both σ_2 and σ_3 are contained. However, their exact location in the great circle has to be determined by the P and T-axes technique (Aleksandrowski, 1985). The coverse axial stress field, where $\sigma_1=\sigma_2$, is not common and does not tend to be considered, but from the geometry of the M-plane technique σ_3 would coincide with the pole to the M-plane girdle or the concentration of intersections. Therefore, while the M-plane method can use data for which the orientation but not the sense of movement is known, in practice slip directions or some other constraints from the tectonic setting are necessary to distinguish the two axes.

The influence of σ_2 on fault planes of various orientations results in a wide range of M-plane orientations. The graphical M-plane method proposed by Aleksandrowski (1985) is applicable to a general triaxial stress state. The technique is based on the pattern of behaviour of M-planes in response to changes in the magnitude ratio between the principal stresses. The technique is used separately to analyse whether a given fault orientation lies within the plane containing a given slip vector. If it does lie within a slip vector plane the orientation can be defined and labelled σ_1, σ_2 or σ_3 from field evidence.

4.3.1.2. P and T-axes Method.

In earthquake first motion studies seismologists define the tension (T) axis as the direction in which compressional first motion outward from the focal sphere is greatest, and the pressure (P) axis as the direction where dilation is greatest (Cox & Hart, 1986). Angelier & Melchler (1977) proposed a technique that is similar to this. The technique identifies the pressure (P) and tension (T) axes, which correspond to the principal shortening and extension axes respectively (Figure 4.4).

The first step in a kinematic analysis is the graphical construction of the principal incremental shortening (P) and extension (T) axes for a given population of faults. The method assumes that only P and T-axes are responsible for the slip vector on a fault

plane, and that P must lie on the M-plane. The P and T-axes method assumes the P-axis is 45° from the pole to fault and the slip vectors (Marrett & Allmendinger, 1990), while the T-axis is 90° to the P-axis (Figure 4.4). The sense-of-slip is necessary to distinguish between the two axes. The following analysis includes only those fault planes that plotted within 5° of the slip vector. On faults in which the sense of slip is known, the intermediate (I) axes are equated with M-poles. With the analysis of a large number of faults the P, I and T-axes are inferred to cluster around the local orientations of σ_1, σ_2 and σ_3 respectively. The P-axes and T-axes can be contoured which effectively averages them and provides descriptions of their directional distributions (Marret & Allmendinger, 1990).

4.3.2. Numerical Method: Reduced Stress Tensor.

A stress tensor is an array of data representing the orientation of magnitude of stresses in space. A stress tensor can be defined for any given fault and defines the stresses required to initate movement in the slip direction of the fault. The last decade has seen a number of methods proposed for determining stress tensors from the inversion of fault data (Etchecopar et.al., 1981; Armijo et.al., 1982; Angelier, 1984; Reches, 1987). All the techniques aim to determine the best stress tensors for a given population of faults by removing the erratic members of the population and analysing these separately.

Problems associated with calculating actual stress magnitudes make derivation of the stress tensor difficult. However, Angelier (1979) has demonstrated that a reduced stress tensor for a given slip vector can be defined by four variables; σ_1, σ_2, and σ_3, (where $\sigma_1 \geq \sigma_2 \geq \sigma_3$) plus a fourth parameter, ϕ, representing the ratio of the principal stress differences:

$$\phi = \frac{\sigma_1 - \sigma_2}{\sigma_2 - \sigma_3}$$

The value of ϕ defines the geometry of the stress ellipse. An array of the four variables only defines a 'reduced' stress tensor as detail of the stress magnitudes in the actual stress tensor are not contained in the reduced stress tensor (Angelier, 1989).

The stress tensor analysis in this study uses a computer program written by Hardcastle and Hills (1991), which uses the philosophy developed for earthquake focal mechanisms by Gephart & Forysth (1984). The program automatically checks approximately 10000 tensor configurations by rotating σ_2 and σ_3 in 10° intervals about σ_1, and in turn moves σ_1, over a lower hemisphere stereonet in 10° increments. In this way all possible stress axes orientations are considered for every fault in the data set. For each, a range of coefficients of friction and fluid pressure are examined using Bott's (1959) techniques. This is done to determine 1) if a fault of that orientation would move under those conditions, and 2) what its motion vector would be. If movement is predicted to occur, the expected slip vector is calculated and compared to the actual measured slip vector, the angle between the two slip vectors representing the angular divergence. If the angular divergence is less than a user defined angle (here 25°) the tensor configuration is recorded as being possible on that fault. These selected faults are weighted for output of results by three levels of certainty recorded in the field from the reliabilty of motion sense indicators. If more than a given percentage of faults (here 25%) are recorded in this way the stress tensor is stored for later plotting. Finally, three equal area stereonet plots of σ_1, σ_2 and σ_3 are contoured. The contours surround the areas in which a stress axis could have been located for a given percentage of the total fault population which has moved. Should any 'erratic' members of the population be present or several populations be indicated, these will appear either on the fringes of the plot or as separate clusters. The resultant plots are a weighted, where each fault is treated discretely, and its motion calculated with minimal assumptions as to the distribution and nature of the total population(s).

4.4. RESULTS OF ANALYSIS.

The kinematic analysis of the mesofaults was carried out at four localities within the cover rocks and at four localities within the Torlesse basement. This was done so as to enable comparisons of the local stress orientations to be made over the field area and also to separate out older deformation in the basement.

Slickenside striation and calcite fibre lineation data were collected from mesofaults developed in the cover sequence at Island Hills, Waitohi Downs, Kanuku Hills and Flaxdown Quarry. Similarly, slickenside striations from the Torlesse basement were collected from mesofaults at the Waitohi Gorge, Hurunui Fault, Island Hills and Taruna areas.

4.4.1. Late Cenozoic Stress Tensors in Cover Rocks.

The cover rocks yielded a total of 183 faults, most with approximately NE-SW and NW-SE orientated planes and moderately to poorly clustered slickenside striations (Figure 4.5., top two rows). The stress tensor data is presented in the lower portion of Figure 4.5. The shaded contours represent the total percentage of the derived stress tensors which fall within the defined areas. The principal stress axes at Island Hills and Waitohi Downs mainly plunge at shallow to moderate angles, but vary in orientation. The Kanuku Hills and Flaxdown Quarry areas are dominated by normal faulting and have undergone local NNW-SSE extension, consequently σ_1 (compression) is the steepest of the three principal stress axes. Surrounding this zone of extension are areas, Island Hills and Waitohi Downs, dominated by compression expressed at the surface as reverse and oblique reverse faults. These areas are characterised by sub-horizontal to moderately plunging SE-ESE orientated σ_1 and moderately plunging σ_2 and σ_3. These orientations and plunges are consistent with the oblique fault motion suggested by the striation data. All four localities are in close proximity to each other implying that changes in the relative values of the principal stresses occur over short (up to 5km) distances.

4.4.2. Late Cenozoic Stress Tensors within Basement Rocks.

Four areas, in or close to, the macroscopic faults in the Torlesse basement were examined for minor slickensided surfaces yielding a total of 88 faults. The faults had scattered to well constrained orientations of planes and slickenside striations (Figure 4.6., top two rows). Reliable motion sense was determined from 25 faults and used for determining the stress tensors (Figure 4.6., lower three rows) in the Waitohi Gorge, Island Hills and Taruna areas.

Figure 4.5. Lower hemisphere equal area contour diagrams of poles to faults and trend and plunge of slickenside striations from four localities within cover are contoured as percentages of the total sample population. Stress tensors ($\sigma 1$, $\sigma 2$ and $\sigma 3$) for the same localities derived from these data are contoured to show the total percent of the derived stress tensors within a given defined area, where 50, 70 and 100% of the stress axes derived within the black, black/striped and black/striped/dotted areas respectively.

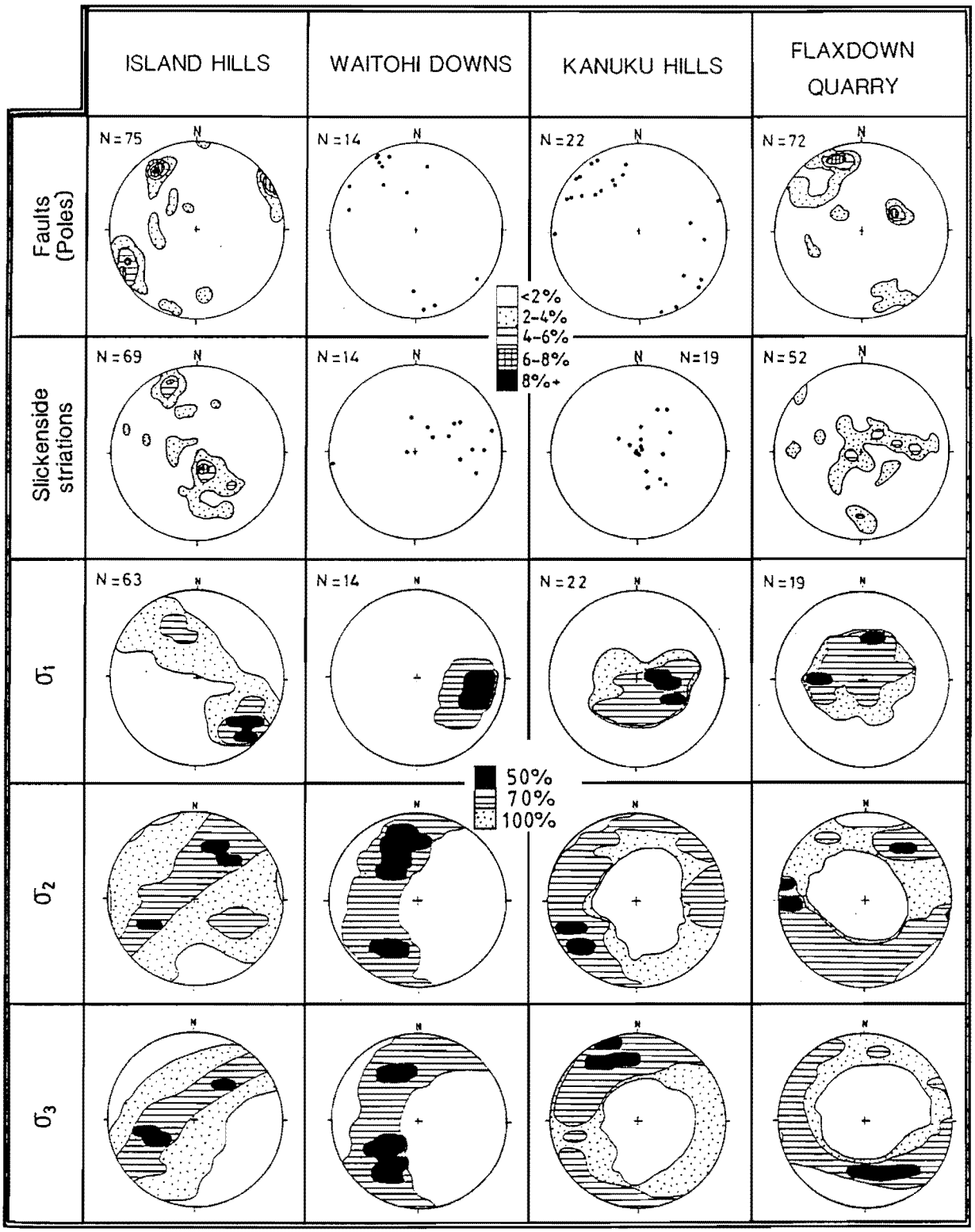
ISLAND HILLS
WAITOHI DOWNS
KANUKU HILLS
FLAXDOWN QUARRY
Faults (Poles)
Slickenside striations
σ_1
σ_2
σ_3
N=75
N=14
N=22
N=72
N=69
N=14
N=19
N=52
N=63
N=14
N=22
N=19
N
<2%
2-4%
4-6%
6-8%
8%+
50%
70%
100%

Figure 4.6. Lower hemisphere equal area contour diagrams of poles to faults and trend and plunge of slickenside striations from four localities within basement are contoured as percentages of the total sample population. Stress tensors ($\sigma 1$,$\sigma 2$ and $\sigma 3$) for the same localities derived from these data are contoured to show the total percent of derived stress tensors within a given defined area; where 50, 70 and 100% of the stress axes derived are within the block, black/striped and black/striped/dotted areas respectively.

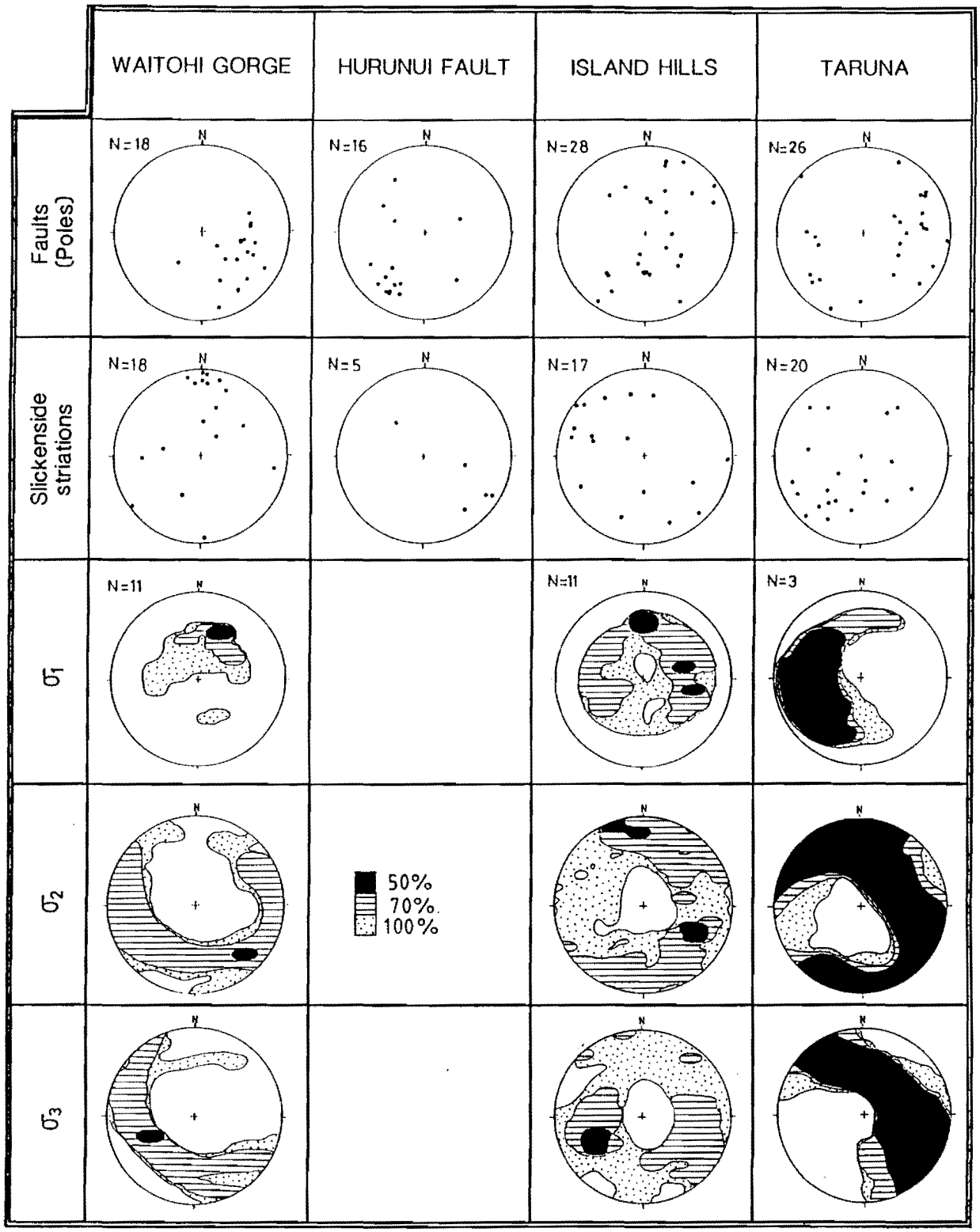
WAITOHI GORGE
HURUNUI FAULT
ISLAND HILLS
TARUNA
Faults (Poles)
Slickenside striations
σ1
σ2
σ3
N=18
N=16
N=28
N=26
N=18
N=5
N=17
N=20
N=11
N=11
N=3
N
50%
70%
100%

The principal stress axes derived for the Waitohi Gorge, Island Hills and Taruna areas are all inclined at shallow to moderate plunges, but vary in orientation. In the Island Hills and Taruna areas the principal compressive stress axis (σ_1) is oriented in the NNW and E, and W respectively. Both these areas display variations in the orientation of σ_1 such that they partially define a small circle. The orientation of σ_2 in the basement at Island Hills is comparable to the σ_1 for the cover rocks at Island Hills. It appears that the orientations of σ_1 and σ_2 may be interchangeable in the basement. This is also the situation in the Waitohi Gorge area where, based on the ESE vergence of the Waitohi Downs Fault, σ_2 appears to have changed with σ_1, with σ_2 now plunging glently SE. Approximately 5km to the NNE σ_1 plunges ESE and σ_2 plunges NNW for the cover rocks at Waitohi Downs. This suggests that as in the cover rocks, changes in the relative values of the principal stresses occur over moderate distances (up to 5km). The change in relative values need not be large and close values for σ_1 and σ_2 suggest constrictional tectonics occur. This is supported by the fault plane orientations and slickenside striation data as well as interference folding in the nearby cover rocks.

At Taruna a movement sense was only determined for three faults giving a poorly constrained σ_1 but one that plunges approximately gently to the W-WSW. Fault orientation and slickenside striation data, oblique reverse and reverse movements on the mesofaults, and field evidence of thrusting suggest the principal compressive stress would have a W-NW to E-SE orientation if the fault movements were associated with the Tommys Stream Fault. The orientation of σ_1, however, suggests that the last fault movement in the Taruna area was associated with the WNW striking Taruna Fault.

It has been found in this study and by Nicol (1991) that sense of movement data from late Cenozoic faults within the basement is best collected from or within close proximity of the late Cenozoic macroscopic faults. Motion sense on faults away from the late Cenozoic faults tends to reflect the principal stresses of pre-late Cretaceous phases of deformation in the Torlesse basement. A further observation to come out of this study is the way in which the principal stress axes plot around partial to near complete small circles. This may show that in, or close (100m) to, the major faults the

orientations of the principal stresses may be rotated. Alternatively, preexisting discontinuities produce failure conditions (e.g. wedge failures) where the fault planes develop movement indicators which differ from those created if the fault formed in a homogeneous mass.

4.4.3. Cumulative Stress Tensors of the Cover and Basement Rocks.

The four areas in the cover rocks were combined as were the three areas in basement to produce plots of the total cover and total basement principal stress axes (Figure 4.7). The total plot of the acceptable stress tensor orientations for the cover rocks displays two dominant orientations for σ_1; 1) moderate to steeply N-NNE plunging and 2) plunging gently to the SE. These orientations lie within a girdle distribution. The NNE plunging σ_1 orientation primarily reflects the result of oblique normal and normal faulting in the Flaxdown Quarry and Kanuku Hills areas respectively. Faulting with a normal component in the Island Hills area (representing 26% of the faults) adds to the concentration.

The less significant SE plunging σ_1 orientation is indicative of the regional NW-SE compression and mainly reflects data sampled from Island Hills. The cumulative plot of data from the cover rocks is statistically dominated by fault and striation measurements from Island Hills. Despite this the cumulative plots still appear to reflect local variations in the principal stress axes orientations. These changes appear to result from local changes in stress tensors causing meso-fault motion, which in turn suggest that strain is also locally variable. This variability may be enhanced by the collection of much of the fault data within confined areas (e.g. the Flaxdown Quarry).

A plot of the total acceptable stress tensors from the basement is similar to that for the cover in that the orientations of the principal axes reflect the orientations of the stress tensors from individual areas. Principal compressive stress (σ_1) in the basement is divided into two populations of differing orientations but similar plunges. The predominant concentration of acceptable σ_1 orientations plunges moderately N-NNE while the second less prominent concentration plunges moderately W-WSW.

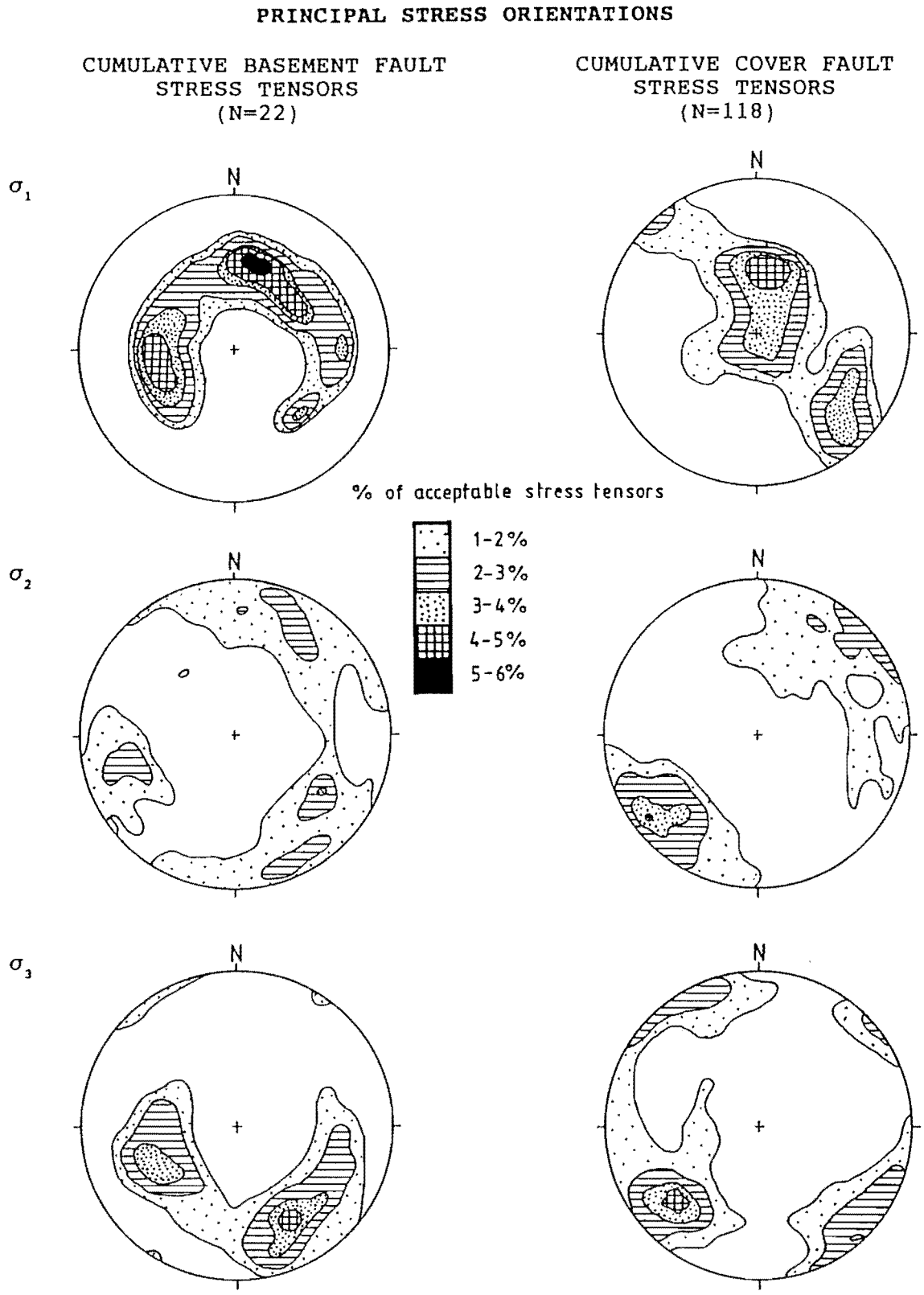

Figure 4.7. A comparison between the principal stress orientations derived via the stress tensor method for basement rock faults and cover sequence faults.

The dominant plunge and orientation of σ_2 in the basement is gently-moderately to the SE. This orientation is approximately perpendicular to the σ_2 orientation in the cover rocks. There is, however, a significant concentration of acceptable σ_2 orientations in the WSW which have a relatively similar orientation and plunge to that of σ_2 in the cover rocks (Figure 4.7). The orientation of σ_3 in the basement shows a similar trend to that of σ_2, in that the dominant concentrations of acceptable σ_3 orientations are approximately perpendicular to each other (Figure 4.7). There is also a significant concentration of acceptable σ_3 orientations that plunge moderately WSW. The orientation of this is slightly W of the σ_3 for the cover rocks and the plunge of the basement σ_3 is somewhat steeper than that for the cover rocks. A feature of the prinicpal stress axes derived from all the basement faults analysed is their partial distribution around small circles, of particular significance is the steep SE plunge of an axis to a cone that defines the distribution of σ_1.

The comparison of the total acceptable orientations of the principal stresses indicates that there is a minor, but significant, correlation between the principal stress orientations of the cover rocks and the basement rock or within close proximity (200m) of the late Cenozoic macroscopic faults. All the principal stress axes shown in Figure 4.7 are gently-steeply inclined to the horizontal indicating oblique motion has occured.

The normal faulting that occurs in the cover rocks is totally absent in the basement, this is exemplified by the absence of σ_1 orientations with steep plunges. The major concentration of σ_1 in the basement results from oblique reverse movements on mesofaults within or close to the NNE-NE striking macroscopic thrusts. The girdle distribution of σ_1 orientations in the cover reflects the affects of folding and associated changes in local strain partitioning. The plot of σ_1 from the basement rocks close or within the late Cenozoic macroscopic faults should, therefore, provide a more reliable indication of the regional stress for the study area. However, the partial fit of the stress tensors to small circles and the movement on the WNW striking faults suggest that defining the principal compression direction is far from simple. Similarly, the diffuse orientations of σ_2 and σ_3 for basement do not help in resolving the orientation of σ_1.

To the south in the mid-Waipara region Nicol & Wise (in press) has found that basement close to the macroscopic faults is rotated, this may explain some of the disparities in the orientations of the principal stress axes from the basement and the cover rocks. It is here inferred that if the unconformity surface could be rotated back to horizontal and the basement mesofaults close to the macroscopic faults could be corrected for this rotation and then the fault data were inverted by the stress tensor method, σ_1 for the basement may prove to be more comparable with the regional stress tensor derived for the cover rocks.

One relevant point that may be rised here is that most of the basement fault data comes from the hanging wall while the cover data comes from the foot wall side of the major faults. Experimental work on the propagation of the effects of reverse faulting in rigid basement into overlying cover rocks (Ameen, 1988) shows that locally strain partitioning is important (Figure 4.8).

4.4.4. Results of the M-Plane Technique.

According to Aleksandrowski (1985) in the case of a radial stress tensor all the movement planes have one common intersection point which coincides either with the position of σ_1 or σ_3, distinguishing between σ_1 and σ_3 can be based on field evidence and/or knowing the movement sense of a few faults. The Hurunui Fault area was the only area in this study to produce a single common intersection point of movement planes in the Torlesse basement (Figure 4.9). The other three areas within basement (Figure 4.9) and all the areas in the cover sequence (Figure 4.10) produced multiple intersection concentrations commonly distributed along a great circle. The M-planes from the Hurunui Fault area are orientated NE-SW and are defined by M-poles that exhibit a partial girdle distibution. This distribution along a single great circle is a trace of the plane containing σ_2 and σ_3 where $\sigma_2=\sigma_3$ for C= ∞ where

$$C = \frac{\sigma_1-\sigma_2}{\sigma_2-\sigma_3}$$ (Aleksandrowski, 1985).

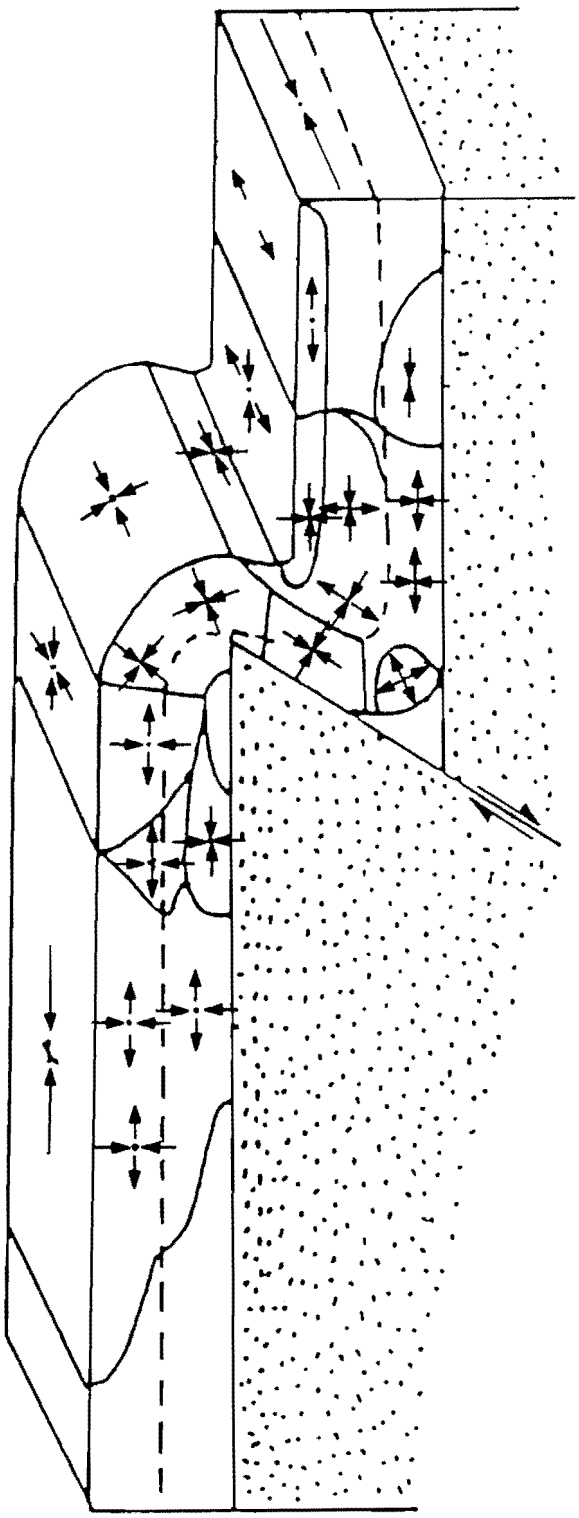

Figure 4.8. An experimental model showing the effects of reverse faulting in a rigid basement on a layered, ductile cover. (After Ameen, 1988).

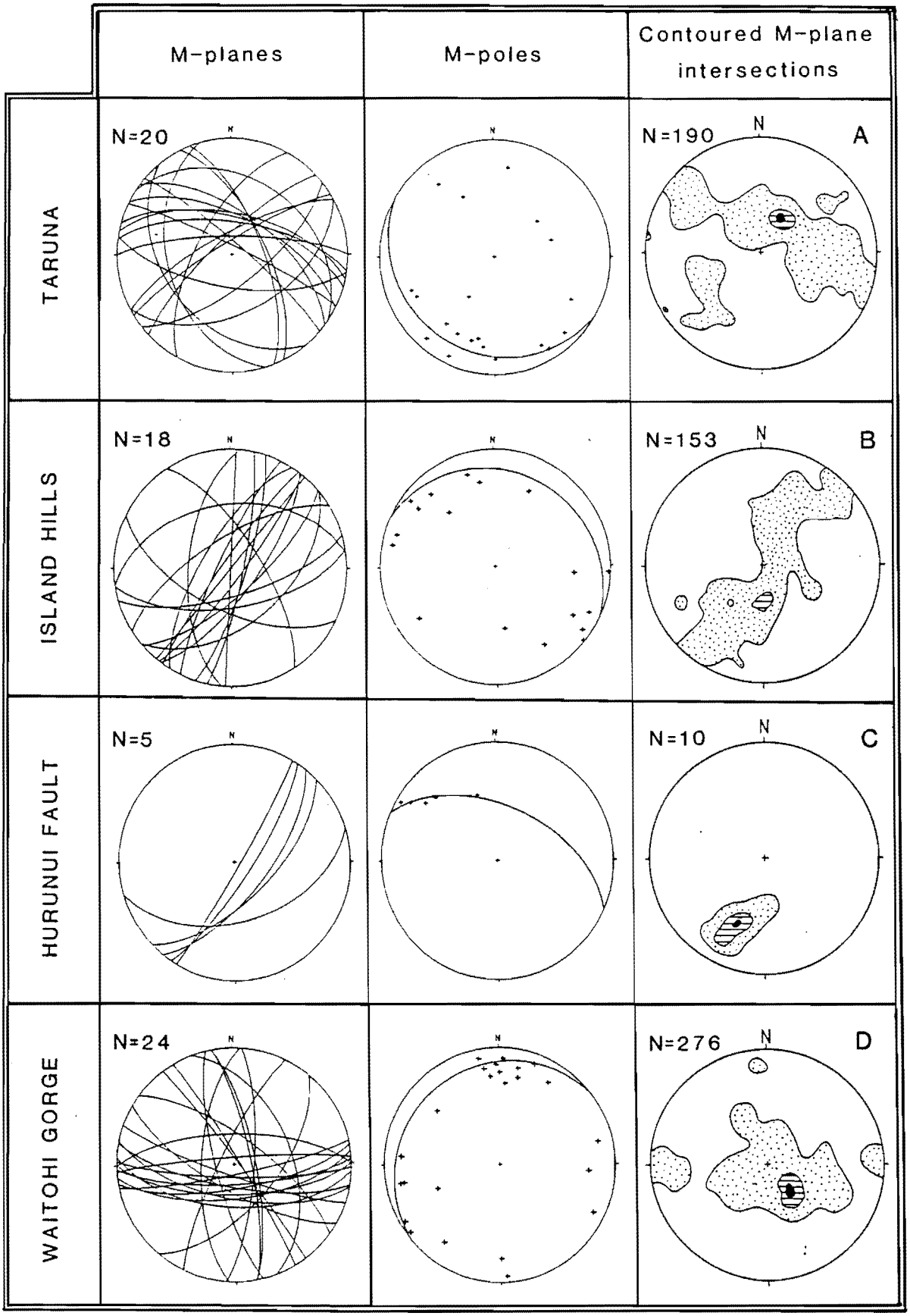

Figure 4.9. Lower hemisphere equal area nets of M-poles for meso-scale faults within the basement rocks. The right hand column is a contoured equal area plot of the M-plane intersections.

Contour intervals for Figure 4.10

A	B	C	D
1–5%	1–7%	1–3%	1–7%
5–9%	7–13%	3–5%	7–13%
9+%	13+%	5%+	13+%

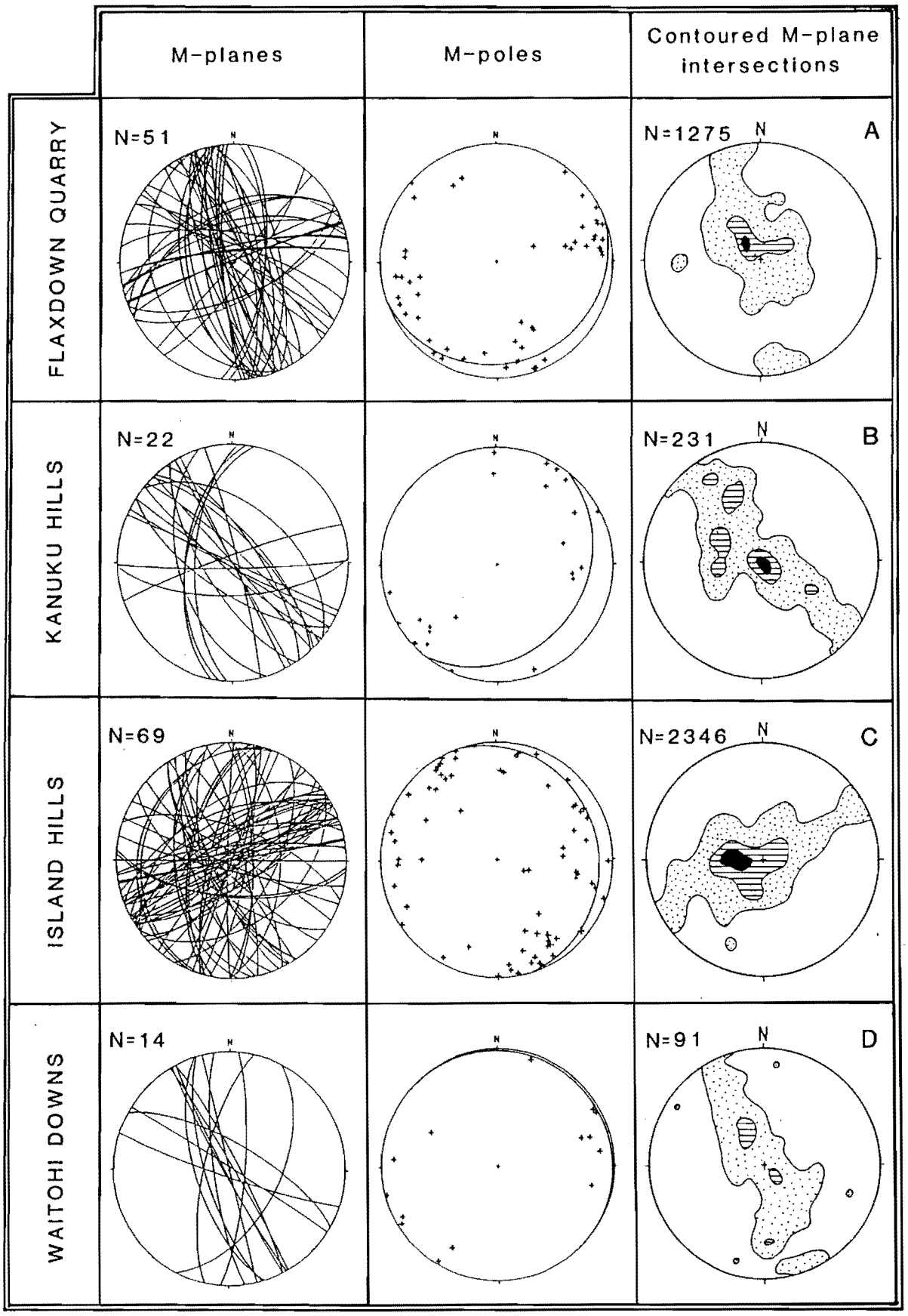

Figure 4.10. Lower hemisphere equal area. nets of M-planes and M-poles for meso-scale faults within the cover sequence. Right hand column is a contoured plot of the M-plane intersections.

4.4.4.1. Basement Fault Data.

A contoured equal area plot of M-plane intersection points (Figure 4.9) from the Hurunui Fault exhibits a single main concentration that equates to the orientation of σ_1 that plunges moderately-gently SSW. Although no reduced stress tensor data was compiled from the area this orientation is interpreted from field observations and structure contouring of SW verging thrusting on the Hurunui Fault to be σ_1.

In the Waitohi Gorge area mesofaults collected from within the highly fractured Torlesse of the Waitohi Downs Fault exhibit two sets of M-planes (Figure 4.9). There is a dominant E-W set and a less prominent more scattered N-S set. The M-poles to the M-planes are predominantly concentrated in the N, W and E sectors and generally do not define a great circle. The main concentration of M-plane intersections plunges steeply to moderatly SE, this, however, results from the intersection of two M-plane sets. This requires separation of the two sets and would probably result in two concentrations of M-plane intersections (σ_1) with one that plunges gently W and another concentration that plunges gently N or S. A gentle E-W plunging σ_1 would be in keeping with the oblique-reverse fault offsetting of pillow lavas within the Torlesse in the Waitohi Gorge area. An E-W orientation for σ_1 is almost perpendicular to the result for σ_1 from the stress tensor method at Waitohi Gorge but coincides with one of the concentrations from the cumulative data. Conversely, if the M-plane intersections equate to σ_3 as occurs in a constrictional environment, then the correlation is quite good.

At Taruna mesofaults from within Torlesse in the fault zone of the Tommys Stream Fault exhibit two sets of M-planes (Figure 4.9). The first set is a minor NE-SW set that is perpendicular to the main W-NW to E-SE set. The M-poles concentrate mainly in the SW and SE quadrants close to the primitive circle and show a crude partial great circle distribution striking WNW-ESE and dipping gently SSW. This suggests that both the σ_2 and σ_3 principal stress axes lie within this plane, however, the dip of the plane differs from that defined by the stress tensor method. The partial fit of a great circle to the M-poles is probably only an apparent feature as the great circle plots through

two concentrates of M-poles that relate to different sets of M-planes. The contoured plot of M-plane intersection points exhibits a main concentration equating to σ_1 that plunges moderately-steeply NNE-NE. It is apparent from the M-planes plot that this concentration is a result of the intersection of M-planes from the two sets observed forming a great circle distribution. If the two sets were analysed independently the dominant W-NW set would display a σ_1 orientation that plunges gently either WNW or ESE, in agreement with the poorly defined σ_1 orientation derived from the stress tensor method.

M-planes from the basement rocks of the Island Hills area (Figure 4.9) form at least two sets, one orientated NNE-ENE to WSW-SSW and a less abundant NW-SE set. The NNE-ENE set predominates with their respective M-poles concentrating in the NW and SE quadrants. The contoured plot of M-plane intersections suggests σ_1 plunges moderately-steeply south. The overall plot of intersection points, however, indicates a NE-SW orientation for σ_1. Both the main and NW-SE concentrations differ from σ_1 derived using the stress tensor method. The stress tensor method suggests that the main concentration of M-plane intersections may correspond to σ_3 and that σ_1 and σ_2 are contained within a moderately plunging, NW striking great circle. This is indicative of extensional faulting, a conclusion supported by numerous oblique normal and normal mesofaults observed within the basement and cover rocks in the Island Hills area. Compressional tectonics, however, are indicated by the asymmetric, Island Hills syncline and the reverse west verging Island Hills Fault. It seems that the M-planes technique may indicate that the concentration of intersections equates to the orientation of σ_3 suggesting that σ_1 and σ_2 are of similar value forming a constrictional stress field in which normal faulting is locally important.

4.4.4.2. Cover Fault Data.

As with the mesofaults in basement the small-scale faults within the cover rocks display at least two sets of M-planes (Figure 4.10), one dominant set that strikes NE-ENE to SW-WSW and another NW-N to SE-S set. The corresponding M-poles plot close to the primitive circle in the SE or NW and NE or SW quadrants respectively,

and exhibit a poor fit with a great circle. Consequently, it is inconclusive as to whether the area is undergoing axial compression. The orientation of the dominant set of M-planes is similar to that of the dominant set in the basement rocks at Island Hills. This feature is supported by the NE-NE to SW-WSW girdle distribution of M-plane intersections. The main concentration of M-plane intersections suggest, however, that σ_1 plunges moderately to steeply west. An orientation such as this differs by approximately 90° to that obtained by the M-plane method for the basement. Similarly, the M-plane method for the cover rocks shows a poor relationship to the gently, SE plunging σ_1 derived from the stress tensor method.

In the Waitohi Downs area the M-planes form three sets (Figure 4.10). The NNW-SSE set is the most abundant while the lesser sets strike approximately WNW-ESE, and NNE-SSW. With the limited data from this area it is difficult to determine whether the M-poles plot along a great circle. It can be said however, that the M-poles to the main set of NNW-SSE M-planes plunge steeply and trend ENE-WSW. If the M-plane sets were analysed individually as suggested by Aleksandrowski (1985) for multi-populations σ_2 and σ_3 would plot in a plane that strikes approximately NE-SW. This is supported by the results of the stress tensor method for σ_2 and σ_3.

Sigma 1 at Waitohi Downs is predicted, using the main concentration, to plunge moderately to steeply NNW-SSE, which differs from the ESE plunge that is derived by the stress tensor method, a difference that may result from the different methodology of the two techniques. The main concentration, however, is a manifestation of the intersection of two (NNW-SSE and WNW-ESE) or possibly three (NNE-SSW) sets of M-planes. The NW-NNW to SE-SSE girdle distribution of M-plane intersections is taken as the orientation of σ_1, while the main set of M-planes inplies a gentle plunge to the NW-NNW for σ_1. A σ_1 of this orientation is also in accord with that from the stress tensor method and agrees with the oblique reverse movement of the Waitohi Downs Fault in this area.

M-planes derived from faults collected in the Kanuku Hills area form three sets. The first and by far the most abundant set strikes NW-SE (Figure 4.10), while the two lesser sets strike N-S and E-W. The NE and SE concentration of M-poles reflects the dominance of the NW-SE striking M-planes. The M-poles exhibit a poor correlation to the best fit great circle, a consequence of the computer program taking into account the three M-pole sets. The contoured equal area plot of M-plane intersections indicates σ_1 to plunge vertically. This is in very close accord with the σ_1 orientation predicted by the stress tensor method. Furthermore, a vertical σ_1 distribution from the M-plane method is in agreement with the macroscopic normal faulting observed in the field at Kanuku Hills.

In the Flaxdown Quarry the mesofaults measured display M-planes that can be grouped into two sets that strike NW-N to SE-S and E-ENE to W-WSW (Figure 4.10). The corresponding M-poles predominantly have steep plunges to ENE-NE, WSW-SW and SSW reflecting the two sets of M-planes. The M-poles display a partial fit to a best fit great circle that strikes WSW-ENE, the great circle does, however, pass through the two sets of M-poles and hence is unlikely to represent the true plane in which σ_2 and σ_3 lie. The resultant equal area contoured plot of M-plane intersections shows a predictable steeply NW plunging concentration for σ_1. If, however, the two sets were individually analysed it is possible that σ_1 for the predominant M-plane set would plunge gently NNW or SSE.

4.4.5. P and T-axes Results.

When a large data set of mesofaults (30+) is analysed by the P and T-axes method of Angelier & Mechler (1977) a clustering of P-axes, I-axes and T-axes will occur that equates to the local orientations of σ_1, σ_2 and σ_3 respectively (Marrett & Allenendinger, 1990).

4.4.5.1. Cover Fault Data.

The analysis of mesofaults on which movement sense was determined in the cover rocks of the Island Hills area, produced a cluster of P-axes equating to a shortening

direction that plunges gently to the SE-SSE (Figure 4.11). The distributions of the intermediate and extension strain axes are similar and suggest that the stress axes may be interchangeable. The result of the P-axes orientation for the shortening axis and the distribution of the intermediate and extension axes agree strongly with the axial compressive stress field defined by the stress tensor method for the cover rocks.

Calculation of P-axes in the Waitohi Downs area defines a cluster of axes equating to a SE orientated, near horizontal principal shortening axis (Figure 4.11). The tight cluster of I-axes defines a gentle plunge to the SW for the intermediate axis while the distribution of T-axes is slightly more scattered. The intermediate and extension axes may be interchangeable suggesting an axial compressive stress field. The results of the P and T-axes method from the Waitohi Downs area display a strong correlation with the orientations derived for the principal stress axes using the stress tensor method. The results of the M-plane method differ in that σ_1 apparently dips moderately NNW, however, this reflects the presence of at least two sets of M-planes. The general girdle distribution of the M-planes do display a similar orientation ($\pm$ 10°) for σ_1 to that of the stress tensor method and the principal shortening direction of the P and T-axes method.

A tight cluster of P-axes from the Kanuku Hills area defines a steeply S-SSE plunging shortening axis (Figure 4.11). The I-axes define a gently S-SW plunging intermediate axis while the T-axes define two clusters for the extension axis that plunge gently SSE and NNW. The principal strain axes are indicative of local axial extension which is in keeping with field observations and the results of the stress tensor and M-plane methods.

A tight cluster of P-axes from the Flaxdown Quarry area define a principal shortening axis that plunges moderately N-NNE (Figure 4.11). There are, however, two other significant clusters of P-axes that warrant discussion. One cluster defines the shortening axis to plunge gently-moderately SE and the other to plunge steeply to near vertically SE (Figure 4.11). The first cluster can be related to the east verging thrusting of the

Contour intervals for Figure 4.11

A	B	C	D
2-6%	2-6%	1-3%	3-9%
6-10%	6-10%	3-5%	9-15%
10%+	10%+	5%+	15+%

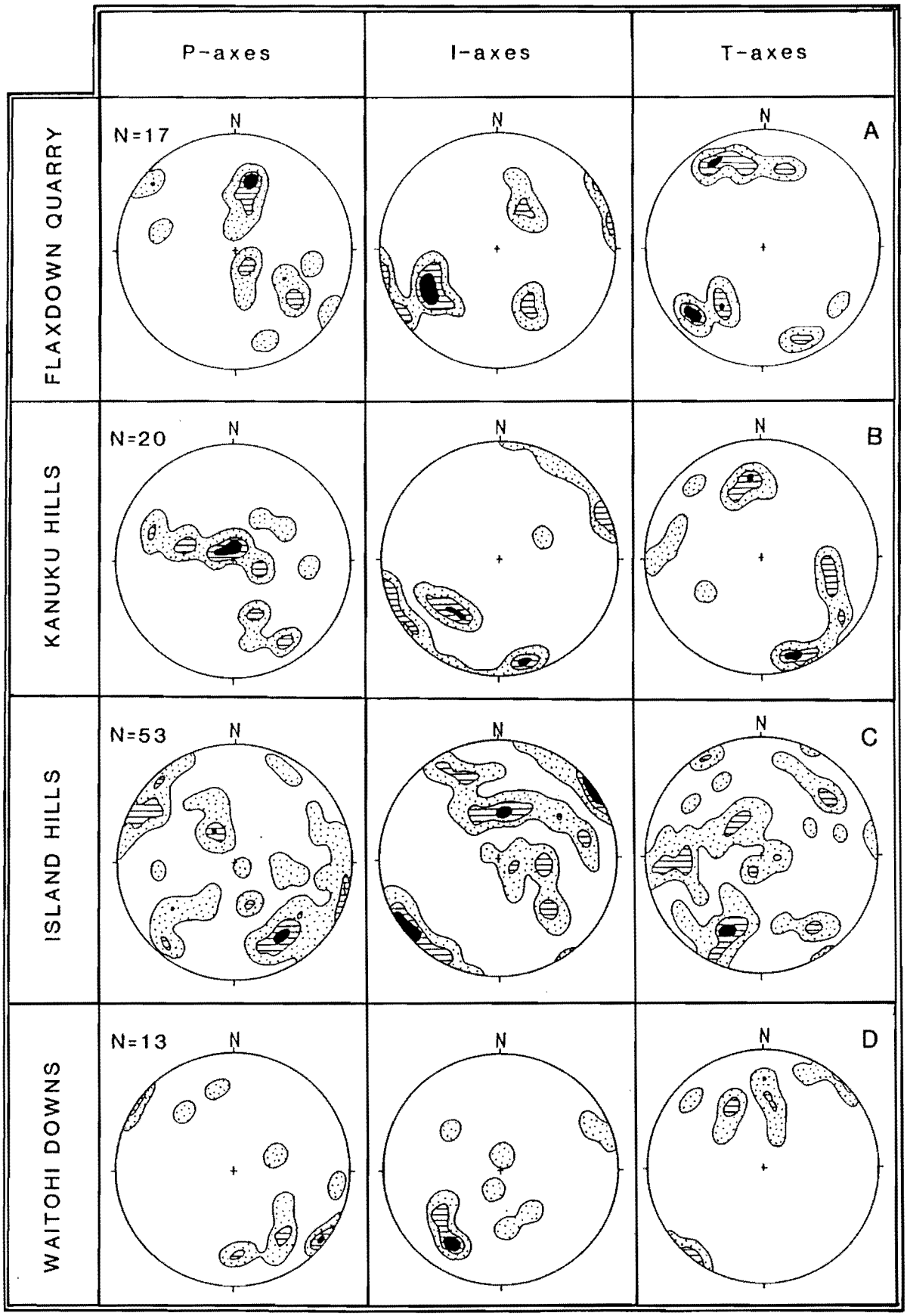

Figure 4.11. Spherical gaussian contoured incremental shortening axes (P-axes), intermediate axes (I) and extension axes (T) for meso-scale faults within the cover sequence.

Waitohi Downs Fault, and the associated folding of the cover rocks. The second cluster relates to local oblique-normal and normal faulting in the Flaxdown Quarry area. This is a result of gravitational collapse because of the location of the cover rocks beneath the fault plane (see Cross sections in Map pocket), and has been predicted from experimental modelling (Ameen, 1988) of stress around reverse faults (Figure 4.8). The main clusters of I and T-axes have a similar gentle plunge to the SW indicating that extensional tectonics are significant in this area. The main clusters of P and I-axes define orientations for the shortening and intermediate axes, respectively, that are consistent with the results from the stress tensor method. The two methods do, however, differ slightly in the orientation of the extension axis, although the methods do display similar plunges. The P and T-axes method defines the extension axis to plunge gently-moderately SW while σ_3 from the stress tensor method plunges SSW-SE.

4.4.5.2. Basement Fault Data.

The orientations of the principal strain axes in the four areas within the basement were resolved using the P and T-axes method. The main cluster of P-axes for the basement rocks at Island Hills equates to a SE orientated, moderately-gently plunging shortening axis. The plots of the T and I-axes are not as tightly defined (Figure 4.12) but may suggest that the basement in Island Hills area is presently undergoing axial shortening. This is comparable to the results obtained from the stress tensor method which indicate σ_1 to plunge gently SE.

The P-axes from the Waitohi Gorge define a shortening axis that plunges moderately to gentle SE. This differs markedly to the σ_1 orientation derived via the stress tensor method. The P-axes definition of the shortening direction is, however, the same as the σ_2 orientation derived from the stress tensor method, suggesting that in this area the P-axes method may be an oversimplification of the local strain given that many of the faults analysed are within volcanics of the Torlesse Supergroup which contain numerous preexisting discontinuities which are not taken into consideration by the technique (see section 4.5). The Waitohi Gorge area may approximate an axial

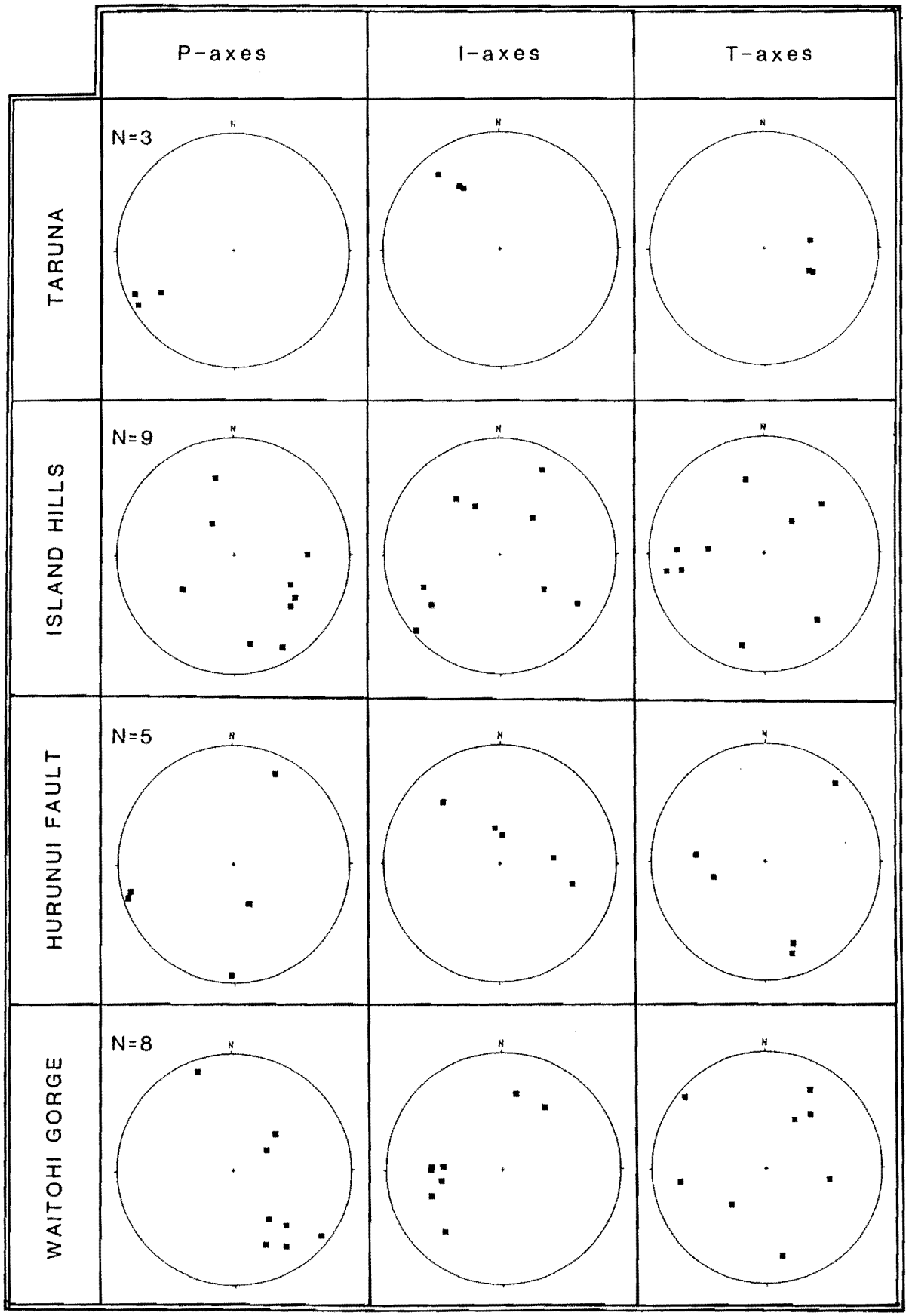

Figure 4.12. Lower hemisphere equal area plots of shortening, (P) intermediate, (I) and tension (T) axes for meso-scale faults within the basement rocks.

compressive stress field, although the results would be better defined with a larger data set.

In the Taruna area movement sense on only three mesofaults was determined, but the results of the P and T-axes method define tight clusters for the P, T and I-axes (Figure 4.12). The P-axes equate to a shortening direction that plunges gently WSW while the intermediate axis plunges moderately to gently NW. From these results, and the ESE verging thrusting of Tommys Stream Fault, it appears that either the shortening and intermediate axes are close in magnitude and changed positions or that the last fault movement in the area has been related to the WNW striking Taruna Fault. Close values for the shortening and intermediate axes infer constrictional tectonics, and this is supported by interference folding in the cover rocks at Mt. Mason. The results from the stress tensor method are poorly defined but indicate σ_1 to plunge moderately-gently SW indicating axial compression which may also be inferred from the P and T-axes method.

Insufficient mesofaults with a defineable movement sense were collected from the Hurunui Fault to delineate the orientation of the principal strain axes by using the P and T-axes method (Figure 4.12). Five mesofaults had slickenside striated surfaces, one was determined to have an oblique normal movement, the other four having been designated a reverse movement sense based on the results of the M-planes method. Field evidence of movement sense on the Hurunui Fault is inconclusive as to whether the fault is oblique reverse or oblique normal, but the topographical high to the NE is suggestive of reverse movement and this is supported by structure contouring of the fault.

The resultant P-axes for the Hurunui Fault display a scattered distribution, the P-axes derived from the oblique normal fault show a steep plunge to the SSE. The P-axes of the reverse faults are distributed in the SW and NE quadrants and all display gentle plunges. Two P-axes plunge gently WSW and are in close accord with the σ_1 orientation predicted by the M-plane method. The I-axes fit an orientation indicating

the intermediate axis may lie within a NW-SE striking NE dipping plane. The T-axes define a partial great circle that strikes NW-SE and dips SW. The small data set does show a crude relationship to the results of the M-plane method if the meso-scale faults have reverse movements, in that the P-axes indicate the shortening axis to plunge gently to the SW quadrant.

4.4.5.3. Cumulative Cover and Basement P-axes.

Cumulative equal area plots were made of all P-axes from both cover and basement rocks (Figure 4.13a & b). These two plots have been combined to produce a cumulative plot of all the P-axes derived from the study area (Figure 4.13c).

The presence of two significant clusters of P-axes in the plot of the cover rocks is indicative of local strain partitioning, the near vertical cluster of axes reflecting the orientation of the shortening axis in the Kanuku Hills and Flaxdown Quarry areas. The dominant cluster of P-axes defines a shortening axis that plunges gently SE-SSE, a consequence of the shortening direction derived from the Island Hills, Waitohi Downs and, to a lesser degree, Flaxdown Quarry areas.

Local strain partitioning is also evident in the cumulative plot of P-axes derived from within the areas of basement rock (Figure 4.13b). Two shortening directions are indicated, one plunging gently to horizontally WSW and the other plunging gently SE. P-axes from Taruna and the Hurunui Fault account for the WSW shortening direction while the Island Hills and Waitohi Gorge areas account for the SE orientation.

The cumulative plot of all the P-axes determined from the cover and basement rocks indicates that the predominant regional shortening axis plunges gently SE-SSE (Figure 4.13c). This orientaion is strongly influenced by the large number of mesofaults collected from within the cover rocks, and in particular from the Island Hills area. A SE-SSE orientation for shortening is, however, compatible with that derived from the cover rocks using the stress tensor method.

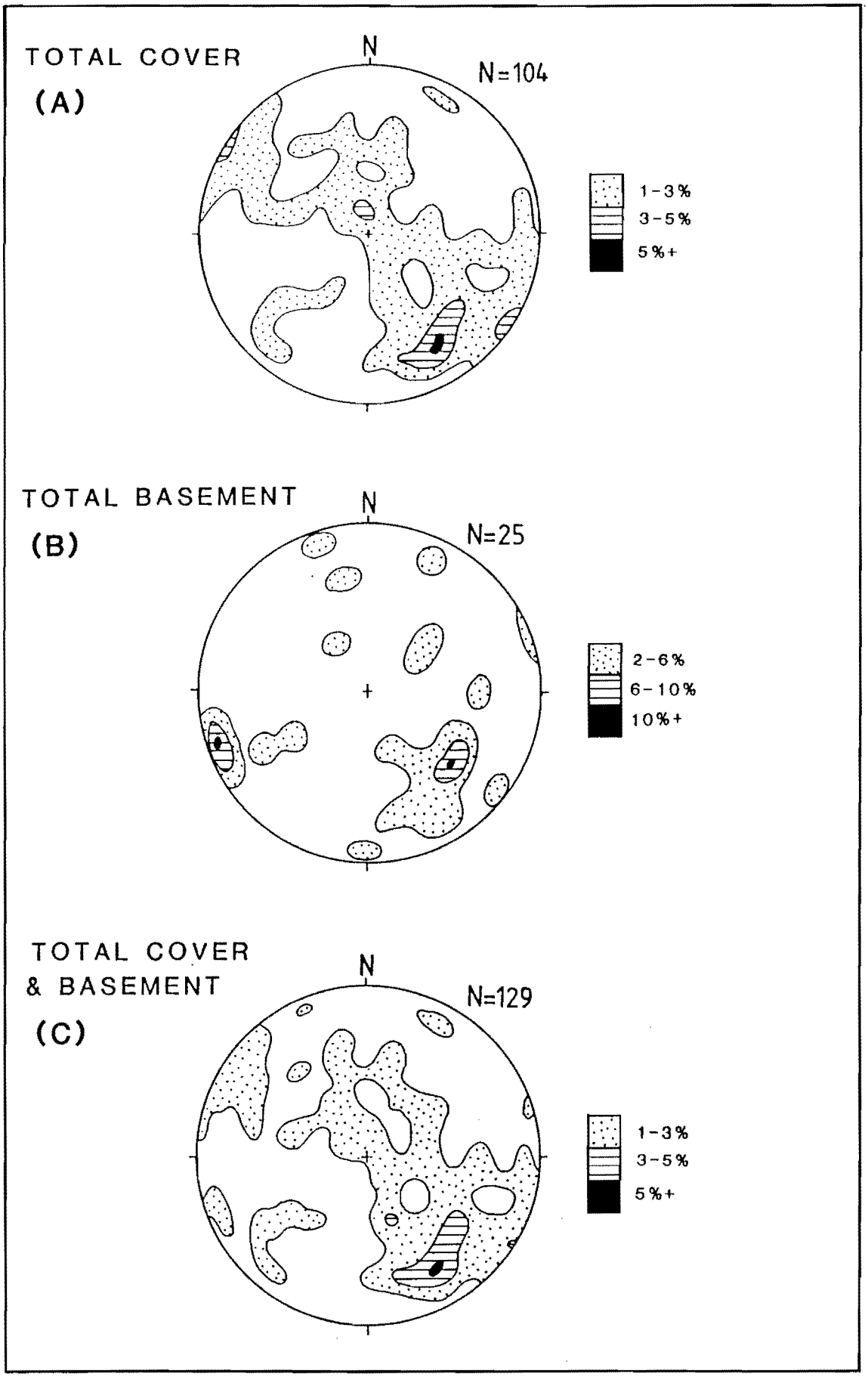

Figure 4.13. Cumlative, spherical gaussian contoured, plots of all principal incremental shortening axes (P) collected from the four areas of cover rock (A), the four areas of basement (B) and a total plot of all P-axes (C).

4.5. COMPARISON OF TECHNIQUES.

The stress tensor and P and T-axes methods exhibit a high degree of consistency between the results obtained. However, with the exception of Hurunui Fault and Kanuku Hills areas the M-plane method produces results incompatible with the first two techniques. The large differences between the M-planes and the other techniques can be partially attributed to differences in methodology and, if multiple populations of M-planes are present, the need for M-plane sets to be analysed individually.

The strength of a rock to resist faulting is derived from two sources. One is the natural cohesive strength (σ_o) of the rock and the second is the internal frictional resistance to faulting. The Mohr-Coulomb law of failure predicts the critical shear stress level (σ_c) which is required to fault a rock.

$$\sigma_c = \sigma_c + \tan\mu\ (\sigma_n)$$

where, σ_c = critical shear stress for the discontinuity
σ_o = cohesive strength
$\tan\mu$ = coefficient of internal friction
μ = angle of internal friction
σ_n = normal stress.

The angle of internal friction (μ) determines the angle (Θ) between the fault surface and the direction of greatest principal stress (σ_1). Based on the geometry of the Mohr stress diagram, $\mu = 90 - 2\Theta$. Since most rocks in nature possess an angle of internal friction (μ) between 25° and 35°, the value of Θ for most fault relationships is also commonly 25-35°.

The P and T-axes method does not take into consideration changes in internal friction resulting from pre-existing discontinuities in rock. Also, the method assumes that failure occurred on the plane of maximum shear stress where Θ is 45°. Experimentally, failure commonly occurs at Θ angles less than 45°, and often about 30° (Hobbs et al., 1976) indicating the P and T-axes method is an over simplification of failure conditions. This is certainly the case in Torlesse basement rocks which have undergone at least two phases of pre-Tertiary deformation and must have contained numerous pre-late Cenozoic discontinuities. These also exist in the cover rocks, and from field evidence are commonly exploited by the late Cenozoic deformation.

Pre-existing discontinuities in the rocks increase the factor of oversimplification as the technique assumes that the principal intermediate axis is always parallel to the fault plane. This is certainly not the case if wedge failure occurs on a pre-existing discontinuity and a late Cenozoic meso-scale fault. Furthermore, the value of the intermediate axis is not considered which may result in many spurious axial orientations.

With the M-plane method the angle of internal friction from the various discontinuites is empirically accounted for. If all the slip vectors are of the same set then failure on all the corresponding faults should have occurred at, or near, the same magnitudes of resolved shear stress. Only in the situation where the most optimally orientated discontinuities fail and the deviatoric stress is prevented from increasing to mobilise a wide range of orientations, will the derived σ_1 be close to the true Θ angle. As more than one population of M-planes exist in all the areas, except at Kanuku Hills and Hurunui Fault, the M-plane method provides a simplification of the Θ angle, and misleading orientations for σ_1.

The M-plane method requires some independent evidence of motion before the concentrations of M-plane intersections, in even a simple axial stress regime, can be assigned to be either σ_1 or σ_3. The technique is also sensitive to sets of M-planes in a few dominant orientations that inevitably intersect to produce a girdle concentration along these directions. The geometric complexity of the intersection patterns for non-axial stress fields makes Aleksandrowski's (1985) method more theoretical than practical, particularly if multiple populations of data are present.

The difference in methodology of the P and T- axes, and M-plane techniques accounts for the angular differences in the Θ angle produced by each method for the Hurunui Fault and Kanuku Hills areas. In the Kanuku Hills area, for example, the macroscopic fault planes strike NE-ENE and have vertical dips. The predicted Θ angle from the M-plane method is approximately 30°, substantially less than the 45° assumed by the P and T axes method, consequently two slightly different σ_1 orientations are produced.

Small differences might be expected between different locations using the M-plane method. Locations with dominantly slickensided faults, such as the basement rocks in this study area, probably remobilised under high transient co-seismic stresses, and from time to time may have periodically exceeded the shear failure limits on a wider range of fracture orientations. Conversely, areas dominated by calcite fibre lineations, such as commonly occurs in the cover rocks, imply positive pore water pressures were prevalent at the time of failure. The magnitude of the stress required for failure is reduced by positive pore water pressures (Hobbs et al., 1976), such that the values may be just large enough to cause failure. In the cover rocks of this study area a Θ angle close enough to the value at which failure may just occur might be expected. Without having separated the various M-plane populations from one another for the individual areas, combined with the small data sets, it has not been possible to juxtapose these effects.

The coefficient of friction, μ, and cohesive strength used in the reduced stress tensor method are determined by the user. In this study μ was set at 0.4, a value that is small enough to allow failure on a wide range of plane orientations relative to σ_1, while a value of zero, based on experimental work, was used for cohesive strength. The large range of orientations of reactivated planes means the value of Θ is typically closer to 45° than the minimum 34° set by the input parameters. This accounts for the consistency between the results of the reduced stress tensor and P and T-axes methods.

The reduced stress tensor method appears the best of the three used for analysing fault-slip data. The method is quickly handled by the Brute3 and Select computer programs (Hardcastle & Hills, 1991) and avoids the time consuming data manipulation that the other two methods require. Furthermore, the reduced stress tensor method uses a methodology applicable to physical failure conditions and allows separation of populations into domains for separate analysis. However, the method is affected by the arbituary input parameters, an effect that becomes particularly important when comparing the results of different users. The M-plane method has a similarly appropriate methodology and is independent of any assumptions, but, is time

consuming, particularly if multiple populations of M-planes exist. Moreover, it is not possible to predict, before applying the method, whether any particular population of data will yield a result (Aleksandrowski, 1985). The P and T-axes method is less time consuming but appears to be an oversimplification of failure conditions and should only be used to support rather than predict results.

All three techniques are affected by the possibility that slip planes formed early in the shear history became rotated out of their original orientation during simple shear on the major fault zones, or during folding of the cover rocks. Inevitably some slip directions are controlled by the geometric constraints on movements where wedge rather than plane failure forces slip parallel to the line of intersection of the two failure planes. Finally, the methods require enough data points to be statistically significant, the collection of which may be limited by limited exposure.

4.6. RESULTS OF KINEMATIC ANALYSIS.

Despite the variations in the results produced by each analysis technique, three differing stress fields are present in the mesofault motion data of this study area. The two compressional and one extensional stress fields reflect that locally strain partitioning is important. The most widely sampled stress field is an axial compression with a gently plunging to horizontal, NW-SE orientated σ_1 indicating the dominant fault movement is one of thrusting. Commonly, σ_2 and σ_3 are of a similar magnitude, σ_2 and σ_3 having moderate plunges to the NE or SW. This stress tensor is consistent in localities influenced by folding, such as the Island Hills and Waitohi Downs synclines, in localities influenced by faulting, (Waitohi Gorge and Island Hills) and in localities influenced by both faulting and folding (Flaxdown Quarry). This consistency indicates folding and faulting are closely related. Curved slickenside striations in the cover rocks at Island Hills and Flaxdown Quarry imply the fault planes have been slowly rotated over time in relation to the compression direction. Likewise, the presence of calcite fibre lineations suggests a relatively long term stress field, with multiple strain increments separated by enough time to allow calcite-crystal growth.

The second axial compressional stress field is observed in the basement in the Hurunui Fault, Taruna and Island Hills areas. The orientation of σ_1, ranges between WSW and SSW and plunges gently to horizontally to the SW or NE. The presence of this stress field is consistent in areas that are influenced by faulting and/or folding.

In the cover rocks at Island Hills and Flaxdown Quarry, where slip vectors associated with both the compressional stress fields are present, the relative age relationship of the sets is ambiguous. This may indicate that the sets have formed synchronously, a conclusion which is in keeping with the synchronous development of macroscopic faults and fault-related interference folding in these areas.

The third stress field is extensional, very localised and formed in close proximity (less than 300m) to the macroscopic thrust faults. The Kanuku Hills area is the best example, with σ_1 being vertical, σ_2 plunges gently to horizontially SE while σ_3 plunges gently-horizontially NNW. Localized, normal mesofaulting also occurs in the cover rocks at Island Hills and Flaxdown Quarry. The occurrence of extensional tectonics in a region dominated by reverse and thrust faults indicates that strain partitioning occurs in this study area across very short distances.

Slip vectors from the Kanuku Hills are predominatly indicative of extension but these cut, or are themselves cut, by meso-scale faults related to NW-SE compression. This relationship is inferred to indicate that the stress fields in this area and the entire study area have formed synchronously.

4.7. COMPARISON OF RESULTS OF KINEMATIC ANALYSIS FROM NORTH CANTERBURY

Since the formation of the North Canterbury Active Tectonics Group two students, Syme (1991) and Nicol (1991), have analysed the kinematics of small-scale structures to determine the local and regional late Cenozoic stress fields in the Marble Point and Mid-Waipara regions respectively.

Syme (1991) investigated four areas within the basement and cover rocks of the Marble Point outlier, located 6km south of the Hope Fault. The same techniques as those used in this study were used to determine the local stress fields from the measurement of mesofaults. Two axial compression stress fields were determined, one with a low angle to horizontal NNW-SSE orientated σ_1 that was observed at all four areas, and another, found only in one of the areas, at a low angle and orientated towards the ENE (Syme, 1991). The regional stress fields are dominated by the NNW-SSE orientated compression, although local strain partitioning is apparent. Where both stress fields are observed the age of the associated slip vectors is ambiguous and may indicate that they formed synchronously.

Nicol (1991) investigated mesofaults within the basement and cover rocks using the stress tensor method. Locally, strain partitioning is observed with σ_1 having various orientations. A total stress tensor plot of all the data from the basement was combined to determine the regional stress field. A similar plot of the total stress tensor data from the cover rocks was produced. Nicol (1991) found that results of the stress tensor method produced σ_1 directions that were comparable, not only with each other, but also with stylolite columns, inferred to be parallel to the principle axis of compression during formation, developed in an Oligocene limestone unit in the cover sequence. Both stress tensor plots, and the late Cenozoic stylolite columns, display σ_1 as gently inclined to horizontal and plunging to the SE.

The orientations of the principal compressive stresses observed by both Syme (1991) and Nicol (1991) are highly comparable with the predominant, gently inclined to horizontal, SE trending principal compressive stress found in this study. The orientations of the principal compressive stresses from all three regions are also in keeping with the N-ENE macroscopic reverse, oblique reverse and thrust faults that dominate the structural grain of these regions. Furthermore, the orientation of σ_1 is comparable with the orientations of the poles to the N-ENE striking, W-NNW dipping axial planes of the macroscopic, asymmetric folds developed in the cover rocks of this study area and in the mid-Waipara region (Nicol, 1992).

Principal incremental shortening and extensional axes have been determined for the Glynn Wye, Hossack and Lottery Stream segments of the Hope Fault using offset geomorphic features documented by Cowan (1990) and McMorran (1991). The movement sense of these features was only used if the strike and dip of the fault plane could be determined. Under these criteria six fault movements were investigated revealing all the P-axes cluster in the SE defining a shortening direction that plunges gently to horizontally to the SE while the T-axes define the extension direction to plunge gently SW (Figure 4.14). It appears from this limited study that the principal shortening stress acting on the right lateral Hope Fault is comparable to the principal compressive stress directions determined in the reverse and thrust fault dominated Marble Point, western Culverden Basin and mid-Waipara regions.

4.8. CONCLUSIONS.

Calcite fibre lineations and slickenside striations developed on mesofaults in the basement and cover rocks along the western margin of Culverden Basin provide a means of analysing the kinematics of fault movements associated with the late Cenozoic deformation in North Canterbury. Two graphical techniques, the M-plane and the P and T-axes methods, and a numerical technique, the reduced stress tensor method, were used to analyse and compare the relationship of mesoscale faulting to the principal stress and strain axes. Within this study area four areas of basement and four of cover rocks containing mesofaults were analysed using all three techniques. The results of the stress tensor and P and T-axes methods produced highly comparable orientations for the principal stress and strain axes. The M-plane technique proved conclusive only when one population of M-planes was observed. In the areas where multiple populations of M-planes occur the results reflect the intersections of different M-plane populations and produce differing orientations for the principal stress axes when compared to the results of the other two methods.

The kinematic analyses reflect that three local stress fields predominate in this study area, two are compressional, the other extensional. The predominant stress field is ubiquitously gently inclined to horizontal and indicates NW-SE compression. The

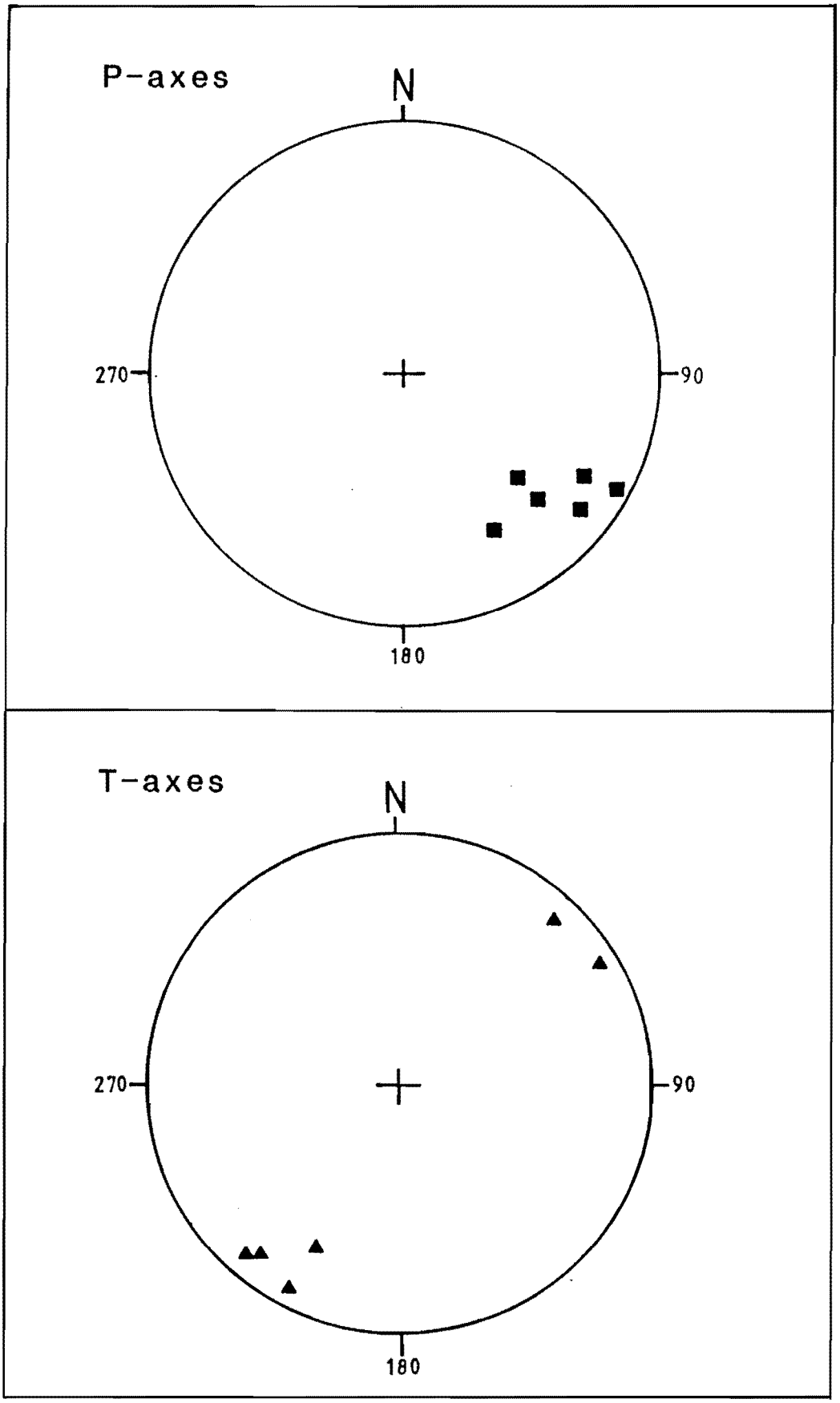

Figure 4.14. Principal incremental shortening axes (P) and tension axes (T), determined from offset geomorphic features, for the Glynn Wye to Lottery Stream segments of the Hope Fault (lowes hemisphere, equal area.

second compressional stress field is intermittently developed, exhibiting a gently inclined to horizontal, SW plunging principal compressive stress. The extensional stress field is not widespread but is locally important and is always moderately inclined to near vertical.

Locally strain is partitioned with the mesofault populations mimicking the style of faulting established by nearby macroscopic faults. Equal area plots of the cumulative stress tensor data and cumulative P and T-axes data for the basement and cover rocks reflect the local strain partitioning. Both the basement and cover rocks, but especially the cover, indicate regional NW-SE compression for this study area. This is comparable to the NW-SE compression direction of the mid-Waipara (Nicol, 1991), and the NNW-SSE directed compression at Marble Point (Syme, 1991) and NW-SE shortening associated with the Glynn Wye to Lottery Stream segments of the Hope Fault. The dominant compressive stress orientation from the western margin of the Culverden Basin is, therefore, part of a regional NW-SE pattern developed in North Canterbury.

CHAPTER FIVE: ACTIVE DEFORMATION.

5.1. INTRODUCTION.

Late Quaternary deformation is recognised in many parts of both North Canterbury and Marlborough (e.g. Falloon, 1954; Clayton, 1966; Campbell & Yousif, 1985; Cowan, 1990 & 1992; Syme, 1991; Nicol, 1991; McMorran, 1991; Garlick, 1992). Locally Quaternary fluvio-glacial deposits of the Culverden Plains and degradation terrace surfaces along the main rivers of this study area provide reference surfaces for documenting deformation and base level changes. Late Quaternary deformation may have occurred as cumulative aseismic strain across the area or as coseismic events on the major faults. Limited data presently constrains the age, amount and rates of deformation in this area. In order to characterise deformation both active faulting and folding are analysed, while landslide data is used to make inferences about paleoseismicity. Dating is provided by lichenometry and weathering rind techniques. From this, a distinction is drawn between aggradation gravel bodies related to Pleistocene fluvio-glacial outwash and the degradation terraces veneered by younger bed load gravels, and given separate nomenclature.

5.2. DESCRIPTION OF QUATERNARY FEATURES.

5.2.1. Glacial Outwash and River Terraces.

Three groups of coarse fluvio-glacial gravel formations and their associated terraces had been recognised previously in the Hurunui River valley and its tributaries. A fourth group of coarse gravel terraces is associated with the present level of the main rivers. Mason (1949) suggested that a flat lying to back-tilted surface, 260m above the present level of the Hurunui River (Figure 5.1A), at Waitohi Downs (M33/714224) may be the oldest glacial terrace in the Hurunui River valley. The name Waitohi Formation is proposed here for this highly weathered, (Figure 5.1B), up to 12m thick, deposit of coarse Torlesse derived gravel. Two terraces, Waitohi Terraces, are developed unconformable on Torlesse basement, the upper surface (elevation 583m) being approximately 30m above a lower degradation surface. The terraces are veneered with a bedload capping of notably less weathered gravel. This terrace surface

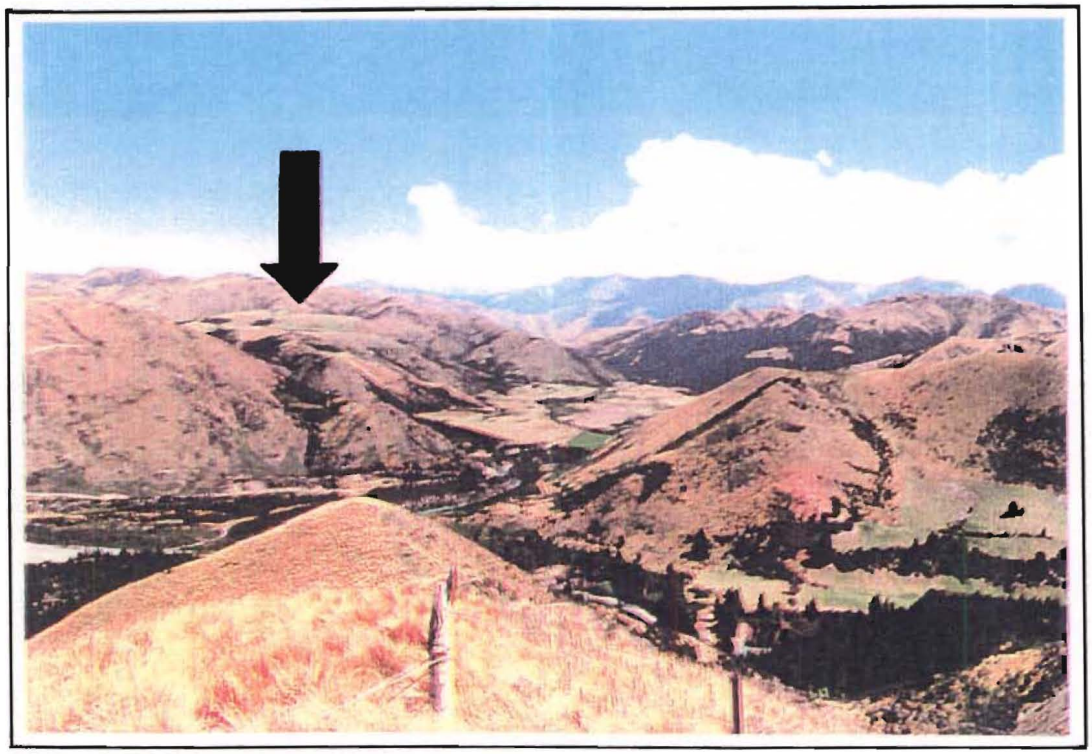

Figure 5.1 A. A view looking southwest showing the flat lying to back tilted Waitohi Terrace surfaces that are approximately 250m above the present floodplain of the Hurunui River.

Figure 5.1 B. Highly weathered Torlesse Supergroup derived gravels that underlie the Waitohi Terrace surfaces.

may correlate with the gently inclined surface developed on Torlesse basement at tha SW end of Sheep Yard Basin (M33/623168). On the basis of weathering of the aggradation gravels and the terrace surface being the highest found in the area, the surface may be attributed to an earlier glacial advance, possibly equivalent to the Avoca or Woodstock deposits of the Waimakariri, but as will be discussed, elevation is not a reliable indication of relative age. No extension of this surface or deposits have been identified in the basin beyond the Waitohi Downs Fault.

In descending elevation the next glacial outwash surface is underlain by coarse gravels of the Windwhistle Formation. These terrace remnants correspond to the High Terrace Remnants and Three Tree glaciation of Powers (1962). Gregg (1964) correlated these deposits with Windwhistle Formation and are attributed to the Otarama glacial advance (70000-40000 years ago; Brown & Wilson, 1988). The terrace surfaces associated with the Windwhistle Formation are here termed Hurunui Terraces on the basis of their ages determined in this study (see section 5.3.2.1).

The Burnham Formation underlies the Main Terraces or Sisters Stream glacial outwash surface of Powers (1962). The aggradation and Hurunui River degradation surfaces, Culverden Terraces, (this study) are the most laterally extensive surfaces developed in this study area. Gregg (1964) suggested that this formation was part of the Blackwater glacial advance (25000-18000 years ago; Brown & Wilson, 1988).

The St. Bernard Formation underlies the youngest glacial outwash surface, Medbury Terraces (this study), found in the Hurunui Valley. Powers (1962) has attributed the surface to the Lake Sumner glacial advance which in turn has been assigned to the Poulter advance (18000-14000 years ago: Brown & Wilson, 1988) by Gregg (1964). The lowest terrace surfaces are close to the present river levels and are non-glacial and formed by Holocene river degradation.

5.2.2. Landslides.

Two large landslides are developed in Torlesse Supergroup sandstone and syenite basement rocks of the Mandamus area. Both are assumed to be seismically triggered due to their large size, the lack of discontinuities in the syenite, the continuous exposure of basement rock in the head scarps, and their proximity (20km) to the major faults of this study area and the strike-slip faults of the Marlborough system. The landslides are complex structures involving both sliding of large blocks, and rolling and flow as streams of rocks fragments. This type of debris deposit places the landslides in the rock avalanche category of the nomenclature of Varnes (1978).

Rock avalanches triggered by seismic events in New Zealand have been found to be associated only with earthquakes of magnitudes M > 6.5 (Eiby, 1968; Cowan, 1992), somewhat larger than the M > 6 found by Keefer (1984). For the larger historical rock avalanches of New Zealand (Whitehouse and Griffiths, 1983) and the world (Voight & Pariseau, 1978), for which a trigger is known, there is a preponderance of association with earthquakes over rainfall. About 90% of rockfalls of sandstone blocks in the northeastern South Island result from seismic shaking (Bull pers.comm).

The Mandamus rock avalanche (M33/740246) is developed in hornfelsic Torlesse Supergroup sandstone and syenite of the Mandamus Igneous Complex. The avalanche debris has a hummocky surface and overlies a paleochannel of the Mandamus River and a Culverden Terrace surface developed on Burnham Formation (Figure 5.2A). It appears the debris dammed the Mandamus River and that the river's present channel, which has a distinct meander form on the upstream side of the avalanche debris, incised into the toe of debris and down into the underlying basement rocks.

The Korari Downs rock avalanche (M33/778260) is developed in syenite of the Mandamus Igneous Complex (Figure 5.2B). The internal disruption of the debris is very high and the debris has a hummocky surface with no soil horizons developed. The Korari Stream is deeply incised into the debris at the toe of the landslide producing a large alluvial fan on a Hurunui Terrace surface at the base of the slope.

Figure 5.2 A. Photograph of the rock avalanche debris that overlie a Culverden Terrace surface (arrow) exposed in the Mandamus River.

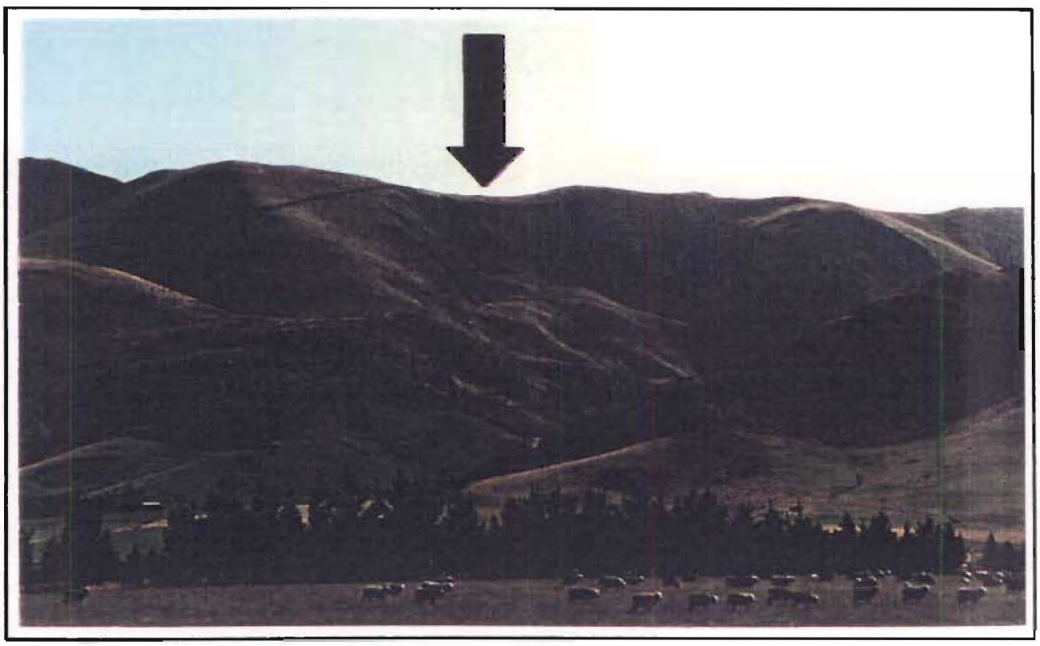

Figure 5.2 B. A view looking northwest at the Korari Downs rock avalanche.

5.2.3. Faulting and Terrace Warping.

A seismic event on a fault is typically evidenced by a surface expression such as a fault scarp. Of all the macroscopic faults observed locally that extend beneath the late Quaternary deposits only the Balmoral Fault exhibits any evidence of ground rupture. This evidence suggests that no seismic event producing ground rupture has occurred on the faults other than the Balmoral Fault since the Hurunui Terrace surfaces formed. However, ground rupturing events may have occurred on the major faults along the segments that juxtapose basement against basement and/or cover rocks. The flat lying Waitohi Terraces on the upthrown side of the Waitohi Downs Fault suggest that these surfaces have been back tilted (Figure 5.1A), but surveying is required to prove this hypothesis. It also appears that remnants of the Hurunui Terraces in the Tommys Stream area (M33/669060) may be back tilted resulting from uplift on the western side of the Tommys Stream Fault.

5.2.3.1. Balmoral Fault.

Terrace warping documented by Powers (1962) is also associated with the southern most extremity of the Balmoral Fault. A WSW transect across the Balmoral Fault along Station Road indicates the Culverden Terrace surface is vertically displaced 1.15 ± 0.15m over a horizontal distance of 30m. Further to the SSE the fault dies out with no visible warping of the terrace surface beyond Duns Road. Striking NNW from Station Road the fault develops into a scarp that displays an increase in vertical displacement to reach a maximum displacement of 5.7±0.5m at the southern edge of Green Hill.

From the fault geometry as it approaches Green Hill, structure contouring of the scarp from orthophotos of 1:2000 and 0.5m contour intervals and the relative displacement a component of reverse movement is evident. This is supported by apparent back tilting of the Culverden Terrace surface on the upthrown side of the fault 100-200m north of Tekoa Road and less obviously to the south along Station Road. Back tilting of the Culverden surface on the upthrown side is further supported by the change in channel pattern of Dry Stream upstream of the fault from braided to straight. The

channel is incised as its nears the fault trace and changes again to a sinuous meander pattern on the downthrown side of the fault.

While the vertical component is the most obvious, with the scarp height rising northwards, a larger component of left lateral movement (12.0 ± 2.0m) is indicated by the offsetting of a Hurunui Terrace scarp where Shortcut Road crosses the fault (M33/848231) (Figure 5.3). As discussed in chapter 3 it appears the Balmoral Fault becomes bedding parrallel where the fault seems to disappear into the Tertiary rocks of Green Hill. Bedding in the Tertiary rocks dips 27°W suggesting that the Tertiary rocks have been exposed due to left oblique reverse movement on the Balmoral Fault.

5.2.3.2. Evidence for a fault along the southern edge of Green Hill.

A left oblique reverse movement on the Balmoral Fault is compatible with reverse movement on a WNW striking NNE dipping fault inferred by the author to abut the Balmoral Fault and run along the southern edge of Tertiary rocks exposed at Green Hill (Figure 5.4). Reverse movement on this WNW striking fault could explain the exposure of Tertiary rocks 210m above the late Quaternary deposits. Evidence for a fault along the range of Green Hill is supported by triangular facets developed on the southern ends of spur ridges, the straight mountain to piedmont junction, and narrow valley floors (Figure 5.4). These geomorphic features are typical of recent episodes of mountain-range uplifts (Wallace, 1978; Bull, 1984). Wallace (1978) developed a model (Figure 5.5) showing the sequence of development of range fronts generated by faults. It is predicted that a WNW striking fault along the southern edge of Green Hill has developed a range front morphology that is intermediate to those of D and E in Figure 5.5. A WNW striking reverse fault at Green Hill is inferred to be a little south of the mountain-piedmont junction, a conclusion supported by the development of alluvial fans, formed from valleys notched into the triangular facets (Figure 5.4) that cover the mountain-piedmont junction. This is indicative of the triangular faceted ridge slopes tending towards a state of equilibrium. Shallow seismic profiling across the mountain-piedmont junction, and in the areas between the alluvial fans, may validate the inferred presence of a WNW striking reverse fault.

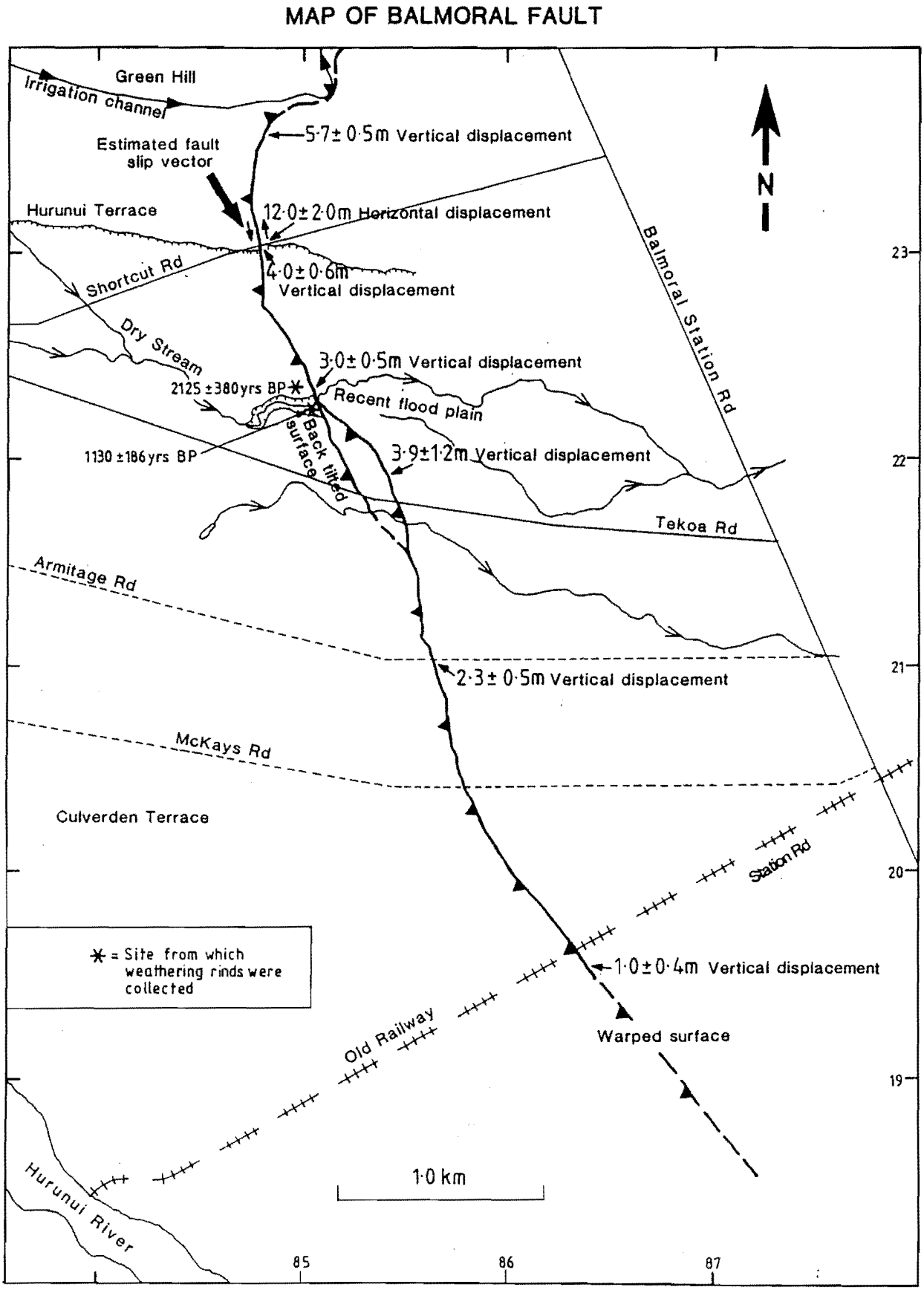

Figure 5.3. A map of the active Balmoral Fault showing vertical and horizontal displacements. Also shown (asterisk) are the sites from which weathering rinds were collected for constraining the age of ground rupture.

Figure 5.4. A plan view of the southern edge of Green Hill. Triangular facets at the piedmont-range front junction suggest a W-WNW striking reverse fault.

PLAN VIEW OF
TRIANGULAR FACETS ON SOUTHERN EDGE OF GREEN HILL

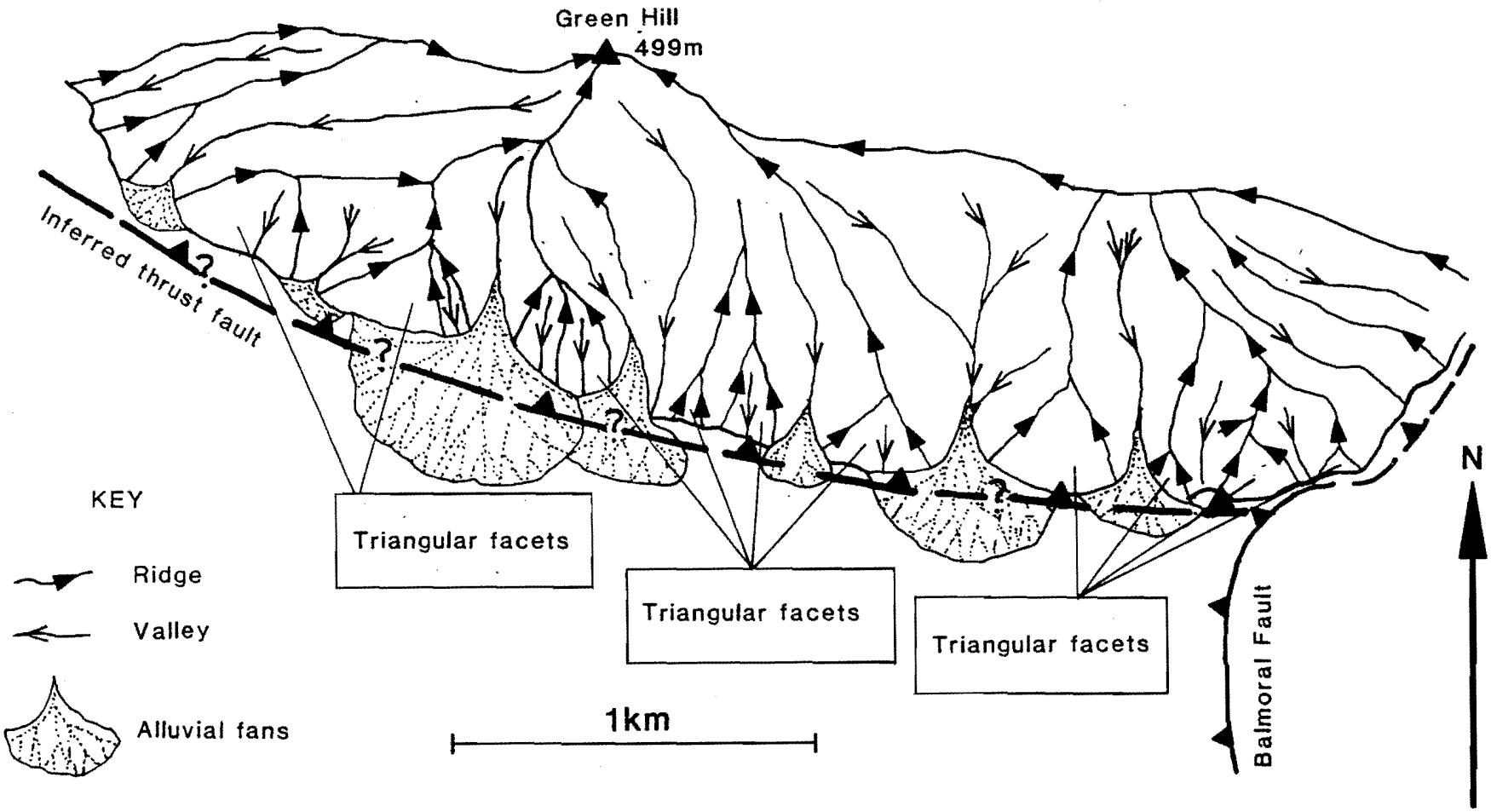

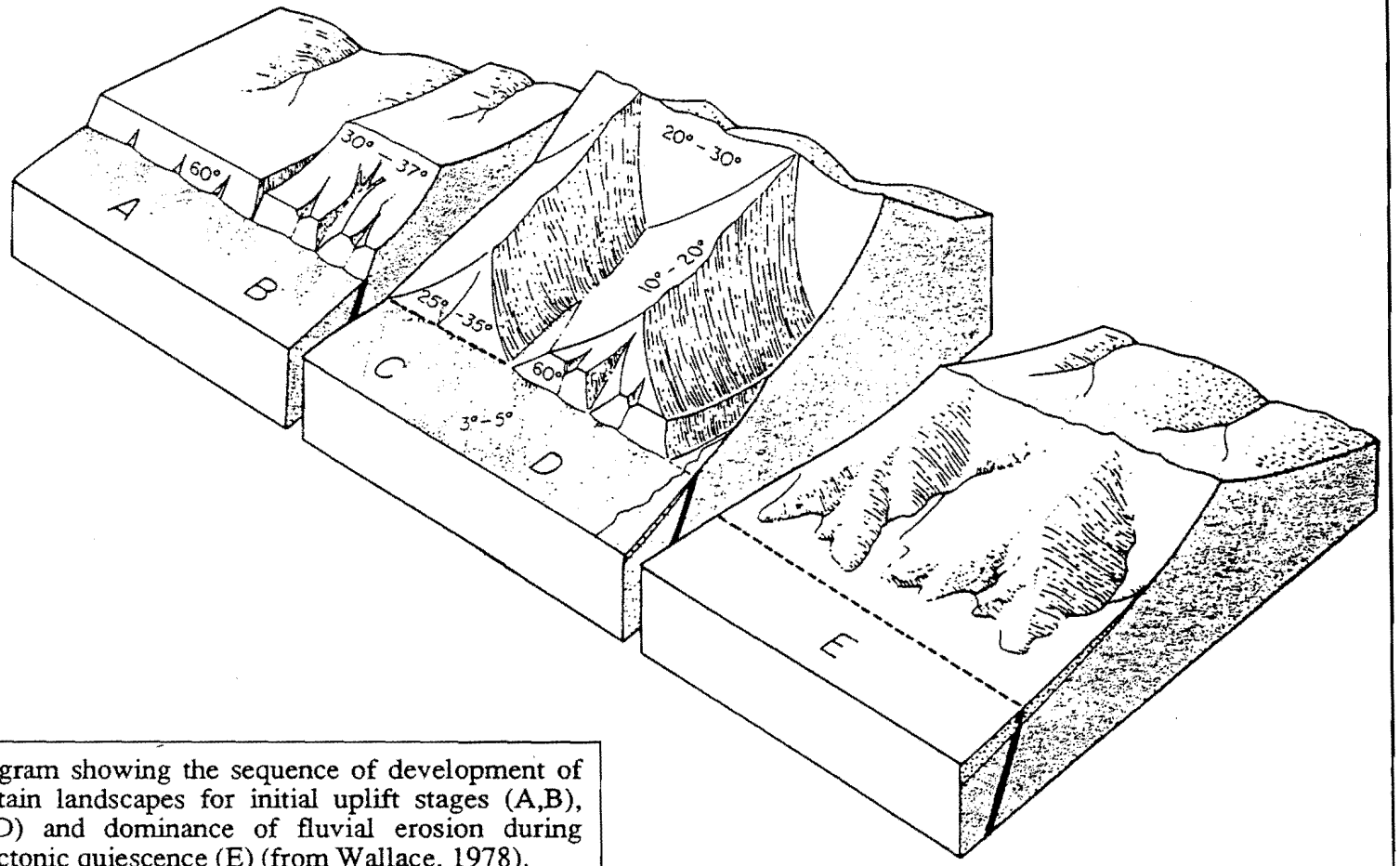

Figure 5.5. Block diagram showing the sequence of development of fault-generated mountain landscapes for initial uplift stages (A,B), maximum relief (C,D) and dominance of fluvial erosion during subsequent stage of tectonic quiescence (E) (from Wallace, 1978).

5.3. AGE OF FEATURES.

5.3.1. Dating Techniques.

Two dating techniques were initally used in the field to establish an estimate of the ages of the landslides and terrace surfaces. Lichenometry was intially used to determine the age of the landslides, this involved measuring the diameter of yellow-green rhizocarpons (Bull pers.comm., 1992) developed on the exposed surfaces of boulders from within the landslide debris. Bull (pers. comm., 1992) has measured lichens developed on boulders of syenite and thermally metamorphosed Torlesse sandstone from within the debris of the two landslides in the study area. Analysis of the lichen data suggested that there is no significant modal lichen diameter from which it is inferred that the landslide exceeds the age limit (1000 years BP) for dating using lichenometry. Previously lichenometry had only been used on prehnite-pumpellyite facies Torlesse sandstones and it has yet to be established how valid the technique is to date lithologies other than Torlesse sandstones under local climatic conditions.

The other dating technique used involves the measuring of weathering rinds (Appendix II) developed on medium grained (0.2-0.6mm) prehnite-pumpellyite metamorphic facies Torlesse sandstones (Chinn, 1981; Whitehouse, et al., 1986). A major difference that arose between the methodologies is the low altitude at which the samples in this study were collected although Whitehouse et al. (1984) found that the effect of changes in altitude are negilible and the method has been used successfully at low altitudes in North Canterbury (Nicol, pers.comm. 1992).

5.3.2. RESULTS.

5.3.2.1. Terrace Surfaces.

The weathering rind technique has been used to date four terrace surfaces, two adjacent to the Balmoral Fault, the Waitohi Terrace surface, and a surface above the confluence of the Mandamus and Hurunui Rivers. The latter is the Culverden Terrace on which the Mandamus landslide is deposited. The two surfaces adjacent to the Balmoral Fault have been used to constrain the age of last ground rupture of the fault. The lower terrace surface is developed along the banks of Dry Stream where it flows

unruptured across the Balmoral Fault (M33/851223). The upper terrace surface that is ruptured by the fault is one of the Culverden Terrace surfaces.

The frequency histogram for weathering rinds measured from the lower terrace has a multimodal distribution analogous to saw teeth (Figure 5.6A). It is assumed that this surface has been disturbed (in this case either by farming practices or episodic flood events in Dry Stream), but that those clasts that date the initial development of the surface will have the thickest rinds. Therefore, the surface age is estimated by determining the modal rind thickness for the peak that represents the thickest rinds and where the peak must exceed random statistics. The age for the lower surface was determined from the saw tooth graph (Figure 5.6A) by passing a line through the apex of the peak defining the thickest significant concentration (1.51mm). Calibrated against the graph of McSaveny (May 1992) an age of 1,130 ± 186 years BP is derived for the surface.

A total of 123 weathering rinds were measured from boulders on the surface ruptured by the fault. Again the distribution of rind thicknesses is multimodal, but with one mode that dominates (Figure 5.6B). In this instance the most significant peak was used for determining the age of the surface. The peak corresponds to a model rind thickness of 2.44mm indicating an age for the surface of 2,125± 380 years BP. It is clear that some uncertainity must remain about this age determination and it is suggested that this be regarded as a minimum age for the surface. A second significant peak to the left of that used to date the surface may equate to the ground rupturing event (1710 ± 215 years BP) of the Balmoral Fault.

From the flat lying to back-tilted surface capping the aggradation gravels of the Waitohi Terraces a total of 117 weathering rinds produced a saw-tooth to slightly bimodal rind thickness distribution (Figure 5.6C). The peak indicating the thickest significant modal rind thickness has been used to determine the minimum age of the Waitohi Terrace surface. This is regarded as a minimum because the terrace surface is exposed to the prevailing wind and due to wind abrasion and/or removal of soil

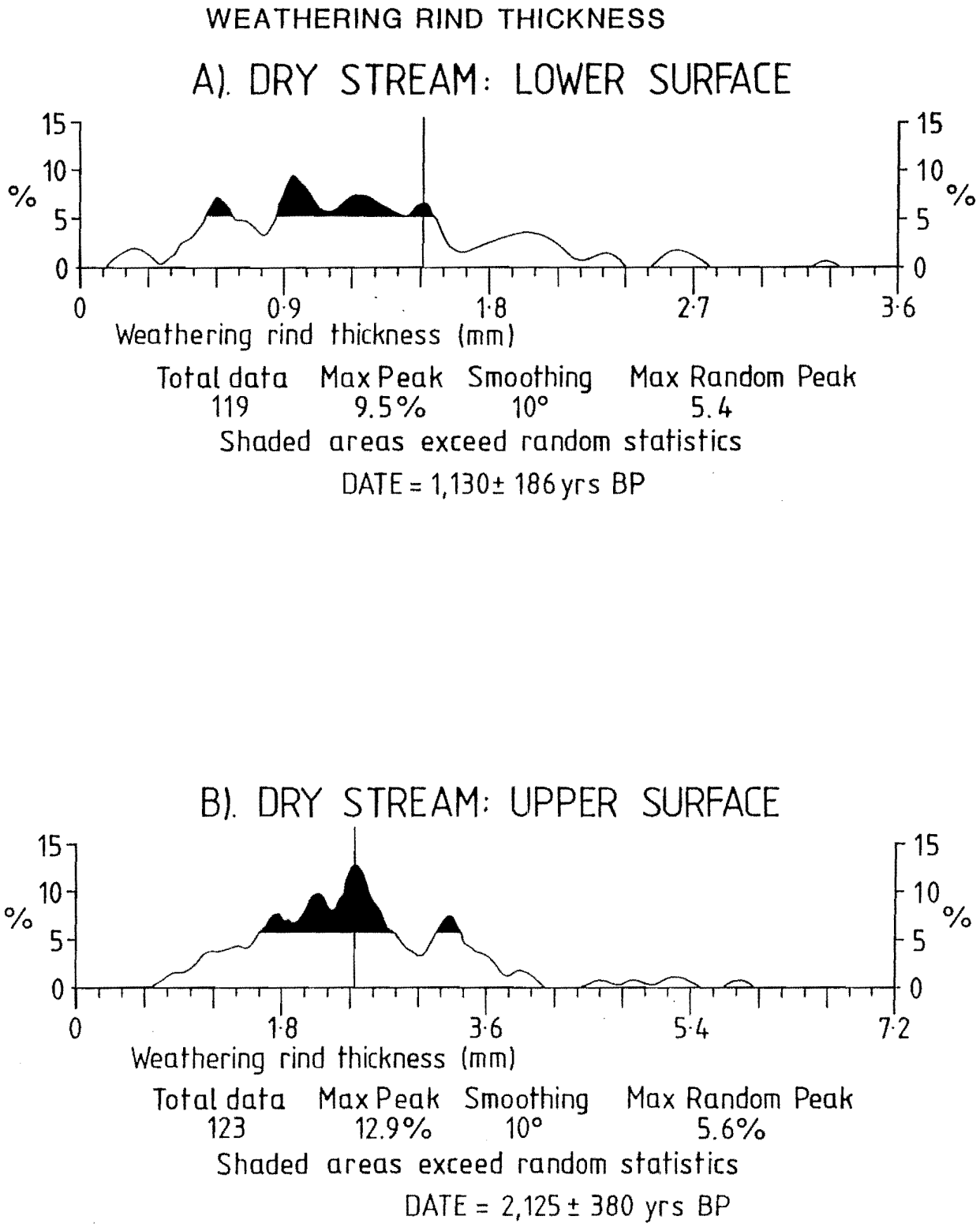

Figure 5.6. Double smoothed frequency histograms of weathering rind thickness for A) Recent flood plain of Dry Stream, B) A Culverden Terrace surface near Dry Stream, C) Waitohi Terrace surface and D) Culverden Terrace surface near the confluence of the Hurunui and Mandamus Rivers.

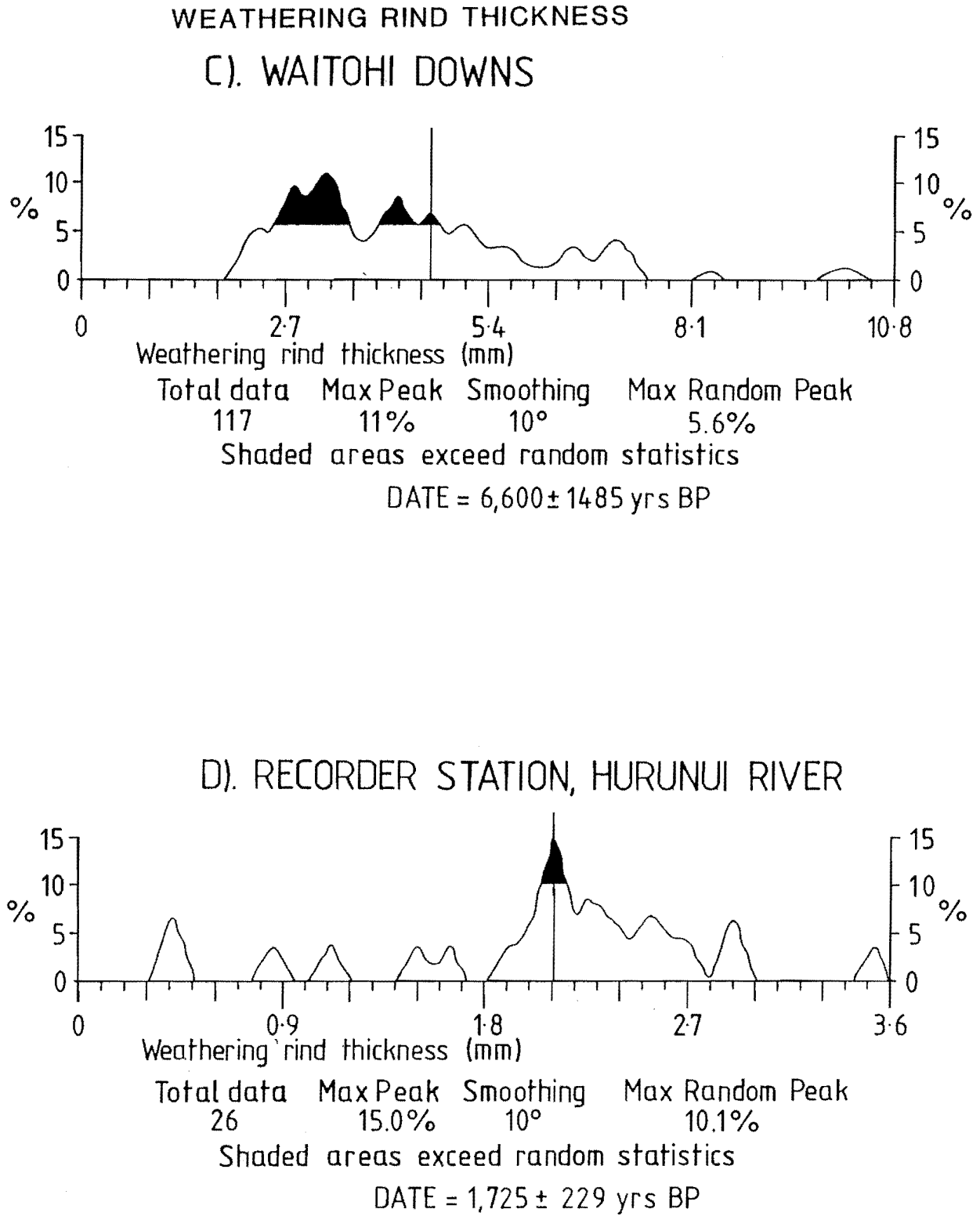

Figure 5.6. Double smoothed frequency histograms of weathering rind thickness for A) Recent flood plain of Dry Stream, B) A Culverden Terrace surface near Dry Stream, C) Waitohi Terrace surface and D) Culverden Terrace surface near the confluence of the Hurunui and Mandamus Rivers.

cover the rinds may be anomalously thin. The peak indicates a thickness of 4.68mm indicating an age of 6,600 ± 1485 years BP for the terrace surface.

The final surface from which weathering rinds were measured is 25± 5m above the current level of the Hurunui River. A total of 26 weathering rinds were measured from the terrace surface. These again produce a multimodal distribution but with one dominant peak with a modal thickness of 2.11mm (Figure 5.6D). This indicates an age of 1,725± 229 years BP.

5.3.2.2. Mandamus River Landslide.

The Mandamus River landslide debris (M33/739245) rests on a terrace surface that is 22± 4m above the current flood plain of the Mandamus River (Figure 5.2A). This terrace is at approximately the same elevation as a terrace on the west bank of the Mandamus River that can be correlated to the Culverden Terrace surface 25± 5m above the Hurunui River (M33/729239). A maximum age for deposition of the landslide of 1725 ± 229 years BP is indicated for the landslide by the age of the Culverden Terrace. The absence of loess on the landslide debris suggests a late Holocene age for the landslide, although the prevailing wind and other climatic conditions may account for the absence of loess.

5.3.2.3. Korari Downs Landslide.

The debris from this landslide is deposited on Torlesse and Mandamus Igneous Complex basement rocks and consequently has not been dated. Korari Stream has eroded its channel into the landslide debris and deposited an alluvial fan on a Hurunui Terrace surface. This surface is dated at between 1745 and 8085 years BP, suggesting that the landslide has been deposited at some time within this range. The absence of loess cover developed on the surface of the landslide also suggests a late Holocene age for the landslide.

5.3.2.4. Downcutting of the Hurunui River.

The dates of the fluvial terraces associated with the Hurunui River have been plotted against the vertical difference in elevation of the top of the terrace surfaces and the current flood plain of the Hurunui River (Figure 5.7). The graph indicates that with decreasing age the rate of downcutting has declined. It should be noted, however, that changes in climatic conditions, the availability of material, its induration and the tectonic uplift rate both locally and regionally can cause changes in downcutting rates. Downcutting may have occurred in the last 8,085 years as a result of either incremental coseismic events on the major faults and/or as cumulative aseismic strain across the area.

5.3.2.5. Displacement events on the Balmoral Fault.

The Balmoral Fault offsets the Hurunui and Culverden Terrace surfaces. A profile of vertical fault displacement (Figure 5.8) shows an increase in displacement of the Quaternary terrace surfaces, from south to north. The profile also indicates a change in the proportion of vertical displacement to distance along the fault, where the Hurunui Terrace scarp crosses the fault at Shortcut Road. This change indicates that there has been two ground rupturing events on the fault pre and post dating downcutting below the Hurunui Terrace surface. Evidence for multiple downcutting events is not strong, but the estimated slip rate for the Shortcut Road-Green Hill segment and the change in profile seem to support two movements.

From the ages of the Culverden Terrace and a floodplain of Dry Stream adjacent to the Balmoral Fault a date for fault movement is in the range 1130-2125 years BP, with the error limits defining a minimum and a maximum age range for ground rupture of the fault of 944 years BP and 2505 years BP respectively. A minimum elapse time since the ground rupturing event on the fault at Dry Stream is 944yrs BP.

Further north along the Balmoral Fault where Shortcut Road intersects the fault a scarp developed in the Hurunui Terrace surface is horizontally (12m) and vertically (4m) displaced by the fault (Figure 5.6) giving a horizontal to vertical ratio of 3:1.

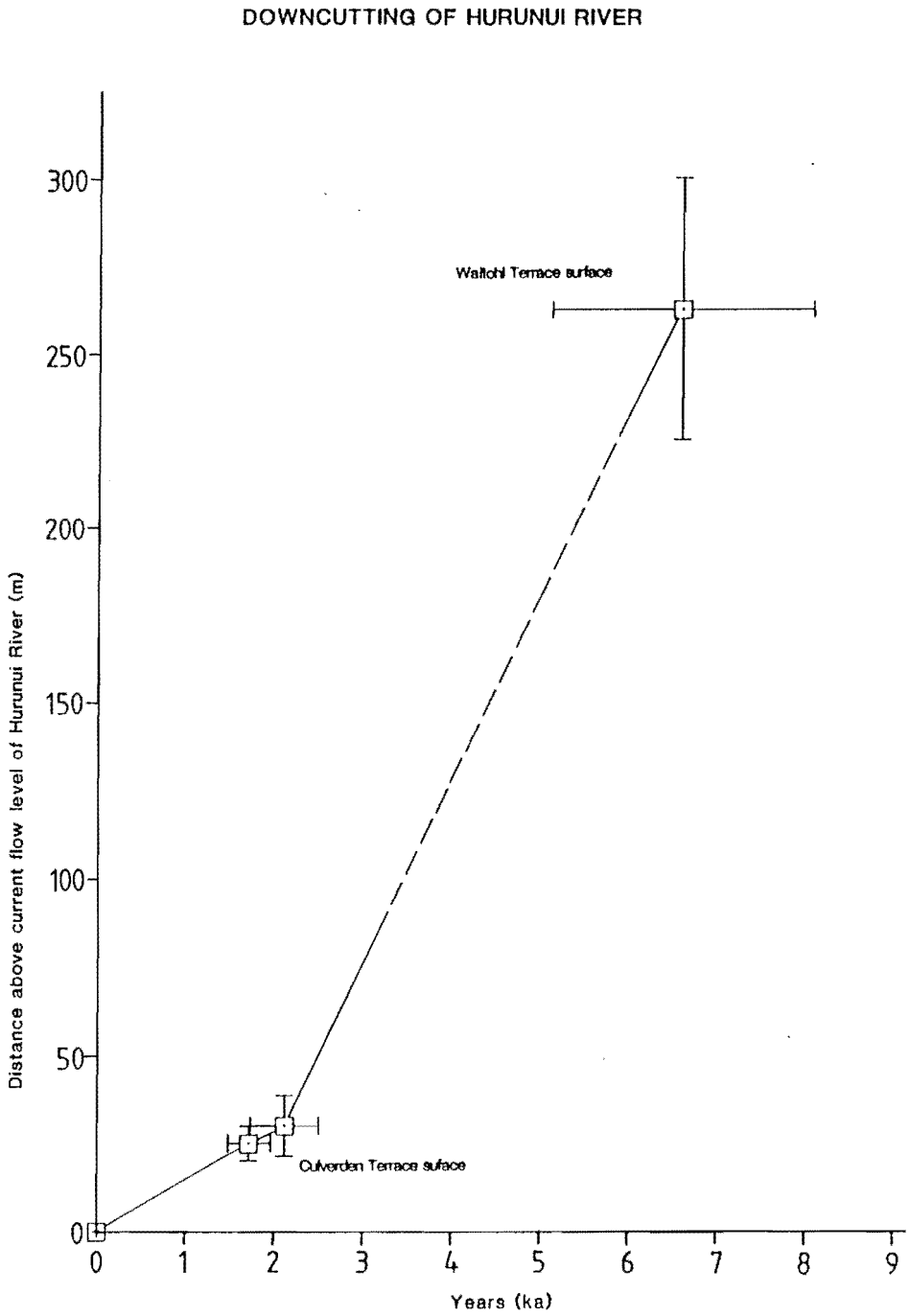

Figure 5.7. A graph illustrating the downcutting of the Hurunui River along the western margin of the Culverden Basin.

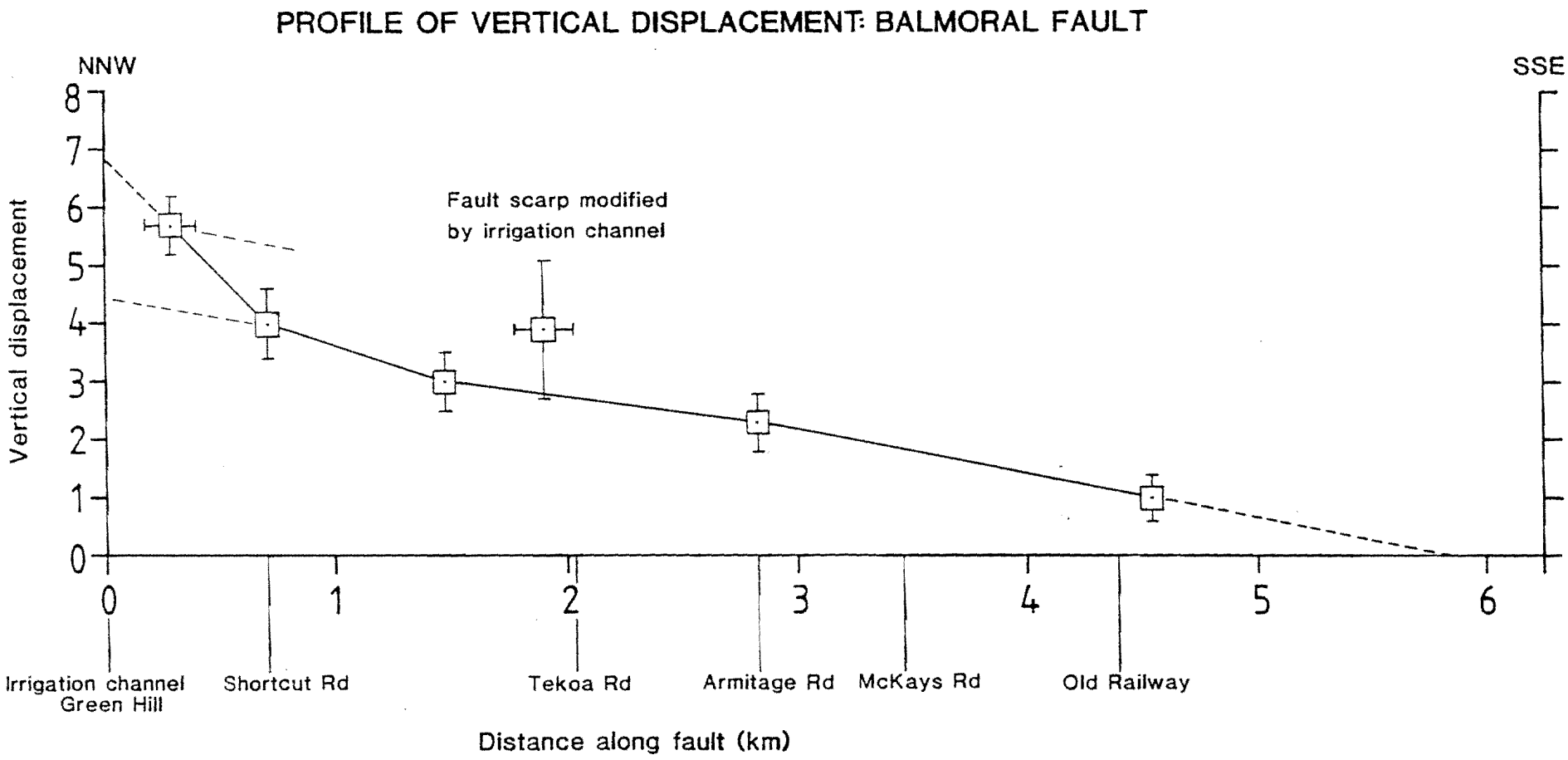

Figure 5.8. A profile of vertical displacement along the Balmoral Fault illustrating the change in displacement from north to south.

These displacements produce a net slip of 13.8m which may or may not equate to a single event. It is inferred from structure contouring at the north end of the fault, and from the dip values of the other major N-NE striking faults, that the Balmoral Fault dips approximately 45° W. A slip vector for the fault at Shortcut Road, assuming the fault dips 45° W and strikes 352°, is 334/18°. The P-axes method, discussed in chapter 4, indicates the principal shortening strain for the Balmoral Fault has an orientation of 304/16°. These values are highly comparable with the NW-SE regional compressional stress and shortening strain discussed in chapter 4.

With only one event to define the elapse time since the last ground rupture, the minimum net slip has been calculated using the date derived for the age of ground shaking event that caused the Mandamus River landslide. This age is used on the basis that it appears the two landslides may have occurred as a result of the ground shaking associated with rupture of the Balmoral Fault.

$$\text{Minimum slip rate} = \frac{\text{net displacement (metres)}}{\text{elapsed time since last event}}$$

$$= \frac{13.8 \pm 2.6\text{m}}{1725 \pm 229 \text{ yrs BP}}$$

$$= 8.0\text{m} \pm 32\% \text{ /1000years.}$$

5.4. INFERENCES FOR ACTIVE DEFORMATION.

If the age estimates calculated are correct they have significant implications for the age and rates of local active deformation. They also suggest that the terrace surfaces of the Hurunui-Culverden region are mid-late Holocene in age and may not correlate readily to those of the Waimakariri Valley. For a number of reasons caution needs to be taken in interpretating these dates. Commonly the boulders from which weathering rinds were collected, especially the older surfaces, are only partially buried in very poorly developed, thin loess. This suggests that winnowing of the soil horizon and the matrix of the fluvio-glacial deposits, where exposed to the prevailing wind, is important. These dates therefore, represent minimum ages for the surfaces and consequently the rates of active deformation determined using these ages must be regarded as maximum values.

5.4.1. DISCUSSION.

It appears from the ages derived for the landslides, and documentation of swarms of landslides resulting from large earthquakes in the Canterbury (Speight, 1933) and Marlborough (Bull pers.comm.) regions, that the two rock avalanches developed in the basement rocks of this study area may have been triggered by the same seismic event. It is also possible within the error limits of the dating technique that the most recent ground rupturing event on the Balmoral Fault may have resulted from the same event that triggered the two rock avalanches. Alternatively the proximity of the two landslides to the major Island Hills, Hurunui, and especially the Waitohi Downs Fault suggests the landslides could also have been triggered by seismic movement on these faults. However, all the latter faults are overlain by terrace surfaces, dated in this study as being Holocene, that exhibit no evidence of ground rupture. It is possible that the fluctuations in downcutting rates of the Hurunui also correspond to the seismic events indicated by the movements on the Balmoral Fault and the landslides. If the last ground rupturing event on the Balmoral Fault is the same as the event that triggered the landslides then it is more than likely, based on the work of Cowan & Nicol (in prep.) that the earthquake was of magnitude M6.5 or greater, particularly if the 13.8m slip represents a single event.

5.5. HAZARD ASSESSMENT.

Seismic activity (minimum estimated elapse time since last rupture of approximately 950 years BP for a M = 6.5 or greater event) may be a significant risk to the inhabitants, and their property, in the Culverden Basin. All of this study area is sparsely populated, farm houses been the only form of settlement. The small townships of Culverden, Waikari and Hawarden are in close proximity to the major faults mapped in this study. Landsliding poses little direct risk to these towns as they are developed in the centre of the Culverden Basin. If a landslide should block one of the major rivers, as has previously happened with the Mandamus rock avalanche, then overtopping or collapse of the natural dam may cause flooding. Landslide debris may also cause destruction of roading and buildings.

The greatest risk is from sudden shaking and/or ground rupture resulting from an earthquake. This is likely to cause widespread destruction of property and possibly loss of human life. Ground rupture of the Waitohi Downs and Balmoral Faults would result in considerable damage to the channels and boarder-dykes of the Balmoral Irrigation scheme. The only intake for the irrigation scheme is on the the upthrown side of the Waitohi Downs Fault, any further movement on this may cause the Hurunui River to change course leaving the intake dry. Similarly, the main channel and a number of smaller channels and numerous broader dykes cross the active trace of the probably Class 1 Balmoral Fault. Again, any continuation of reverse movement on this fault could cause enough change in elevation that the channels will be back tilted, resulting in considerable expense to rectify the problem. Ground shaking and/or rupture is also likely to have a destructive effect on the Balmoral Forest.

Christchurch lies 75km south of the Balmoral Fault and although an earthquake of M=6.5 would not cause widespread destruction a larger event on the fault or the continuous Waitohi Downs Fault may be destructive. Three earthquakes with M≈7 have been recorded in North Canterbury (Hope Fault, 1888; Cheviot, 1901 & Arthurs Pass, 1929) and an event of this size in the Culverden Basin would certainly cause widespread structural damage both locally and possibly as far south as Christchurch.

5.6. CONCLUSIONS.

Dates obtained from measurement of weathering rinds on Torlesse sandstone boulders indicate that the ages of all the terrace surfaces in this study area are probably younger than the aggradation gravels beneath them. These terrace surface ages have been useful for constraining the age of two rock avalanches (inferred to be seismically triggered) formed in the basement rocks, and of ground rupturing event(s) on the Balmoral Fault. The profile of vertical fault displacement with distance along the fault indicates that it has had at least two ground rupturing events in the Holocene. The fault has been estimated to have a dip of 45°W allowing the calculation of net slip and of the principal extension and shortening strain axes, the shortening axis exhibiting the same NW-SE orientation found from meso-scale faulting in basement and cover rocks.

No loess cover on the Mandamus and Korari Downs landslides suggests both are probably of Holocene age. The terrace surface upon which the Mandamus River landslide debris is deposited is 1725± 229 years BP providing a maximum age for the landslide. The Korari Downs landslide was probably deposited in the period 1745-8085 years BP. The two landslides and the last ground rupturing event on the Balmoral Fault may have occurred during the same seismic event or it is possible that the Korari landslide may reflect an earlier event that has been reactivated, the constraints on the ages are not precise enough to prove these alternatives. From the weathering rind dating of the terrace surfaces it is inferred that they are considerable younger than the underlying aggradation gravels and also appear to be much younger than the terrace ages inferred in previously published accounts of the region. If we believe the dates then we must accept that the landscape is locally very young, with many geomorphic elements being Holocene in age.

CHAPTER SIX: SYNTHESIS AND REGIONAL TECTONICS.

6.1. SYNOPSIS OF WESTERN MARGIN OF CULVERDEN BASIN.

Along the western margin of the Culverden Basin, on the eastern edge of the New Zealand plate boundary, associated shallow crustal (<3km wave amplitude) deformation has produced structures within the thin (<2.4km) Late Cretaceous-early Pleistocene sedimentary cover rocks. The major structures developed in the cover sequence indicate that they were formed or reactivated during the early Pleistocene, and focal mechanism and geodetic data testify to the ongoing strain. The major faults and folds are intimately related with predominantly NNE-NE and WNW-NW orientations, producing a structural grain that is similar to the rest of North Canterbury. The major faults are predominantly oblique reverse and thrust faults that verge ESE-SE, SSW-SW and NW, and major right lateral strike-slip faults are absent.

The major macroscopic folds are steeply inclined, gently but variably plunging, asymmetric syncline-anticline fold pairs, whose dimensions reflect the proximity to the major faults. The folds are non-cylindrical and geometrically distinctive and can be defined by a series of conical segments. The intersection of the orthogonal folds produces non-classical irregular basin and dome interference patterns. Corrugated hose, T-shaped and triangular outcrop interference patterns predominate. Secondary folds are developed at various oblique angles to the major fold sets.

The major folds have developed in response to fault propagation and displacement within the basement, combined with shortening within the fault bounded blocks. The major folds tend to be asymmetric with the steep (60° to overturned) limb closest to the fault and the relatively shallow (10-30°) limb further from the fault. Propagation of the major faults through the cover rocks results in truncation of the axial plane of the major fault-related synclines at some structural level higher than that now exposed. Both faulting and folding appear to have been active simultaneously during the Cenozoic. The basement rocks are not folded by simple flexure, rather, deformation has occurred on numerous small-scale faults and a few major macroscopic faults.

Deformation in the basement rocks is most intense, and wedged shaped, adjacent to the major faults and beneath the hinge zones of the major folds.

Bedding parallel pressure solution seams in Oligocene limestone indicate vertical compression resulting from the volume of overlying sediments. Orthogonal joints in the cover sequence indicate a weak deformational phase concurrent with the initiation of the Alpine Fault. Mesofaults and calcite veins both pre-date and, along with macrofractures, have developed synchronously with mid-Pleistocene-Recent deformation.

Mesofaults with movement indicating structures developed on the fault planes were kinematically analysed by two graphical and one numerical technique to determine local and regional stress and principal strain axes. Of the three methods the reduced stress tensor technique is the most useful as it is less time consuming, is more applicable to physical failure conditions and allows seperation of populations into domains for separate analysis. Despite the variations in the methodology of each analysis technique, and some problem in relating results from cover and basement, three different stress fields are distinguished, one extensional and two compressional. The most widely observed stress field is axial compression with a gently plunging to horizontal, NW-SE orientated σ_1 indicating the dominant fault movement is one of thrusting. The second axial compressional stress field is locally significant with σ_1 plunging gently to horizontally NE or SW. In the third stress field σ_1 is steeply inclined giving rise to very localised extension, which formed in close proximity to the major thrust faults. Although locally strain partitioning during the late Cenozoic deformation is important, the dominant compressive stress orientation is at a high angle to the northeast strike of the faults of the Marlborough system and is part of the regional NW-SE compression, a similar pattern to that observed by Zoback et.al. (1987) for the San Andreas Fault.

Two seismically triggered landslides and ground rupturing events on a major thrust fault testify to a continuation of regional shortening strain during the Holocene. The calculation of modal weathering rind thickness for fluvio-glacial and fluvial terrace surfaces has proven that the degradation surfaces are significantly younger than the gravel formations they overlie. This has important connotations for assessing and displaying active deformational structures in a seismically active region such as the Culverden Basin.

The major faults and folds have comparable kinematics, both in the short and long terms, and appear not to have changed much since the inception of late Cenozoic deformation. The complexity of the deformation along the western margin of the Culverden Basin may partially reflect interference between reactivated faults of Late Cretaceous age and younger faults formed during the late Cenozoic. This complexity may explain the synchronous development of the orthogonal faults and their associated folds.

6.2. LATE CENOZOIC DEFORMATION IN NORTH CANTERBURY.

The style of deformation along the western margin of the Culverden Basin is in many respects similar, but also shows some significant atypical features, to that which occurs in North Canterbury, between the Hope Fault and the Porters Pass-Amberley Fault Zone. This region south of the Hope Fault is dominated by valley and ridge topography which reflects the locations of the major faults and folds. These structures appear to be mainly contractional, having developed in response to regional NW-SE compression (Nicol, 1991; Syme, 1991; this study). Contractional deformation extends to at least Marble Point in the north (Syme, 1991) suggesting that strike-slip deformation may be confined to the Hope Fault zone in a similar way to that described for the San Andreas Fault (Zoback et.al., 1987). There is, however, a significant component of left lateral movement on the major faults developed along the western margin of the Culverden Basin, indicating their relationship to the Hope Fault is not as simple as the San Andreas Fault model.

6.2.1. THE CULVERDEN BASIN.

The Culverden Basin is approximately 15x55km, elongate in a NE-SW direction and crudely rhomboidal (Figures 1.2 & 6.1). Because of the proximity of the basin to the lateral faults of the Porters Pass-Amberley Fault Zone and the Marlborough system it has been suggested that this is possibly a composite pull-apart basin (Hicks, 1989), formed at an extensional jog along a strike-slip fault. From the results of this study, work at the southern end of the basin, and gravity survey data (Dibble, unpublished) it has been found that at present the basin is bounded and penetrated by thrust faults.

The west verging thrusting on the Lowry Peaks Fault has developed a relatively straight margin to the southeast edge of the basin (Figure 6.1). Discontinuous faults to the north and northwest produce a more irregular basin edge. The straight western margin of the basin is dominated by thrust and reverse faults (this study) that, south of the Hurunui River, strike obliquely across this margin into the basin. North of the Hurunui River the range front parallels the major faults. Gravity data (Hicks, 1989) indicates a significant basin (1km to basement) is present beneath the Hurunui River between Hurunui Mound and the northern end of the Waitohi Downs Syncline. The swing in strike, from N to NE, of the Waitohi Downs Fault adjacent to this basin suggests that the basin may have some controlling effect on the fault, this, however, is geometrically impossible. Rather than a basin a structural high is required to produce the concave SE jog in the strike of the fault. This change in strike of the fault suggests that may be some other pre-late Cenozoic structure has had an influence on the devolpment of the western margin of the Culverden Basin.

The straight western edge to the basin forms a continuation of a N-NNE striking lineament that can be traced from Mt. Grey in the south north through the Mandamus River valley to the Hope Fault (Figure 1.2). The decrease in elevation from west to east across the lineament suggests that the eastern block has been downthrown (Mason, 1949). To the east of the Mandamus River the Pahau River follows a parallel N-NNE lineament, that from a change in topography, appears to be downthrown to the east. To the west of the N-NNE striking Mt. Grey to Hope Fault lineament, the

Figure 6.1. Geology of the Culverden Basin, North Canterbury. Cross sections are drawn normal to the basin at natural scale (after Nicol, 1991).

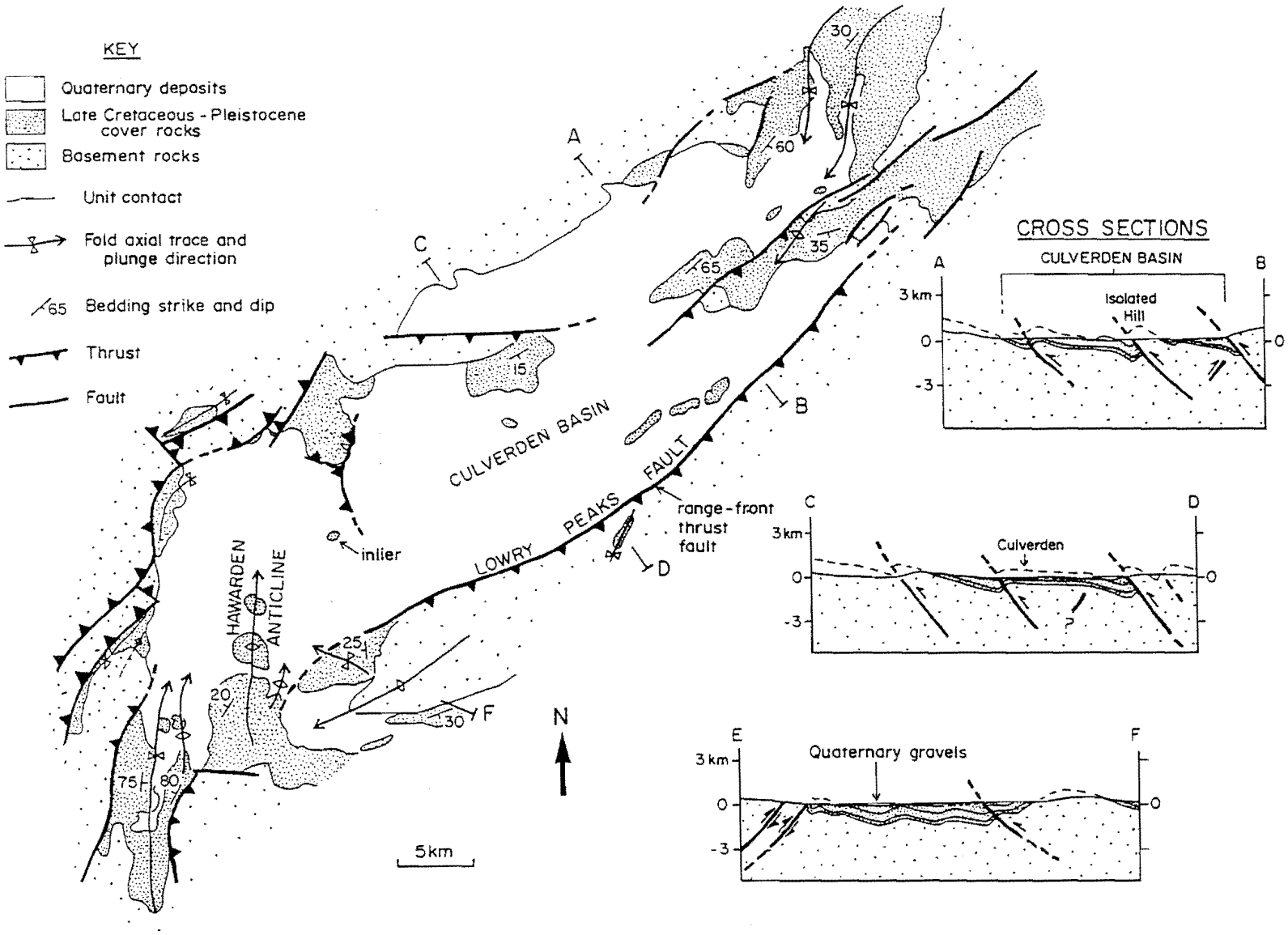

GEOLOGY OF THE CULVERDEN BASIN

Torlesse Supergroup contains uncommonly high occurrences of spilitic volcanics. South of Mt. Grey the lineament may continue south to Rangiora, possibly contributing to the Rangiora Sub-Basin that is developed to the east of the projection of the lineament. Furthermore, five rhyolite domes on the flanks of Banks Peninsula have a N-NNE trend (Cowan, pers.comm. 1992) that lines up with straight western margin of the Culverden Basin. To the north, the Mandamus Igneous Complex lies along the trace of the lineament. Freund (1971) has estimated a dextral strike-parallel offset of 19km from the projection of lithological changes in the Torlesse Supergroup across the Hope Fault. Using this value the lineament may continue N-NNE through Jollies Pass north of the Hanmer Basin. It is in this area that the dextral strike-slip Jollies Pass Fault takes a jog to the north in a linear valley along which the upper reaches of the Clarence River flow. The lineament may then be dextrally offset by the Clarence Fault and strike along the Acheron River.

The question that arises from this is does the Culverden Basin overprint some older N-NNE striking structural low or basin. The possible continuation of the lineament, the coincidence of the west edge of a Miocene sedimentary basin with the present western edge of the Culverden Basin (Figure 2.2), the occurrence of the Mandamus Igneous Complex and the increased volume of volcanics in the Torlesse Supergroup to the west of the lineament suggest that possibly it may mark a N-NNE striking weak zone. Tertiary volcanism in the Island Hills and Pahau areas of this study and in the Mason River to the north (Coote, 1987) are on or in close proximity to this N-NNE lineament. It appears that the western margin of the Culverden Basin, and in particular the Waitohi Downs Fault, have exploited this weak or structurally low zone, which may be related to proposed N-S Late Cretaceous extension (Browne & Field, 1988).

Subsidence of the present basin is controlled by N-NE to S-SW trending folds. Thus the irregular rhomb-shaped basin geometry is a result of thrust faulting and folding rather than the strike-slip faulting that is expected if the basin were a pull-apart structure.

A number of inliers that protrude through the Quaternary gravel that infill the basin suggest that the post Quaternary gravel deposits are relatively thin and that the structural relief within the basin is closely related to the pattern of faulting. Estimates of the structural relief, from cross sections (Figure 6.1, cross sections C-D) and gravity data within the basin indicate that the deepest parts of the basin are along the SE edge adjacent to the Lowry Peaks Fault. Up to 3.5km of elevation difference between the basement-cover unconformity within the basin and the surrounding peaks can be inferred. Adjacent to the Waitohi Downs Fault a structural elevation difference of 3.2 km on the present unconformity is estimated from cross sections (Map pocket) that strike perpendicular to the fault for this part of the basin.

The inference, from the thrust and reverse faulting and folding along the basin margins and the estimated small structural elevation differences, is that the Culverden Basin is relatively shallow and developed during the late Cenozoic in a contractional tectonic environment. A contractional basin, like the Culverden Basin, will only form in a structurally low region when the upper surface of the basin passes below the base level of sedimentation. With the contractional deformation that is active within the Culverden Basin it is likely that its depositional phase will be short lived (<3ma).

The Culverden Basin has formed from a combination of predominantly NE-SW faulting and fault-related folding while the basin width is controlled by strike-normal distance between the major faults and the rate of relative subsidence. Other elongate basins in North Canterbury (eg. Cheviot Basin, see Figure 1.2 & 6.2) probably have had a similar structural history. The larger size of the Culverden Basin may be explained by the greater amount of area that is below the present base level of sedimentation. Tertiary inliers in the Quaternary gravels (e.g. Hurunui Mound), active thrust faulting (e.g. Balmoral Fault), and the propogation of the Hawarden Anticline into the basin suggest, however, that the basin is being exhumed.

Figure 6.2. Map of the major structures and basins in North Canterbury (modified after Nicol et al., 1992).

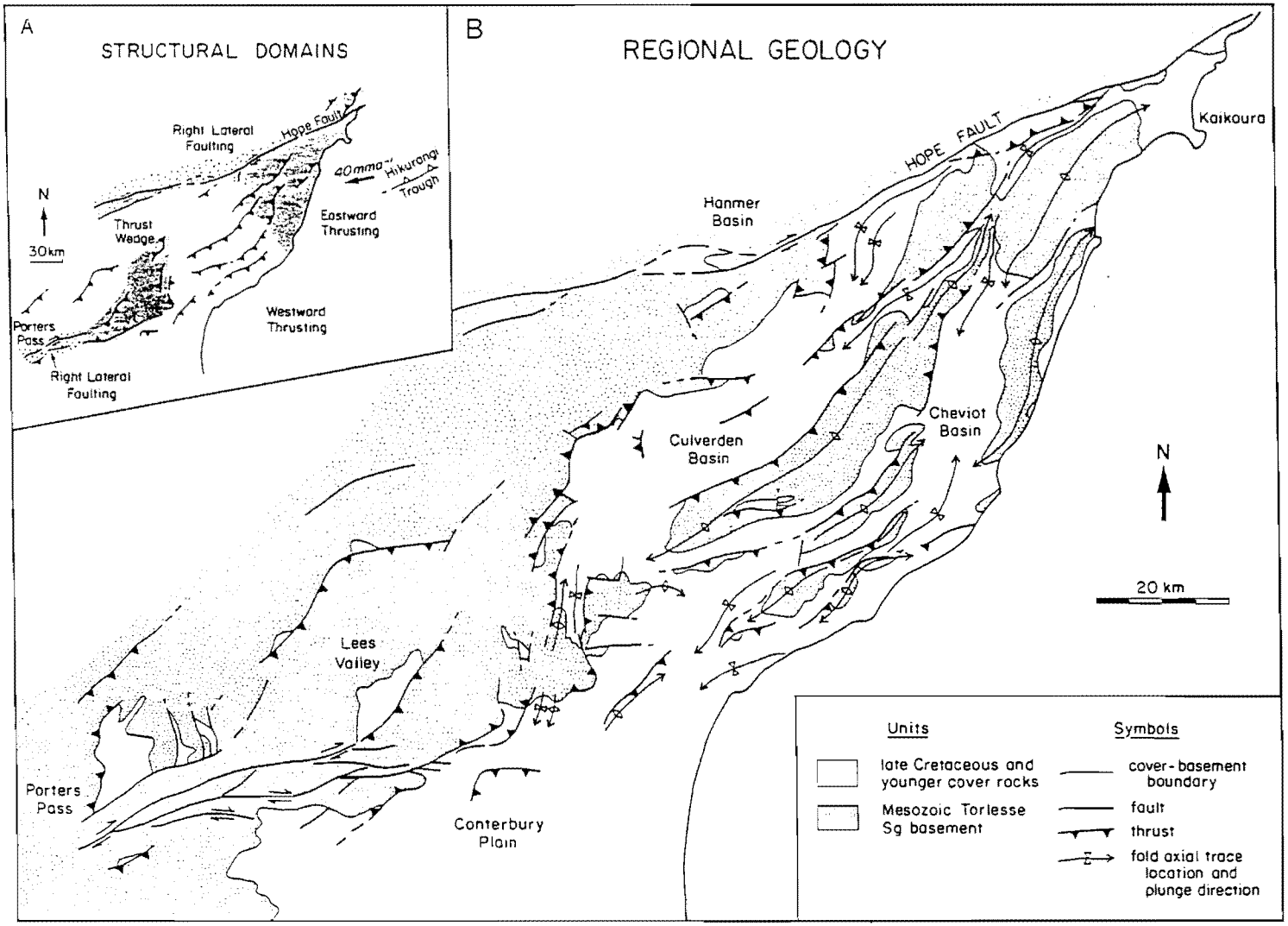
A
STRUCTURAL DOMAINS
Right Lateral Faulting
Hope Fault
40mma⁻¹
Hikurangi Trough
N
30km
Thrust Wedge
Eastward Thrusting
Westward Thrusting
Porters Pass
Right Lateral Faulting
B
REGIONAL GEOLOGY
HOPE FAULT
Kaikoura
Hanmer Basin
Culverden Basin
Cheviot Basin
N
20 km
Lees Valley
Porters Pass
Canterbury Plain
Units
late Cretaceous and younger cover rocks
Mesozoic Torlesse Sg basement
Symbols
cover-basement boundary
fault
thrust
fold axial trace location and plunge direction

6.3 LATE CENOZOIC FINITE STRAIN

Finite strain has been calculated using the deformed late Cretaceous unconformity surface as a marker horizon. Data for the estimates were derived from cross-sections constructed perpendicular to the strike of the major faults and their related folds. The calculations represent minimum values as no account is taken of strain accommodated by the thickening and thinning of the cover sequence in association with folding. Estimates of the finite strain associated with fault displacement are conservative as only the present day eroded surface of the upthrown block has been used on the assumption that the unconformity lies only a small distance above the current topography.

The amount of shortening along the western margin of the basin varies from $<12\%$ (NE-SW between the Tommys Stream and Mt. Mason Synclines) to approximately 60% at the southern end of the Waitohi Downs Syncline. Mean values of shortening of 32% and 13% have occurred in NW-SE and NE-SW directions respectively. The NE-SW shortening is comparable to the regional values (14%, Nicol 1991) derived via the same method as used here. The NW-SE shortening, however, is over double the regional (North Canterbury) value of 15% (Nicol 1991) derived via the same methods. Nonetheless the 32% is less than the 60% estimated by Syme (1991) for the Marble Point area. Of the strain estimated at the surface in this study area 9-28% can be attributed to faulting. Strain across the Island Hills to Green Hill area related to faulting is approximately 23%, a value very close to the 20% for coastal North Canterbury (Norris 1979).

Given the value of 15% shortening between the Hope Fault and the North Canterbury coastline the region has contracted by 11km. Furthermore, using 15%, the Mandamus-Pahau area will have contracted by 0.6km since the Pliocene in a NW-SE direction. A minimum rate of shortening of 6 ± 2mm a^{-1} (Nicol 1991) has been calculated for the region between the Hope Fault and the coast, in a NW-SE direction, for the post-early Pleistocene period.

6.4. DEFORMATION OF THE CULVERDEN BASIN IN THE CONTEXT OF PLATE COLLISION.

Mesoscale structures in the cover sequence, particularly in the Oligocene limestones (Chapter 3), imply two episodes of plate boundary deformation in the Culverden Basin. The first involved weak deformation during the Oligocene and may relate to the development of the Alpine Fault as a plate boundary transform structure (e.g. Carter & Norris, 1976). The orthogonal joints formed during this deformation are the only indication of post late Cretaceous, but pre Pliocene deformation in North Canterbury, and may indicate that the plate boundary zone was narrower in the Oligocene and Miocene than at present. The second period of deformation began along the western margin of the Culverden Basin during the late Pliocene. This deformation was marked by the formation of mesofaults, veins, joints along with macrofractures and macroscopic folds and faults. This second period of deformation indicates the increasing strain and widening of plate boundary deformation which commenced in Marlborough during the Pliocene (Lamb & Bibby, 1989).

The Hikurangi Trough terminates offshore, south of Kaikoura, at the edge of the New Zealand continental crust. Onshore there is a significant change in the style and magnitude of deformation between North Canterbury and Marlborough. Firstly, the major faulting style in North Canterbury is predominantly oblique thrust and oblique-reverse dip-slip as opposed to major right lateral strike-slip faulting in Marlborough. Secondly the lateral extent of the major faults in North Canterbury is considerably less than those in Marlborough. Furthermore the rates of deformation, derived from seismic data (Reyners, 1989), fault offsets (Bull, pers.comm., Cowan, 1990), and uplift rates (Lamb & Bibby, 1989), increase from North Canterbury to Marlborough. Finally, ridge and valley topography resulting from oblique-reverse and thrust faulting and fault-related folding in the Culverden Basin and North Canterbury is in contrast to the regional uplift in Marlborough.

There is, however, a similarity in vergence direction between the anomalous E-SE verging thrusts of the western margin of the Culverden Basin and the Pliocene and younger thrusts in Marlborough. A notable transition zone strikes NNW to the Hope Fault, from where the projection of the Hikurangi Trough intersects the present coastline. To the NNE of this zone E-SE verging thrusting predominates. South of this line E-SE verging thrusts are anomalous, while NW directed thrusting predominates. The intersection of the transition zone and the coastline may mark the southern onshore limit of the subduction of the Pacific Plate beneath the overriding Australian Plate.

6.5. CRUSTAL DETACHMENT FAULTING IN NORTH CANTERBURY.

Norris et.al. (1990) have inferred a mid to lower crustal décollement, from their application of critical wedge mechanics to the analysis of uplift of the Southern Alps, beneath the Otago region. Nicol (1991) has inferred from surface observations that a similar mid to lower crustal detachment fault exists in the Pacific Plate beneath North Canterbury. An aseismic zone located between 12-17km beneath the surface in North Canterbury (Cowan, 1992) is inferred to represent a ductile zone which probably equates to a detachment zone in the upper crust of the region. From the field mapping and analysis of macro- and mesoscopic structures of this study area the author infers that the thrust faults along the western margin of the Culverden Basin, and possibly the Mt. Noble fault to the west, shallow as they approach the inferred detachment zone (see Block diagram in Map pocket).

The right lateral strike-slip movement on the Hope Fault, and the same movement sense on the Porters Pass-Amberley Fault Zone, produces a region between the two faults that is subjected to contractional shortening and complex shear. This combines upthrow on the NNW sides of the faults, in response to the NW-SE regional shortening, with the SE verging left lateral oblique-reverse to oblique-thrust faults along the western margin of the Culverden Basin. This is supported by the SE vergence of the major thrust and oblique-reverse faults and the predominance of left over right lateral strike-slip mesofaults along the western margin of the Culverden

Basin (this study & Nicol, 1991). Furthermore the relative oblique uplift associated with the NW side of the Porters Pass-Amberley Fault Zone and relative oblique downthrow on the SE side of the Hope Fault suggest that the Culverden Basin will be exhumed from the south to north. This is supported by the uplift of the Mt. Grey to Mt. Oxford range front (Cowan pers.comm., 1992) and propagation of the Hawarden Anticline into the Culverden Basin at its southern end. Active faulting near Green Hill also suggests that the basin is being exhumed from the NW. The development of the Balmoral Fault and the upthrown block of Tertiary rocks at Green Hill, at a constraining bend in the Waitohi Downs Fault, has analogies with the "bends" area of the Alpine Fault. The left lateral component of the Waitohi Downs Fault is opposite to the movement sense on the Alpine Fault but the oblique thrusting and associated structures at both localities are similar. Contractional deformation at the restraining bend in the Waitohi Downs Fault is further evidence that the Culverden Basin is being exhumed and that it is likely to be short lived (<3ma).

Any further studies of the contractional deformation of the Culverden Basin and North Canterbury on the outer edge of the plate boundary zone need to be based on field mapping and kinematic analysis of both macro- and mesoscale structures within both the basement and cover rocks. Furthermore sub-surface data and geodetic triangulation should be incorporated into the studies to adequately explain both the surface and sub-surface geology of North Canterbury.

ACKNOWLEDGEMENTS

This thesis has received invaluable assistance from numerous people and organisations. Funding was received from the Mason Trust while a field vehicle was purchased for the North Canterbury Active Tectonics Group from funds provided by the Earthquake and War Damage Commission. I thank my supervisors Jocelyn Campbell and Jarg Pettinga who set up and obtained funding for the Active Tectonics Programme and who suggested the study area. In particular I thank Jocelyn for her assistance with this project and providing a guiding hand with the problems encountered. Jarg is thanked for his discussions and guidance on the production of the map. Andrew Nicol, a post Doctorate fellow, is thanked for his help and for enlarging my knowledge of structural geology, in particular the analysis of small scale structures. Similarly, Alastair Syme is thanked for his help with the computer based analysis of small scale structures.

Bill Bull, on sabbatical leave from the Department of Geoscience at the University of Arizona, provided very helpful assistance with the dating of the landslides in this study.

Mapping and data collection were undertaken with Jarg Pettinga, Andy Nicol, Richard Garlick and my fiancée, Debbie Nicholl. Andy, Richard and Hugh Cowan are thanked for their involvements in discussions on local and regional geology.

I wish to thank Jane Newman for her assistance with the analysis of the coal samples and Kerry Swanson and Malcolm Warnes for their work on the bugs. All technical staff of the Geology Department, University of Canterbury, are acknowledged for their assistance. Tracey is thanked for her help with the printing.

Carter Holt Harvey Limited and numerous farmers are acknowledged for allowing access to their land for fieldwork. In particular the Shands of Island Hills, Popes of Kanuku Hills and the Barkers of Mt. Mason are thanked not only for land access but their friendly assistance with accommodation. Helen, my sister, and her husband Jimmy are also thanked for their encouragement as well as providing accommodation.

I wish to thank Simon Ward, Richard Garlick and Brydon Hughes for their assistance in many ways during this thesis. I also thank all my friends and Deb's parents for their assistance and encouragement.

To Debbie, a BIG THANK YOU, not only for the word processing, but also for all her understanding, support and encouragement throughout.

Finally, and most importantly, I would like to thank my dad and my late mother. Mum provided a lot of support and encouragement throughout my education and most of this thesis. To dad I owe a big thank you for his support and encouragement throughout. I must also thank dad for his assistance and cooking, especially of the porridge, while in the field.

P.S. I must thank Watties for the tomato sauce that made many a pie eatable and of course Nescafe for the coffee.

REFERENCES.

Aleksandrowski, P., 1985: Graphical determination of principal stress directions for slickenside lineation populations: an attempt to modify Arthaud's method. Journal of Structural Geology 7, 73-82.

Ameen, M.S., 1988: Forced folding of layered cover due to dip-slip, basement faulting. Unpublished Ph.D. Thesis, University of London.

Anderson, E.M., 1951: The Dynamics of Faulting, Oliver and Boyd Ltd., London, 206p.

Andrews, P.B., 1960: Sedimentary history of the lowermost Otaian horizon in North Canterbury, New Zealand. Unpublished M.Sc. Thesis, University of Canterbury, Christchurch. 129pp.

Andrews, P.B., 1963: Stratigraphic nomenclature of the Omihi and Waikari Formations, North Canterbury. New Zealand Journal of Geology and Geophysics. 6, (2): 228-56.

Andrews, P.B., 1968: Patterns of Sedimentation during early Otaian (Early Miocene) time in North Canterbury. New Zealand Journal of Geology and Geophysics 11, 722-52.

Andrews, P.B., Speden I.G., Bradshaw, J.D., 1976: Lithological and paleontological content of the Carboniferous-Jurassic Canterbury Suite, South Island, New Zealand. New Zealand Journal of Geology and Geophysics 19, 792-819.

Angelier, J., 1975: Sur l'analyse de mesures recueillies dans des sites faillés: L'utilité d'une confrontation entre les méthodes dynamiques et cinématiques. C.r. Acad. Sci., Paris D281, 1805-1808.

Angelier, J., 1979: Determination of the mean principal stresses for a given fault population. Tectonophysics 56, T17-T26.

Angelier, J., 1984: Tectonic analysis of fault slip data sets. J. Geophys. Res. 89, 5953-5848.

Angelier, J., 1989: From orientation to magnitudes in paleostress determinations using fault slip data. Journal of Structural Geology 11, 37-50.

Angelier, J., & Mechler, P., 1977: Sur une méthode graphique de recherche des constraintes principales également utilisable en tectonique et en séismologie: la méthode des dièdres droits. Bull. Soc Géol.Fr. 19, 1309-1318.

Angelier, J., Tarantola, A., Valette, B., Manoussis, S., 1982. Inversion of field data in fault tectonics to obtain the regional stress. I. Single phase fault populations: a new method of computing the stress tensor. Geophys. J. R. Astr. Soc 69, 607-621.

Armijo, J.A., Carey, E., Cisternas, A., 1982: The inversion problem in microtectonics and the separation of tectonic phases. Tectonophysics 82, 145-160.

Armijo, R. & Cisternas, A., 1978: Un problème inverse en microtectonique cassante. C.r. Acad-Sci., Paris D287, 595-598.

Arthaud, F., 1969: Méthode de détermination graphique des directions da raccourcissement, d'allongement et intérmediare d'une population failles. Bull. Soc. Geol. Fr. 11, 729-737.

Aydin, A. & Nur, A., 1982: Evolution of pull-apart basins and their scale independence. Tectonics 1, 91-105.

Berg, R.R., 1962: Mountain flank thrusting in the Rocky Mountain Foreland, Wyoming and Colorado. American Association of Petroleum Geologists Bulletin 46, 2019-2032.

Botsford, J.W., 1983: The Esk Head Mélange in the Esk Head/Okuku area, North Canterbury. Unpublished M.Sc. thesis, University of Canterbury, Christchurch, New Zealand.

Bott, M.H.P., 1959: The mechanics of oblique slip faulting. Geological Magazine 96, 109-117.

Bradshaw, J.D., 1972: Stratigraphy and structure of the Torlesse Supergroup (Triassic-Jurassic) in the foothills of the Southern Alps near Hawarden (S60-61), Canterbury. New Zealand Journal of of Geology and Geophysics 15, 71-87.

Bradshaw, J.D., 1973: Allochthonous fossil localities in mélange within the Torlesse rocks of North Canterbury. Journal of the Royal Society of New Zealand 3, 161-167.

Bradshaw, J.D., 1975: The folds at Castle Hill (Canterbury) and their bearing on Kaikouran deformation style in the Canterbury Basin. Journal of the Royal Society of New Zealand 5, 209-217.

Bradshaw, J.D., 1989: Cretaceous Geotectonic Patterns in the New Zealand region. Tectonics 8, 803-820.

Bradshaw, J.D., Adams, C.J., Andrews, P.B., 1981: Carboniferous to Cretaceous on the Pacific margin of Gondwana: and the Rangitata Phase of New Zealand. In: Cresswell, M.M. and Vella, P. (Eds.) Fifth International Gondwana Symposium. Balkema, Amsterdam 217-221.

Brown, L.J. & Wilson, D.D., 1988: Stratigraphy of the Quaternary deposits of the Northern Canterbury Plains, New Zealand. New Zealand Journal of Geology and Geophysics 31, 305-335.

Brown, W.G., 1988: Deformational style of Laramide uplifts in the Wyoming Foreland. In: C.J. Schmidt and W.J. Perry (Jr) (Eds.) Interaction of the Rocky Mountain Foreland and the Cordilleran Thrust Belt. Geological Society of America Memoir 171, 1-26.

Browne, G.H., 1984a: The Balmoral Forest Inlier, North Canterbury. Immediate Report, New Zealand Geological Survey.

Browne, G.H., 1984b: Geological features related to the excavation in early 1984 of the Balmoral Irrigation Scheme Race, Green Hill, North Canterbury. Immediate Report, New Zealand Geological Survey.

Browne, G.H. & Field, B.D., 1985: The lithostrigraphy of Late Cretaceous to early Pleistocene rock of North Canterbury, New Zealand. New Zealand Geological Survey Record 6.

Browne, G.H. & Field, B.D., 1988: A review of Cretaceous-Cenozoic sedimentation and tectonics, East Coast, South Island, New Zealand. In: D.P James and D.A. Leckie (Eds.) Sequences, stratigraphy, sedimentology: surface and subsurface. Canadian Society of Petroleum Geologists Memoir 15, 37-48.

Buchanan, J., 1868: Kaikoura District. New Zealand Geological Survey report of Geological Explorations 4, 34-41.

Buchner, F., 1981: Rhine graben, horizontal stylolites indicating stress regimes of earlier states of rifting. Tectonophysics 73. 113-118.

Bull, W.B., 1984: Tectonic Geomorphology. Journal of Geological Education 32, 310-324.

Campbell, J.D. & Warren, G., 1965: Fossil localities of the Torlesse Group in the South Island. Transactions of the Royal Society of New Zealand 3, 99-137.

Campbell, J.K., 1973: Displacement data from the Alpine Fault at Lake Rotoiti and its relevance to glacial chronology and the tempo of tectonism. Abstracts from the IXth INQUA Congress, Christchurch, 57-58.

Campbell, J.K. & Yousif, H.M.K., 1987: Tectonic Geomorphology of the lower Waipara Gorge, North Canterbury. Geological Society of New Zealand Miscellaneous Publication 32b, 53-65.

Carey, E. & Brunier, B., 1974: Analyse théorique et numérique d'un modèle mécanique élémentaire appliqué à l'étude d'une population de failles. C.r. Acad. Sci., Paris D179, 891-894.

Carter, R.M. & Carter, L., 1982: The Motunau Fault and other structures at the southern edge of the Australian/Pacific Plate Boundary, offshore Marlborough, New Zealand. Tectonophysics 88, 133-159

Carter, R.M. & Carter, L., 1985: The Motunau Fault revisited. Tectonophysics 115, 164-166.

Carter, R.M. & Norris, R.J., 1976: Cainozoic history of southern New Zealand, an accord between geological observations and plate tectonics predictions. Earth and Planetary Science Letters 31, 85-94.

Chester, J.S., Spang J.H., Logan J.M., 1988: Comparisons of thrust fault rock models to basement-cored folds in the Rocky Mountain Foreland. In: C.J. Schmidt and W.J Perry (Jr) (Eds.) Interaction of the Rocky Mountain Foreland and the Cordilleran Thrust Belt, Geological Society of America Memoir 171, 65-74.

Chinn, T.J., 1981: Use of rock weathering rind thickness for Holocene absolute age dating in New Zealand. Artic and Alpine Research 13, 33-45.

Christoffel, D.A., 1971: Motion of the New Zealand Alpine Fault deduced from the pattern of sea-floor spreading in Recent crustal movements. Royal Society of New Zealand Bulletin 9, 25-30.

Clayton, L.S., 1966: Tectonic depressions along the Hope Fault, a transcurrent fault in North Canterbury. New Zealand Journal of Geology and Geophysics 9, 95-104.

Cook, D.G., 1983: The Northern Franklin Mountains, NW Territories Canada, a scale model of the Wyoming Province. In: J.D. Lowell and R.R. Gries (Eds.) Rocky Mountain Foreland basins and uplifts. Rocky Mountain Association of Geologists, 315-338.

Cook, D.G., 1988: Balancing basement cored folds of the Rocky Mountain Foreland. In: C.J. Schmidt and W.J Perry (Jr) (Eds.) Interaction of the Rocky Mountain Foreland and the Cordilleran Thrust Belt, Geological Society of America Memoir 171, 53-64.

Cooper, A.F., Barreiro, D.L., Kimborough, D.L., Mattinson, J.M., 1987: Lamprophyre dike intrusion and the age of the Alpine Fault, New Zealand. Geology 15, 941-944.

Coote, A., 1987: Cenozoic volcanism in the Waiau area, North Canterbury. Unpublished MSc Thesis, University of Canterbury, Christchurch.

Cowan, H.A., 1990: Late Quaternary displacements on the Hope Fault at Glynn Wye, North Canterbury. New Zealand Journal of Geology and Geophysics 33, 285-293.

Cowan, H.A., 1992: Structure, Seismicity and Tectonics of the Porters Pass-Amberley Fault Zone, North Canterbury, New Zealand. Unpublished Ph.D. Thesis University of Canterbury, Christchurch.

Cox, A. & Hart, R.B., 1986: Plate Tectonics: how it works. Blackwell Scientific Publications U.S.A. p. 392.

Coyle, S.A., 1988: The Porters Pass Fault. Unpublished M.Sc Thesis, University of Canterbury, Christchurch.

Cutten, H.N.C., 1979: Rappahannock Group: Late Cenozoic sedimentation and tectonics contemporaneous with Alpine Fault movement. New Zealand Journal of Geology and Geophysics 22, 535-553.

de Mets, C., Gordon, R.G., Argus, D.F., Stein, S., 1990: Current plate motions. Geophysical Journal International 101, 425-428.

Dibble, R.R., Unpublished: Gravity data, with map and cross sections, from the Culverden Basin Area, North Canterbury, New Zealand.

Durney, D. & Ramsay, J.G., 1973: Incremental strains measured by syntectonic crystal growths. In De Jong, K.A. and Scholter, R. (Eds.) Gravity and Tectonics, John Wiley and Sons Inc, New York.

Eiby, G.G., 1968: A descriptive catalogue of New Zealand earthquakes. Part.1 shocks felt before the end of 1945. New Zealand Journal of Geology and Geophysics 11, 630-647.

Endharto, M.A., 1987: Upper Cretaceous-Tertiary geology of the Wandle River-Whales Back area, Northern Waiau, North Canterbury. Unpublished M.Sc. Thesis, Department of Geology, University of Canterbury, Ghristchurch.

Engelder, T. & Geiser, P., 1980: On the use of regional joint sets astrajectories of paleostress fields during the development of the Appalachian Plateau, New York. Journal of Geological Research 85, 6319-6341.

Etchecopar, A., Vasseue, G., Daignieres, M., 1981: An inverse problem in microtectonics for the determination of stress tensors from striation analysis. Journal of Structural Geology 3, 51-65.

Falloon, A.S., 1954: Geology of the Culverden Basin, North Canterbury, New Zealand. Unpublished M.Sc. Thesis, University of Canterbury, Christchurch.

Field, B.D. & Browne G.H., 1989: Cretaceous and Cenozoic Sedimentary Basins and Geological Evolution of the Canterbury Region, South Island, New Zealand. New Zealand Geological Survey Basin Studies 2. New Zealand Geological Survey, Lower Hutt, New Zealand.

Field, B.D. & Odin, G.S., 1981: K-Ar dating of Paleocene glaucony from North Canterbury, New Zealand. New Zealand Geological Survey report G45.

Fletcher, R.C. & Pollard, D.D., 1981: Anticrack modal for pressure solution surfaces. Geology 9, 419-424.

Friedman, M., Handin, J., Logan, J.M., Min, K.D., Stearns, D.W., 1976: Experimental folding of rocks under confining pressure; Part III, faulted drape folds in multi-lithologic layered specimens. Bulletin of the Geological Society of America 87, 1049-1066.

Frizzell, V.A. & Zoback, M.L., 1987: Stress orientation determined from fault slip in Hampel Wash area, Nevada, and its relation to contemporary regional stress field. Tectonics 8, 89-98.

Gangi, A.F., Min, K.D., Logan, J.M., 1977: Experimental folding of rocks under confining pressure: Part 4. Theoretical analysis of faulted drape-folds. Tectonophysics 88.

Garlick, R.D., 1992: Lees Valley Fault, North Canterbury. Unpublished B.Sc. (Hons) Thesis, Department of Geology, University of Canterbury, Christchurch.

Gephart, J.W. & Forsyth, D.W., 1984: An important method for determining the regional stress tensor using earthquake focal mechanism data: application to the San Fernando earthquake sequence. Journal of Geophysical Research 89, 9305-9320.

Gregg, D.R., 1964: Sheet 18, Hurunui (1st edition). Geological map of New Zealand 1:250.000. Department of Scientific and Industrial Research, Wellington, New Zealand.

Gregg, R.C., 1965: Pre-Quaternary geology of an area around Waiau, North Canterbury. Unpublished M.Sc. Thesis, Department of Geology, University of Canterbury, Christchurch.

Haast, J., 1871: On the geology of the Amuri district in the province of Nelson and Marlborough. New Zealand Geological Survey reports of geological exploration 6, 25-46.

Haast, J., von 1879: Geology of the Province of Canterbury and Westland, New Zealand. A report comprising the results of offical explorations. Times Office, Christchurch.

Hamilton, D., 1950: Geology of the Waikari Valley and its northern ridges, North Canterbury. Unpublished M.Sc. Thesis, Department of Geology, University of Canterbury, Christchurch.

Hancock, P.L., 1985: Brittle microtectonics, principles and practice. Journal of Structural Geology 7, 437-457.

Hardcastle, K., 1989: Analysis of veins and faults along a cross section of the New England Appalachians: clues to the brittle history of an orogenic belt. Unpublished Ph.D. Dissertation, University of Massachusetts at Amherst.

Hardcastle, K.C. & Hills, L.S., 1991: Brute3 and Select: Quickbasic 4 programs for determination of stress tensor configurations and seperation of heterogeneous populations of fault-slip data. Computers and Geosciences 17, 23-43.

Hicks, S.R., 1989: Structure of the Canterbury Plains, New Zealand, from Gravity Modelling. Research Report 222. Geophysics division. D.S.I.R. Wellington New Zealand.

Hobbs, B.E., Means, W.D., Williams, P.F., 1976: An outline of structural geology. John Wiley and sons Inc., New York.

Hoskins, R.H., 1969: Planktonic foraminiferida and the Paleocene-Eocene boundary of the middle Waipara Gorge, North Canterbury, New Zealand. Unpublished M.Sc. Thesis, Geology Department, University of Canterbury.

Hutton, W.F., 1878: Report on the geology of the northeast portion of the South Island, from Cook Strait to Rakaia. New Zealand Geological Survey report of Geological Explorations, 1873-1874: 27-58.

Jenkins, T.B.H. & Jenkins, D.J., 1971: Conodonts of the Haast Schist and Torlesse groups of New Zealand. PART 1. New Zealand Journal of Geology and Geophysics 14, 782-94.

Kamp, P.J.J., 1986: The mid-Cenozoic Challanger Rift System of western New Zealand and its implications for the age of the Alpine Fault inception. Bulletin of the Geological Society of America 97, 255-281.

Keefer, D.K., 1984: Landslides caused by earthquakes. Geological Society of America Bulletin 94, 406-421.

Kneupfer, P.L.K., 1984: Tectonic geomorphology and present-day tectonics of the Alpine Shear System, South Island, New Zealand. Unpublished Ph.D. thesis, University of Arizona, Tucson.

Laird, M.G., 1981: The late Mesozoic fragmentation of the New Zealand segment of Gondwana. Fifth International Gondwana Symposium. Wellington, New Zealand, February, 1980, 311-318

Lamb, S.H., 1988: Tectonic rotations about vertical axes during the last 4 ma in part of the New Zealand plate-boundary zone. Journal of Structural Geology 9, 877-891.

Lamb, S.H. & Bibby, H.M., 1989: The last 25 ma of rotational deformation in part of the New Zealand plate-boundary zone. Journal of Structural Geology 11, 473-492.

Lammerink, W.L., 1976: The structure and some sedimentological aspects of the Mount Highfield area, North Canterbury. Unpublished B.Sc.(Hons) Thesis, Department of Geology, University of Canterbury, Christchurch.

Le Pichon, X., 1968: Sea-floor spreading and continental drift. Journal of Geophysical Research 73, 3661-3697.

Lensen, G.J., 1962: Sheet 16, Kaikoura (1st edition). Geological Map of New Zealand 1:250 000. Department of Scientific and Industrial Research, Wellington, New Zealand.

Letouzey, J. & Tremolieres, P., 1980: Paleo-stress fields around the Mediterranean since the Mesozoic derived from microtectonics; comparison with plate tectonic data. Mem. Bur. Rech Geol. Min. 115. 261-273.

Lewis, K.B., Bennett, D.J., Herzer, R.H., von der Borch, C.C. 1985: Seismic stratigraphy and structure adjacent to an evolving plate boundary, Western Chatham Rise, New Zealand. Initial Reports of the Deep Sea Drilling Project XC, Washington.

Lisle, R.J., Styles, P., Freeth, S.J., 1990: Fold interference structures: the influence of layer competence contrast. Tectonophysics 172, 197-200.

McCulloch, B.A., 1981: Geology of the Mount Brown beds. Unpublished M.Sc. Thesis, Department of Geology, University of Canterbury, Christchurch.

McKay, A., 1890: On the earthquakes of september 1888, in the Amuri and Marlborough districts of the South Island. New Zealand Geological Survey report of geological exporations 20, 1-16.

McKay, A., 1892: On the geology of the Middle Waipara and Weka Pass districts, North Canterbury. New Zealand Geological Survey of Geological Exporations 1890-1891 21, 97-103.

McMorran, T., 1991: The Hope Fault at Hossack Station east of Hanmer Basin, North Canterbury. Unpublished M.Sc. Thesis, Department of Geology, University of Canterbury, Christchurch.

Marrett, R. & Allmendinger, R.W., 1990: Kinematic analysis of fault-slip data. Journal of Structural Geology, 973-986.

Mason, B.H., 1947: Tertiary rocks at Marble Point, Waiau, North Canterbury. New Zealand Journal of Science and Technology B29, 116-120.

Mason, B.H., 1949: The geology of Mandamus-Pahau district, North Canterbury. Transactions of the Royal Society of New Zealand 77, 403-428.

Mason, B.H., 1951: The Syenite and Associated Rocks of the Mandamus-Pahau Area, North Canterbury, New Zealand. Transactions of the Royal Society of New Zealand 79, 260-275.

Means, W.D., 1987: A newly recognised type of slickenside striation. Journal of Structural Geology 9, 585-590.

Michael, A., 1984: Determination of stress from slip data: faults and folds. J. Geophys. Res. B89, 11,517-11,526.

Middleton, L.M.H., 1978: Upper Triassic and Upper Jurassic Torlesse volcanic associations in the Waitohi Hills and Mt Mason districts, NW Canterbury, New Zealand. Unpublished M.Sc. Thesis, Department of Geology, University of Canterbury, Christchurch.

Molnar, P., Atwater, T., Mammerickx, J., Smith, S.M., 1975: Magnetic anomalies, bathometry and the tectonic evolution of the South Pacific since the late Cretaceous. Geophysical Journal of the Royal Astronomical Society 40, 383-420.

Nicol, A., 1991: Structural styles and kinematics of deformation on the edge of the New Zealand Plate Boundary Zone, Mid Waipara region, North Canterbury. Unpublished Ph.D. Thesis, Department of Geology, University of Canterbury, Christchurch.

Nicol, A., 1992: Oligocene limestone tectonic structures and their implications for New Zealand plate boundary deformation in North Canterbury. New Zealand Journal of Geology and Geophysics 35, 353-362.

Nicol, A. & Campbell, J.K., 1990: Late Cenozoic thrust tectonics, Picton, New Zealand. New Zealand Journal of Geology and Geophysics 33, 485-494.

Norris, R.J., 1979: A Geometric Study of finite strain and bending in the South Island. In: R.I. Walcott and M.M. Cresswell (Eds.) Origin of the Southern Alps. Bulletin of the Royal Society of New Zealand 18, 21-28.

Norris, R.J., Koons, P.O., Cooper, A.F., 1990: The obliquely-convergent plate boundary in the South Island of New Zealand: implications for ancient collision zones. Journal of Structural Geology 12, 715-725.

Petit, J.P., 1987: Criteria for the sense of movement on fault surfaces in brittle rocks. Journal of Structural Geology 9, 597-608.

Powers, W.E., 1962: Terraces of the Hurunui River, New Zealand. New Zealand Journal of Geology and Geophysics 5, 114-129.

Prucha, J.J. & Nickelsen, R.P., 1965: Basement controlled deformation in Wyoming province of Rocky Mountain Foreland. American Association of Petroleum Geologists Bulletin 49, 966-992.

Ramsay, J.G., 1962: Interference Patterns produced by superposition of folds of "similar" type. Journal of Geology 60, 455-481.

Ramsay, J.G., 1967: Folding and Fracturing of Rocks. McGraw Hill Inc.

Ramsay, J.G. & Huber, M.I., 1987: The Techniques of Modern Structural Geology Volume 2: Folds and Fracture. Academic Press Inc., London.

Read, J.R.L., 1964: The geology of the Hurunui River valley between Lake Sumner and the Mandamus River, North Canterbury. Unpublished M.Sc. Thesis, Department of Geology, University of Canterbury, Christchurch.

Reches, Z., 1978: Development of monoclines: part I. Structure of the Palisades Creek branch of the East Kaibab monocline, Grand Canyon, Arizona. In: V. Matthews III (Ed.) Laramide folding associated with basement block faulting in the Western United States. Geological Society of America Memoir 151, 235-273.

Reches, Z., 1987: Determination of the tectonic stress tensor from slip along faults that obey the coulomb yield condition. Tectonics 6, 849-861

Reches, Z. & Johnson, A.M., 1978: Development of monoclines: part II. Theoretical analysis of monoclines. In: V. Matthews III (Ed.) Laramide folding associated with basement block faulting in the Western United States. Geological Society of America Memoir 151, 273-312.

Reid, D.L., 1972: A petrological study of the Mandamus Igneous Complex, North Canterbury. Unpublished M.Sc. Thesis, Department of Geology, Victoria University of Wellington.

Reyners, M., 1989: New Zealand Seismicity 1964-87: an interpretation. New Zealand Journal of Geology and Geophysics 32, 307-315.

Schofield, J.C., 1949: The Geology of the MacDonald Downs and Waikari Districts, North Canterbury. Unpublished M.Sc. Thesis, Department of Geology, University of Canterbury, Christchurch.

Sevon, W.D., 1969: Stratigraphy and sedimentology of the Tertiary rocks of the Mandamus-Dove River area, North Canterbury, New Zealand. New Zealand Journal of Geology and Geophysics 12, 283-309.

Shelley, D., Smale, D., Tulloch, A.J., 1977: Boehmite in syenite from New Zealand. Mineralogical Magazine 41, 398-400.

Speight, R., 1915: The intermontane basins of Canterbury. (Part 1) Transactions of the New Zealand Institute 47, 336-353.

Speight, R., 1918: Structural and Glacial Features of the Hurunui Valley. Transactions of the New Zealand Institute 50, 93-105.

Speight, R., 1926: Intermontane basins of Canterbury (part 2) Transactions of the New Zealand Institute 56, 355-360.

Speight, R., 1933: The Arthurs Pass earthquake of 9th march 1929. New Zealand Journal of Science and Technology 15, 173-182.

Sporli, K.B. & Anderson, H.J., 1980: Paleostress axes from mineral striations in faulted Mesozoic basement, Auckland, New Zealand. New Zealand Journal of Geology and Geophysics 23, 155- 166.

Stauffer, M.R., 1964: The geometry of conical folds. New Zealand Journal of Geology and Geophysics 7, 340-347.

Stauffer, M.R., 1988: Fold interference structures and coaptation folds. Tectonophysics 149, 339-343.

Stearns, D.W., 1971: Mechanisms of drape folding in the Wyoming province. Wyoming Geological. Association 23rd Annual Field Conference, Wyoming Tectonics Symposium Guidebook, 125-143.

Stearns, D.W., 1978: Faulting and forced folding in the Rocky Mountain Foreland. In: V. Matthews III (Ed.) Laramide folding associated with basement block faulting in the Western United States. Geological Society of America Memoir 151, 1-37.

Stearns, D.W. & Weinberg, D.M., 1975: A comparison of experimentally created and naturally formed drape folds. Wyoming Geological Association 27th Annual Field Conference, Geology and mineral resources of the Bighorn Basin, Guidebook, 159-166

Stock, J. & Molnar, P., 1982: Uncertainties in the relative positions of Australia, Antartica, Lord Howe and Pacific plates since the late Cretaceous. Journal of Geophysical Research 87, 4679-4714.

Strong, C.P., 1984: Cretaceous-Teritary boundary, mid Waipara River Section, North Canterbury, New Zealand.

Suggate, R.P., 1965: Late Pleistocene geology of the northern part of the South Island, New Zealand. Bulletin of New Zealand Geological Survey 77.

Suppe, J., 1985: Principals of Structural Geology. Prentice-Hall, New Jersey.

Syme, A.R., 1991: Structural Analysis of the Deformation of the Marble Point Outlier, Waiau River, North Canterbury. Unpublished B.Sc.(Hons.) Thesis, Department of Geology, University of Canterbury, Christchurch.

Systra, Y.U.I. & Skornyakova, N.I., 1980: Conical folds in ancient complexly folded metamorphic formations in Northern Karelia. Geotectonics 14, 17-25.

Theissen, R.L., 1986: Two dimensional refold interference patterns. Journal of Structural Geology 8, 563-573.

Theissen, R.L. & Means, W.D.,1980: Classification of fold interference patterns: a reexamination. Journal of Structural Geology 2, 311-316.

Thomson, J.A., 1920: The Notocene geology of the middle Waipara and Weka Pass district, North Canterbury, New Zealand. Transactions of the New Zealand Institute 52, 322-415.

Tulloch A.J., 1991: Alkaline Plutonic and Volcanic Rocks of the Late Cretaceous Mandamus Igneous Complex, North Canterbury. New Zealand Geological Survey Record 43, 15-23.

Van Dissen, R. & Yeats, R.S., 1991: Hope Fault, Jordan thrust, and uplift of the Seaward Kaikoura Range, New Zealand. Geology 19, 393-396.

Van der Lingen, G.J., 1984: Surface textures on quarts grains from the Leeston-1 oil exploration well, Canterbury, New Zealand. Research notes, New Zealand Geological Survey record 3, 45-66.

Varnes, D.J., 1978: Slope movement and types and processes. In: Schuster, R.L. & Krizek, R.J. (eds) Landslides: Analysis and Control. Transportation Research Board Special Report 176. Washington DC, National Academy of Sciences: 11-33.

Voight, B. & Pariseau, W.G., 1978: Rockslides and Avalanches: An introduction, In: Voight, B. (Ed.) Rockslides and Avalanches 1. Developments in Geotechnical Engineering 14a. Amsterdam, Elsvier, 1-67.

Walcott, R.I., 1978: Present tectonics and late Cenozoic evolution of New Zealand. Geophysical Journal of the Royal Astronomical Society 52, 137-164.

Walcott R.I., 1984: Reconstructions of the New Zealand region for the Neogene. Palaeogeography, Palaeoclimatology, Palaeoecology 46, 217-231.

Walcott R.I., 1987: Geodetic strain and the deformation history of the North Island during the late Cenozoic. Philosophical Transactions of the Royal Society of London A321, 163-181.

Wallace, R.E., 1951: Geometry of shearing stress and relation to faulting. Journal of Geology 59, 118-130.

Wallace, R.E., 1978: Geometry and rates of change of fault generated range fronts, north-central Nevada. United States Geological Survey Journal of Research, 637-650.

Warren, G., 1978: Torlesse supergroup eastern South Island, 271-277. In: R.P. Suggate, G.R. Stevens, and M.T. Te Punga (Eds.) The Geology of New Zealand. Wellington Government Printer (2vols).

Warren, G. & Speden, I.G., 1978: The Piripauan and Haumurian stratotypes (Mata Series, Upper Cretaceous) and correlative sequences in the Haumuri Bluff district, South Marlborough (S56) New Zealand Geological Survey Bulletin 92.

Weaver, S.D. & Pankhurst, R.J., 1991: A precise Rb-Sr age for the Mandamus Igneous Complex, North Canterbury, and regional tectonic implications. New Zealand Journal of Geology and Geophysics 34, 341-345.

Webb, B.C. & Lawerence, D.J.D., 1986: Conical fold terminations in the Bannisdale States of the English Lake District. Journal of Structural Geology 8, 79-86.

Weingberg, D.M., 1978: Some two-dimensional kinematic analysis of the drape-fold concept. Geological Society of America Memoir 151, 51-78.

Wellman, H.W., 1953: Data for the study of recent and late Pleistocene faulting in the South Island of New Zealand. New Zealand Journal of Science and Technology B34, 270-288.

Whitehouse, I.E. & Griffiths, G.A., 1983: Frequency and hazard of Large Rock Avalanches in the central Southern Alps, New Zealand. Geology 11, 331-334.

Whitehouse, I.E., McSaveney M.J., Knuepfer P.L.K., Chinn T.J.H., 1986: Growth of Weathering Rinds on Torlesse Sandstones, Southern Alps, New Zealand. In: S.M. Colman and D.P. Dethier (Eds.) Rates of Chemical Weathering of Rocks and Minerals. Academic Press.

Wilson, D.D., 1963: The Geology of the Waipara Subdivision. New Zealand Geological Survey Bulletin 64.

Wilson G.J., 1967: The geometry of cylindrical and conical folds. Proceedings of the Geological Association 78, 179-209.

Wilson, G.D., 1976: Report on a late Jurassic and early Cretaceous dinoflugellate assemblage from Torlesse sediments in the Cheviot, Culverden, Parnassus and Hanmer areas. Unpublished New Zealand Geological Survey Report. GJW 63.

Wilson, G.D., 1978: Kaiwarodinium., a new dinoflagellate genus from the Late Jurassic of North Canterbury, New Zealand. New Zealand Journal of Geology and Geophysics 21, 81-84.

Wilson, G.D., 1984: Two new dinoflagellates from the Late Jurassic of North Canterbury, New Zealand. Journal of the Royal Society of New Zealand 14, 215-221.

Wise, D.U. & McCrory, T.A., 1982: A new method of fracture analysis, azimuth versus traverse distance plots. Geological Society of American Bulletin 93, 889-897.

Wise, D.U. & Fleischmann K., 1990: A program for smoothing, plotting and placing statistical limits on rose diagrams, submitted to Computers and Geology.

Yeats, R.S., 1987a: Active faults related to folding. In: Active Tectonics. National Academic Press, 63-79.

Yeats, R.S., 1987b: Coseismic folding. In: Active Tectonics. National Academic Press, 163-172.

Yeats, R.S. & Berryman, K.R., 1987: South Island, New Zealand, and Transverse Ranges, California: A seismotectonic comparison. Tectonics 6, 363-376.

APPENDIX I: COAL DATA.

Six coal samples, 3 from conglomerates within the Torlesse Supergroup, 2 from the late Cretaceous Broken Rover Formation and 1 from the Pliocene to early Pleistocene Kowai Formation (see Stratigraphic Column) were analysed using proximate (performed by the Coal Research Association of New Zealand, CRA), and vitrinite reflectance analyses (carried out by Dr J. Newman). All proximate analyses are on an air dried basis. The results are presented below.

Torlesse Supergroup.

Coal clasts were collected from a conglomerate within the Torlesse Supergroup on the banks of the Hurunui River (M33/697227). All three clasts are mineralised wood; minerals include quartz, pyrite, carbonate, iron oxide (hematite) and some authigenic clay. Some areas are more intensely mineralised than others while margins of unmineralised grains have occasional inclusions of minerals from previously adjacent grains.

The quartz veining (Figure 7.1) is pre coalification and infills prevasive fractures, this is supported by the lack of quartz veining in the host rock compared to the abundant carbonate replacement of the host rock. The carbonate is clearly post coalification as angular vitrinite floaters occur in the carbonate veins and carbonate infilled pore spaces.

Sample HR 3 has an average vitrinite reflectance (Ro) value of 0.88%.
HR 5 has a bimodal reflectance curve with a low peak of Ro = 0.66% while the main mode is Ro = 0.79%.
HR 6 reflectance is unimodal with Ro = 0.79%.

Figure 7.1. A fracture developed in quartz mineralised wood from within a conglomerate horizon in the Torlesse Supergroup, Hurunui River, North Canterbury (M33/697227). The fracture is smeared with organic material which appears to postdate the mineralisation (horizontal field of view = 0.25mm).

Figure 7.2. A photograph of a possible echinoderm fragment (single crystal) in coal sample BR1 from Coal Creek, Island Hills, North Canterbury (View is in cross polarised light and horizontal field of view = 0.25mm).

Figure 7.3. A photograph of framboidal pyrite (white-yellow) in KHC2 from the the Kowai Formation in the core of the Waitohi Downs Syncline, North Canterbury. Also present in this view (horizontal field = 0.25mm) is quartz silt.

Broken River Formation Coal.

There are two components to this sample from Coal Creek, Island Hills 1) wood with Ro = 0.32%

2) coal, with vitrinite, inertodetrinite (oxidised fragments), quartz and sparse fossil fragments (Figure 7.2). Ro = 0.49%.

The two components occur interlayered, the wood lacking any remnant porosity, but it is severely weathered while the coal is less weathered.

Broken River Formation CRA Proximate Analysis.

Sample number corresponds to CRA reference 49/155.

Moisture	9.60%
Ash	45.6%
Volatile matter	20.8%
Fixed carbon	24.0%
Sulphur	1.80%
Volatile dmmSf	39.8%

Volatile dmmSf = volatile matter corrected for moisture and mineral matter.

Kowai Formation Coal.

Two samples were collected from Kanuku Stream in the core of the Waitohi Downs Syncline.

KHC1 is suberinitic wood with well preserved vascular structure. Some cell lumens are filled (phlobaphenite) while others have remnants of their original porosity (implies very low rank). The sample is not mineralised other than containing pyrite and shows little sign of weathering. An Ro value of 0.20% to 0.25% was measured from the phlobaphenite while Ro = 0.20% was recorded on telinite (cell walls).

Kowai Formation CRA Proximate Analysis.

Sample number corresponds to CRA reference 49/156.

Moisture	17.4%
Ash	5.20%
Volatile matter	39.1%
Fixed carbon	38.3%
Sulphur	1.40%
Volatile dmmSf	50.1%

Volatile dmmSf = volatile matter corrected for moisture and mineral matter.

KHC2 has an association of various macerals indicating that this sample is a coal, originating from peat (as opposed to the peatified wood). The pyrite is distinctly framboidal (Figure 7.3), implying a marine influence during peat accumulation (an environment supported by the overlying beds containing bivalve fragments and slightly glauconitic quartzose sandstones). Ro values are bimodal with Ro = 0.28% and Ro = 0.48% with an average Ro = 0.36%.

APPENDIX II: WEATHERING RIND MEASUREMENT & DATING.

Chinn (1981) proposed a technique for establishing the age of medium grained (0.2-0.6mm) prehnite-pumpellyite metamorphic facies Torlesse Supergroup sandstones. Whitehouse et al. (1986) modified the simple relaxation law derived by Chinn (1981). The same methodology and relaxation law has been used in this study to that used by Whitehouse et al. (1986). The age of a dated feature is determined by deriving the modal weathering rind thickness for a given population and comparing this, via a calibration curve, to data from sites where both weathering rind and radiocarbon information is available. The calibration curve used in this work is that of McSaveny (May, 1992).

The weathering rinds were measured using digital verneer calipers that measure to the nearest hundreth of a millimetre. The digital display was turned away to reduce recorder bias in determining the rind thickness. Wherever possible a sample population of at least one hundred weathering rinds were collected and measured.

The modal rind thickness was determined using a computer based Quickbasic 4.5 program written by Wise & Fleischmann (1990). The program plots a histogram of rind thickness against a concentration factor, where the concentration factor is defined as the number of times the data are concentrated over and above an absolutely uniform distribution (Wise & McCrory, 1982). For the purposes of presenting the data the concentration factors have been converted to percent by dividing the sample window size by the total spread of rind thicknesses. The histogram is then double smoothed, so as to avoid skewing the peaks, in 0.01mm intervals using a 0.10mm sample window. The program shades those peaks that exceed the maximum value for randomly generated statistics. Shaded peaks are regarded as significant at one standard deviation.

Diagram to accompany thesis by Richard James Mould "Structure and Kinematics of late Cenozoic Deformation along the Western Margin of the Culverden Basin, North Canterbury, New Zealand."

BLOCK DIAGRAM OF THE CULVERDEN BASIN